

Review Article

Mohsin Saeed, Umer Shahzad, Muhammad Fazle Rabbee, Jehan Y. Al-Humaidi, Hadi M. Marwani, Shujah Ur Rehman, Anam Shabbir, Muhammad Naeem Ayub, Raed H. Althomali, Muhammad Nadeem Asghar and Mohammed M. Rahman*

Comprehensive reviews on the potential applications of inorganic metal sulfide nanostructures in biological, environmental, healthcare, and energy generation and storage

<https://doi.org/10.1515/revic-2024-0016>

Received March 12, 2024; accepted April 29, 2024;
published online May 31, 2024

Abstract: The versatile nature of metal sulfide nanostructures has led to their meteoric rise in popularity. The compositions, morphologies, and sizes of these nanostructures may be tuned, giving them distinct features. Here we look at the many uses of metal sulfide nanostructures, with an emphasis on their possible benefits in

the fields of biology, ecology, and energy storage. Because of their remarkable optical characteristics and high degree of biocompatibility, metal sulfide nanostructures have great potential in the biological fields of bioimaging, medication administration, and photothermal treatment. Additionally, because of their large surface area and adsorption capability, these nanostructures show outstanding performance in environmental remediation, which includes pollutant removal and wastewater treatment. Because of their great conductivity and electrochemical activity, metal sulfide nanostructures are also in great demand for energy storage applications such as supercapacitors, hydrogen storage, and lithium-ion batteries. This review provides a comprehensive analysis of recent progress in synthesizing various metal sulfides with transition metal elements. Effective physiochemical and biological approaches are employed in their production to control the structures, dimensions, and compositions of these sulfides.

Keywords: supercapacitor; solar cell; photocatalysis; metal sulfides; bioimaging; cancer photothermal therapy

Mohsin Saeed, Umer Shahzad and Muhammad Fazle Rabbee are contributed equally to this work.

*Corresponding author: **Mohammed M. Rahman**, Department of Chemistry, Faculty of Science, King Abdulaziz University, Jeddah 21589, Saudi Arabia; and Center of Excellence for Advanced Materials Research (CEAMR), King Abdulaziz University, Jeddah 21589, Saudi Arabia, E-mail: mmrahman@kau.edu.sa

Mohsin Saeed and Umer Shahzad, Department of Chemistry, Faculty of Science, King Abdulaziz University, Jeddah 21589, Saudi Arabia

Muhammad Fazle Rabbee, Department of Biotechnology, Yeungnam University, Gyeongsan 38541, Republic of Korea

Jehan Y. Al-Humaidi, Department of Chemistry, College of Science, Princess Nourah Bint Abdulrahman University, P.O. Box 84428, Riyadh 11671, Saudi Arabia

Hadi M. Marwani, Department of Chemistry, Faculty of Science, King Abdulaziz University, Jeddah 21589, Saudi Arabia; and Center of Excellence for Advanced Materials Research (CEAMR), King Abdulaziz University, Jeddah 21589, Saudi Arabia

Shujah Ur Rehman, Institute of Energy & Environmental Engineering, University of the Punjab, New Campus, Lahore, Pakistan

Anam Shabbir, Department of Chemistry, Forman Christian College University, Lahore, Pakistan

Muhammad Naeem Ayub, Department of Chemistry, The University of Lahore, Lahore, Pakistan

Raed H. Althomali, Department of Chemistry, College of Art and Science, Prince Sattam Bin Abdulaziz University, Wadi Al-Dawasir 11991, Saudi Arabia

Muhammad Nadeem Asghar, Department of Chemistry, Forman Christian College University, Lahore, Pakistan

1 Introduction

Nanotechnology has garnered significant interest in the 21st century because of its wide-ranging applications in several fields, for example, biomaterials, energy storage, water purification, and medicine. Nanostructures (NSs) with dimensions ranging from 1 to 100 nm are crucial in advancing nanotechnology. Their remarkable control over a wide range of physical and chemical properties including melting point, electrical and thermal conductivity, catalytic activity, light absorption, and scattering explains why. Consequently, NSs exhibit superior performance compared to bulk materials. Various physiochemical and biological techniques have produced a diverse

range of nanostructures (including zero-dimensional, one-dimensional, two-dimensional, and three-dimensional structures). Among the many uses for these nanostructures are electrical appliances, sensors, catalysts for light, antibacterial substances, and catalysts.^{1–3} Many classes of nanomaterials exist, including carbon-based materials, ceramics, polymers, metal sulfides, metal oxides, and metals. Their size, shape, and a plethora of properties including electrical, optical, magnetic, chemical, and mechanical traits affected by their constrained dimensions form the basis of this categorization.^{4–7} MOs and MSs, as nanomaterials, have exceptional semiconductor properties that enable them to efficiently capture solar radiation over a wide range of wavelengths, the ultraviolet (below 300 nm), visible (between 300 and 700 nm), and infrared (beyond 700 nm) wavelengths. For years, nanomaterials incorporating MOs and MSs have been employed in photocatalysis, water splitting, and photovoltaics.

An important fact is that several MOs possess a significant band gap energy. This is because the band of energy levels occupied by valence electrons is exclusively made up of deep $2p$ oxygen orbitals, resulting from their restricted structure. Additionally, hole carriers in MOs have a comparatively high effective mass.^{8–14} The chemical composition of MSs differs from MOs in a few keyways. One reason is the disparity in atomic numbers and dimensions between oxygen (O) and sulfur (S) atoms, as well as the dissimilarity in negatively bivalent anions that attach to them. For example, the ionic radius of O^{2-} ranges from 1.35 to 1.42 Å, and the ionic radius of S^{2-} is 1.84 Å.^{15–17} Accordingly, S exhibits greater average polarizability ($\alpha_S = 2.90 \times 10^{-24} \text{ cm}^3$) compared to O ($\alpha_O = 0.802 \times 10^{-24} \text{ cm}^3$).¹⁸ The electronegativity of sulfur (S) is significantly less than that of oxygen (O), indicating that the M–S interaction is more covalent than the M–O link.¹⁹ Compared to MOs, MSs have several desirable properties, such as extended lifespan, low melting point, nanocrystalline shape, low redox potential, exposed active sites, strong photosensitivity, and appropriate electronic band gaps and locations.²⁰ MSs, M_2S , M_3S_4 , and MS_2 , are stoichiometric compositions of compounds formed by sulfur anion and cationic metal or semimetal, abbreviated as MX Sy.²¹ Ammonium sulfide, thiols (such as decanethiol or DDT), and organo-sulfur compounds (such as thiourea and thioacetamide) are sources of the comparatively cheap and readily handled element sulfur.

MSs have attracted much attention as potential catalysts or photocatalysts for various applications in the last few decades. A few instances involve sensors, power sources, splitting of water by photo electrochemistry (PEC), electrocatalytic hydrogen generation, environmental cleanup, and many more.²² Metal sulfides (MSs) have garnered growing interest

in diverse fields including medical, electrochemistry, absorption, capacitors that store energy and rechargeable.^{23,24} 3D transition metal dichalcogenides, such as FeS_2 , are electronic materials with structures that span both the localization and itinerant regimes of 3D electron properties. There is great promise for using FeS_2 nanosphere material in inexpensive solar systems.

Various methods, both vertical and horizontal, are currently employed to produce high-quality mono-, bi-, and multi-MS nanomaterials with precise sizes and structures. Top-down synthesis techniques include ball-milling, sputtering, lithography, and etching processes. Bottom-up approaches encompass chemical vapor deposition, laser pyrolysis, atomic condensation, and spray pyrolysis. Given the significant influence of nanoscale structures (NSs) on functional properties, there is a growing focus on research aimed at controlling morphologies, such as nanoparticles (NPs), nanorods (NRs), nanotubes, nanoplates, nanofibers (NF), nanosheets, nanowires, and nanoflakes, within the realm of nanotechnology.

This study explores recent advancements in synthesis techniques for producing MSs. These methods facilitate large-scale production of MSs with high efficiency and moderate cost. MSs can exhibit structures ranging from zero to three dimensions. Each MS is summarized, emphasizing its key features and potential applications across various fields including sensing, photocatalysis, antimicrobial properties, manufacturing, medical science, and energy storage and conversion, encompassing technologies like solar panels, solid-state batteries, and supercapacitors.

This review article provides a comprehensive analysis of recent progress in synthesizing various metal sulfides, including manganese sulfide (MnS), iron sulfide (FeS), cobalt sulfide (CoS), nickel sulfide (NiS), copper sulfide (CuS), zinc sulfide (ZnS), silver sulfide (AgS), cadmium sulfide (CdS), tungsten sulfide (WS), tin sulfide (SnS), lead sulfide (PbS), and molybdenum disulfide (MoS_2). It highlights the significance of metal sulfide nanoparticles in addressing contemporary challenges such as environmental contamination and sustainable energy storage needs, driven by population growth, industrialization, and urbanization.

The review emphasizes the diverse applications of metal sulfide nanoparticles in fields like health, biology, environmental remediation, and energy generation and storage. It underscores their optical properties, high specific capacitance, photocatalytic abilities, and light-absorbing capacities, which make them promising candidates for various technological advancements.

Furthermore, the review discusses recent advancements in utilizing metal sulfide nanoparticles as electrode materials

for solar cells, supercapacitors, and ion batteries, including those based on lithium, sodium, potassium, and magnesium. It also explores their capabilities in gas and chemical sensing, electrocatalysis for oxygen and hydrogen evolution, and remediation of polluted areas when employed as catalysts or photocatalysts.

A unique aspect of this review is its focus on identifying cost-effective methods for mass-producing high-quality metal sulfides, heterogeneous structures, and composites. It discusses effective physiochemical and biological approaches employed in the production process to control the structures, dimensions, and compositions of these sulfides, aiming to unlock their full potential for various applications.

Overall, this review provides valuable insights into the current state of research on metal sulfide nanoparticles and their diverse applications, offering a comprehensive overview of their synthesis methods, properties, and potential implications across different fields.

2 Metal-sulfide classification

MSs can be classified based on the number of metal elements they contain, leading to alternate names such as ternary (e.g., ZnIn_2S_4 , CuInS_2) and binary (e.g., Ag_2S , CuS), or polymer (e.g., $\text{Cu}_2\text{ZnSnS}_4$). These materials may feature sulfide 3D electrons, which can either be confined or migratory, or even both. The stability of the cation of the nearest neighbor is upheld by sulfide 3s and 3p orbitals, in conjunction with various forms of anion arrays such as trigonal, octahedral, and tetrahedral. These arrangements facilitate the formation of covalent bonds between metals (M–M) and sulfur (S–S). The interaction between layered sheet formations is reinforced by enhanced polarization and covalency, mediated through van der Waals interactions. MSs are typically composed of atomic

configurations, ionic sizes, and charges, which form various close-packing combinations.

Several sulfur-containing nanoscale structures, such as metal sulfides, lithium sulfide materials, sulfur-containing organosilicon compounds, sulfur-containing quantum dots, have been documented.^{25–28} Figure 1 demonstrates the growing global research interest in many nanomaterials, elements such as manganese, iron, copper, zinc, molybdenum, silver, lead, zinc, and WS.

3 Applications in synthesis, biomedicine, the environment, and energy

3.1 Manganese sulfide (MnS)

The electrochemical and magneto-optical characteristics of manganese sulfide (MnS) are unique, and it has been successfully synthesized in a variety of morphologies, including NPs, spherical, NR, nanotube, nanosheet, microfiber, and nanoflakes.^{29–32} There are three different polymorphic forms of manganese sulfate: α -MnS, the one with the rock salt framework, the one with the zinc blende framework, and the one with the spherite and the quartz arrangement, γ -MnS. Among these compounds, α -MnS is the most stable across a wide range of ambient temperatures and pressures, instead β -MnS and γ -MnS need specific conditions in the lab to be manufactured.^{33–38} Molten salts can be made in several different ways. Still, the most common ones are chemical pathways, as well as the thermolysis process, chemical-based bath accumulation, sol-gel synthesis, hydrothermal processes, solvothermal processes, and wet chemical methods.^{39,40} A combination of the α -MnS phase's polymorphism, thermodynamic stability, and plentiful and inexpensive manganese makes it an

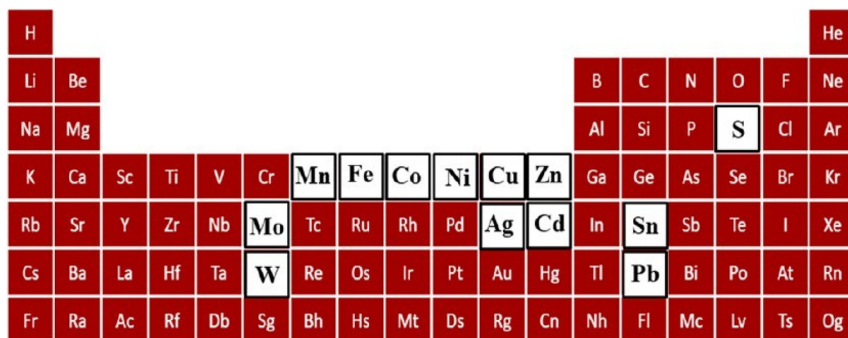
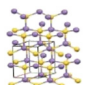
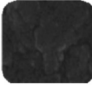

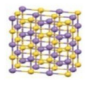
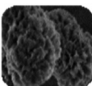

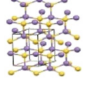

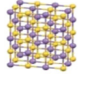
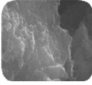
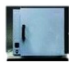
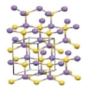


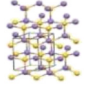
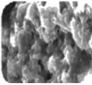

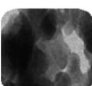
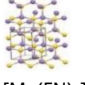


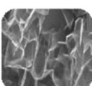

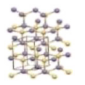
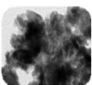


Figure 1: MS synthesis chemical.

attractive candidate for energy storage applications.^{41–43} However, due to its poor cycling efficiency, it is not suitable to be employed as an electrode material in supercapacitors and low inherent electrical conductivity.^{44,45} Investigators have mostly focused on studying the electrochemical characteristics of the α -MnS transition in lithium-ion batteries and supercapacitors, rather than γ -MnS and associated combined stages.^{46–49} This choice is because γ -MnS has better electrical conductivity than other materials.^{50–53} This is because its layered Wurtzite structure makes it easier for electrolytes to penetrate and ions to intercalate and deintercalate.

Table 1 and Figure 2 highlight the extensive efforts of various research groups in controlling synthesis methods to achieve desired morphologies, crystalline phases, and applications of MnS nanosheets (NSs). Table 1 illustrates the diverse uses of MnS in recent studies. Investigations have focused on applications such as supercapacitors, which exhibit an energy storage capability of 91 Wh kg^{-1} at 7.78 kW kg^{-1} , lithium-ion batteries with an energy capacity of 495 mAh g^{-1} at 2000 mA g^{-1} , drug removal with an efficiency of 80 %, and the degradation of malachite green oxalate dye, achieving a breakdown rate of 56 %.

Table 1: A recent research investigation delved into the synthesis of manganese sulfide (MnS), exploring its formation, crystal structure, particle dimensions, and potential applications.^{54–67}

Materials	Precursors	Synthesis techniques	Crystal structure	Morphology	Applications
MnS films	$(\text{CH}_3\text{COO})_2$, $(\text{CH}_3\text{CSNH}_2)$, $(\text{C}_6\text{H}_5\text{Na}_3\text{O}_7)$, $(\text{NH}_3/\text{NH}_4\text{Cl})$	Chemical deposition	Hexagonal 		
MnS ₂	$\text{C}_4\text{H}_6\text{MnO}_4$, CH_3CSNH_2	Solvothermal 			Electrochemical detection of cortisol in bio-fluids e.g., human serum, urine, and milk
MnS NSs	$\text{C}_4\text{H}_6\text{MnO}_4$	Thermolysis 	Hexagonal 		
MnS NPs		Plasma evaporation			Li-ion storage with capacities 705, 684, 643, 578, and 495 mAh g^{-1} at current densities 100, 200, 500, 1000, 2000 mA g^{-1}
MnS NPs	$\text{MnCl}_2 \cdot 4\text{H}_2\text{O}$, $\text{Na}_2\text{S} (\text{CH}_2\text{OH})_2$	Solvothermal 	Hexagonal 		
Nanosheets	Tu, $\text{MnCl}_2 \cdot 4\text{H}_2\text{O}$	Hydrothermal 	Hexagonal 		Photocatalytic degradation of (MV, MG, MB and RhB) dyes. In batteries electrochemical discharge at voltage 0.2–3.2 V
MnS NPs	$\text{MnCl}_2 \cdot 4\text{H}_2\text{O}$, $\text{Na}_2\text{S} \cdot n\text{H}_2\text{O}$	Solvothermal 			Photovoltaic thin film solar cells
Microspheres 2018s	Wurtzite 				Magnetic resonance imaging with a coercivity of 3320 Oe and magnetization 17 emu g^{-1}
Nanoflakes	$[\text{Mn}(\text{EN})_3]^{2+}\text{CS}_2$	Hydrothermal 			
	$\text{MnCl}_2 \cdot 4\text{H}_2\text{O}$, $\text{Na}_2\text{S} \cdot 9\text{H}_2\text{O}$	Hydrothermal 			Supercapacitor demonstrated.

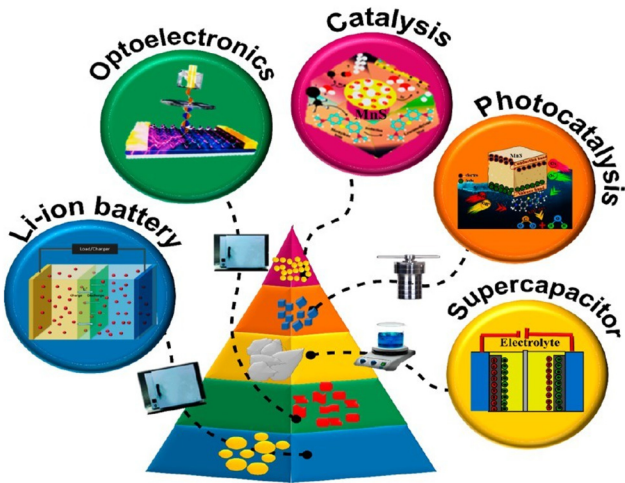


Figure 2: Diagram showing MnS production methods, morphologies, and applications. Permission to reproduce references.^{68–70} 2018, 2019, and 2020 copyrights.

3.2 Iron sulfide

Various phases of FeS exist with Fe:S ratios ranging from 0.5 to 1.05, encompassing minerals such as marcasite, troilite, mackinawite, pyrrhotite, smythite, and greigite. The Fe:S proportions for these phases are as follows: pyrite, marcasite, troilite, smythite, greigite, hexagonal-Fe₃S₄, smythite, and greigite-Fe₃S₄. The electrical and magnetic properties of iron sulfide minerals are influenced by both their crystal morphology and the stoichiometric balance of iron to sulfur.⁷¹ Concerning magnetic characteristics, naturally occurring

FeS crystals include electromagnetically active pyrite and marcasite, ferromagnetic greigite and pyrrhotite, paramagnetic mackinawite, and antiferromagnetic troilite.⁷²

Due to its diverse array of beneficial electrical, magnetic, and optical characteristics, iron chalcogenide (FeS) has attracted considerable attention from researchers across multiple fields. Exciting advancements have been made in various applications, including medicine, environmental remediation, energy storage (such as in solar cells and lithium-ion batteries), and catalysis. Particularly noteworthy is its role in addressing soil and groundwater pollution caused by both organic compounds like trichloroethene and tetrachloroethene, as well as inorganic contaminants like uranium, chromium, selenite (Se-IV), and mercury.⁷³

Under reduced and anoxic conditions, FeS maintains its thermodynamic stability. It is typically synthesized through coprecipitation in oxygen-depleted water.⁷⁴ Pyrite FeS₂, prevalent across vast regions of the Earth’s surface, is valued as a low-cost mercury adsorbent due to its abundance and high surface reactivity. However, natural FeS₂, characterized by its dense structure, exhibits limited mercury absorption capacity, achieving rates of less than 42 % at temperatures ranging from 40 to 100 °C. FeS₂ synthesized via solvothermal methods demonstrates optimal performance only within the temperature range of 60–100 °C.⁷⁵ Subjecting pyrite FeS₂ nanospheres to a brief heat treatment at 500 °C can transform them into hexagonal FeS nanosheets.⁷⁶

Researchers are currently focusing on using FeS nanosheets by physiochemical synthesis methods, which lead to various shapes and crystal morphology, as described in Table 2

Table 2: Recent FeS fabrication research involves structure, crystal structure, particle dimensions, and uses.^{71,72,74–84}

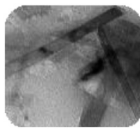
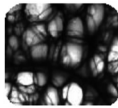
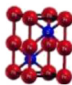
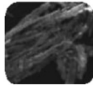
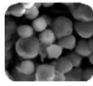

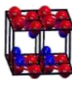
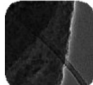

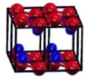

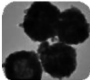
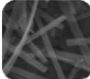

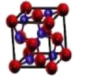


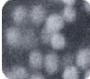
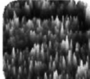
Materials	Precursors	Synthetic techniques	Crystal structures	Morphology	Applications
FeS ₂ NRs 2022		Molten salt			Removal of Hg efficiency (96.2 %)
FeS NPs	FeSO ₄ ·7H ₂ O and Na ₂ S FeSO ₄ ·7H ₂ O and Na ₂ S				
FeS ₂ NRs					
FeS ₂ NPs 2021	FeCl ₃ ·6H ₂ O SC(NH ₂) ₂	Polyol/coprecipitation			
FeS NPs	FeCl ₃ ·6H ₂ O Na ₂ S·xH ₂ O				

Table 2: (continued)

Materials	Precursors	Synthetic techniques	Crystal structures	Morphology	Applications
FeS NPs	$(\text{NO}_3)_3 \cdot 9\text{H}_2\text{O}$ $\text{C}_4\text{H}_4\text{Na}_2\text{O}_6 \cdot 2\text{H}_2\text{O}$	 Chemical reduction	Tetragonal 		
FeS ₂ NPs 2020	$\text{FeCl}_3 \cdot 6\text{H}_2\text{O}$, $\text{C}_3\text{H}_3\text{NaO}_2$, $\text{Na}_3\text{C}_6\text{H}_5\text{O}_7$				Biosensing application for detection of H_2O_2 and glutathione
FeS ₂ Nanowire	$(\text{NO}_3)_3 \cdot 9\text{H}_2\text{O}$ $\text{CH}_4\text{N}_2\text{S}$				Remediation
FeS ₂ nanosheets (NS) 2020	FeCl_3 and sulfur				Pseudocapacitive sodium storage with capacity 391 mAh g^{-1} at current density 10 Ag^{-1}
FeS ₂ Nanosphere 2018	$\text{FeSO}_4 \cdot 7\text{H}_2\text{O}$ $\text{CH}_4\text{N}_2\text{S}$	Solvothermal 	Hexagonal		Solar absorber
FeS ₂ thin film	$\text{FeSO}_4 \cdot 7\text{H}_2\text{O}$		Electrochemical deposition		Photovoltaic application with superior catalytic and photocurrent properties

and Figure 3. FeS₂ nanoparticles have been fabricated for diverse purposes using several synthesis processes, fluid-phase removal, solvothermal processes, and molten salt extraction, as shown in recent works. It is incredible how well these

applications work. For example, they remove mercury 96.2 % of the time, store 391 mA s of electricity in a gram at a current density of 10 A per g, and store 900 mA s of electricity in a gram at a current density of 0.1 A per g, as shown in Table 2.



Figure 3: Illustrates graphical representations of FeS synthesis routes and their resulting morphologies tailored for various applications. Permission has been obtained to reproduce content from references,^{76,79,85–87} copyrighted in 2020, 2020, 2020, 2018, and 2018, respectively.

3.3 Cobalt sulfide

CoS belongs to a group of II–IV semiconductor materials, which can exist in various stoichiometric compositions and phases, including CoS₂, CoS, Co₂S₃, Co₉S₈, Co₃S₄, Co₄S₃, and Co_{1-x}S. Synthesis methods have yielded diverse morphologies of CoS, such as nanotubes, nanowires, and hollow spheres. Factors like temperature, reaction duration, and reactant concentrations significantly influence the shape and size distribution of these particles in the samples.^{88–102} Structural materials prone to corrosion may exhibit two crystalline forms, cubic and hexagonal. Introducing sulfide, produced by bacteria through sulfate reduction or from inorganic sources, is a promising approach to manage heavy metals like cobalt (Co) in low-oxygen environments. Metal sulfides (MSs) formed by the rapid reaction of sulfide with metal cations are insoluble precipitates, enhancing the sequestration of aqueous metal cations, especially in nanoparticle (NP) synthesis, due to the significantly lower solubility of MSs in anaerobic to subtoxic conditions.^{103,104} The sulfidic waters of early Earth may have naturally facilitated this process, potentially impacting life development by limiting cobalt supply.^{105,106} Cobalt sulfides (CoS) attract considerable interest for their unique chemical, electrical, physical, and optical properties, finding applications in electrochemical supercapacitors, solar energy devices, ultra-high-density magnetic recording, hydrodesulfurization and dehydrodearomatization catalysts, and lithium-ion batteries. Among various stoichiometries, Co₉S₈ is a frequently studied transition metal chalcogenide with potential in battery and supercapacitor technologies. However, its mechanical stability

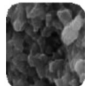
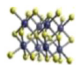

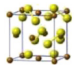
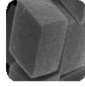
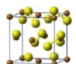
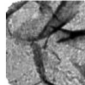

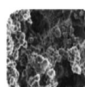
and poor electrical conductivity currently limit its use as an energy storage device.^{93,107}

Table 3 and Figure 4 provide comprehensive insights into the various structures, stages of crystallization, and applications of CoS nanomaterials, showcasing diverse manufacturing techniques. In a recent study, CoS nanosheets (NSs) were extensively utilized in supercapacitors, demonstrating remarkable performance with a specific capacitance of 1072 Fg⁻¹ at a scan rate of 100 mV/s. These nanosheets also exhibit promising applications in Na-ion storage, achieving a capacity of 705 mAh g⁻¹ at a current density of 0.2 Ag⁻¹. Additionally, Table 3 highlights the successful synthesis of CoS, Co₉S₈, and CoS_{1.97} nanosheets through combustion methods, which proved highly effective in degrading methylene blue (MB) dye with an efficiency of 89.5 %.

3.4 Nickel sulfide

Nickel sulfide (NiS) may be found in many forms, including α-NiS and β-NiS, NiS₂, Ni₃S₄, Ni₃S₂, Ni₇S₆, and Ni₉S₈. The development of various phases of NiS is greatly influenced by factors such as reaction temperature, duration, quantity of reagents, and pH level.¹¹⁹ One of the primary phases is rhombohedral β-NiS at low temperatures, while the other is hexagonal α-NiS at high temperatures. According to reference¹²⁰, the α-NiS undergoes a phase change at a temperature of 282 °C. There are several applications for the various NiS phases; for example, Ni₃S₂ conductors have the potential

Table 3: Recent research explored CoS production, structure, crystalline structure, dimensions of particles, and uses.^{108–116}

Materials	Precursors	Synthetic techniques	Crystal structures	Morphology	Applications
Cobalt	Co(NO ₃) ₂ ·6H ₂ O CH ₄ N ₂ S and glycine	Combustion method			MB dye degradation
CoS nanocrystal 2019	Cobalt chloride sulfanilamide	Hydrothermal			Supercapacitors with capacity 1072 Fg ⁻¹ and retention of 1000 cycles at 100 mV/S
CoS hollow structure 2019	ZIF-67 nano cubes, ethanol, deionized water, Na ₂ S	Reflux reaction			Li/S batteries
Co ₃ S ₄ nanosheets 2018	Lamellar CO ₃ S ₄ /TETA	Plasma inducing dry exfoliation.			Hydrogen evolution performance at over-potential 18 mV and 63 mV for 10 mA cm ² .
CoS ₂ NPs 2017	CO ₆ Al ₂ CO ₃ ·4H ₂ O	Hydrothermal			Electrochemical supercapacitors as specific capacitance 507 Fg ⁻¹ at scan rate 5 mVs ⁻¹

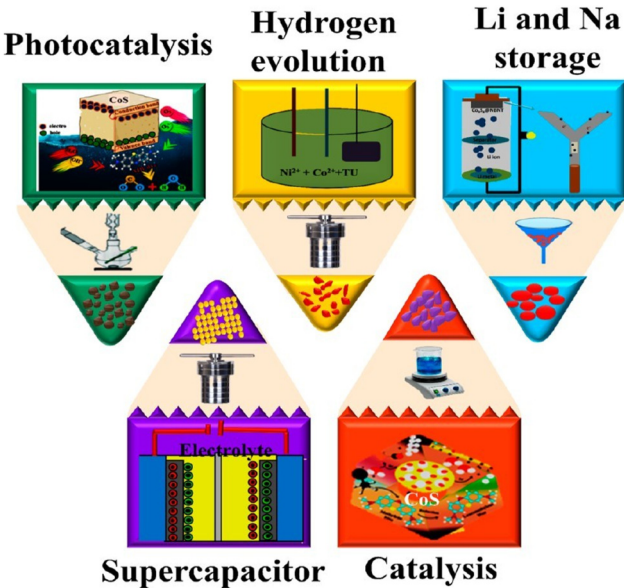


Figure 4: Illustrate the synthesis pathways of CoS, the structures of matter and their uses. Reproduced with authorization from.^{68,117,118} 2020–2019–2017 copyrights.

to enhance the performance of sodium-ion rechargeable batteries, sensors, storage devices, and thermoelectric appliances, while fluorescence devices and hydrogen evolution reactions can make use of NiS₂.¹²¹ There are two main phases of NiS₂: the triclinic stages are used in the processes of producing hydrogen through photocatalytic processes and supercapacitors, while the cubic phase is more effective in

HER. Additionally, in a basic solution, NiS₂ may effectively function as a catalyst for HER in water splitting.¹²² More precisely, structures with a pentlandite-type composition (Ni₉S₈) have shown superior performance in the hydrogen evolution process, because of their inherently high conductivity.¹²³





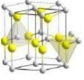
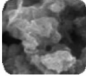
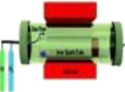
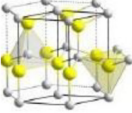
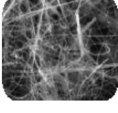
Several fabrication techniques, including microwave, solvothermal, hot injection, and hydrothermal methods, have been investigated to achieve precise synthesis of different phases of NiS.¹¹⁹ These methods result in NiS with unique properties attributed to characteristics such as high durability, low resistivity (approximately $1.2 \times 10^{-4} \Omega \text{ cm}$), excellent dye adsorption capabilities, affordability, abundant availability, electrostatic forces, hydrogen bonding, surface/pore diffusion, coordination effects, and hydrophobic interactions. Various industries, particularly those involved in electrocatalytic water splitting, manufacturing dye-sensitized solar cells, water treatment, and production of electrical energy storage devices like batteries and Li/Na/K ion batteries, have shown significant interest in NiS.^{84,124–127}

Table 4 and Figure 5 document the utilization of NiS nanoparticles across various applications, emphasizing the production methodologies enabling precise control over their phases and morphologies. Recent research, as depicted in Table 4, illustrates how NiS nanomaterials can enhance the electrochemical performance of Na/K ion batteries. At current densities of 0.2 Ag^{-1} and 100 Ag^{-1} they exhibit capacities of 610 and 154 mAh g⁻¹, respectively. Additionally,

Table 4: Recent studies have focused on the production of NiS isotopes, as well as exploring their structure, crystallization system, particle dimensions, and applications.^{119,121,123–125,127–135}

Materials	Precursors	Synthetic techniques	Crystal structures	Morphology	Applications
NiS NPs	(Ni (SO) ₄) ₂ H ₂ O		Hexagonal		Catalytic and photovoltaic activities
Mesopores Nis NPs	Acetate tetrahydrate and thioacetamide	Solvothermal 			Photothermal chemotherapy of cancer
NiS nanomaterial	Nickel acetate tetrahydrate, glutathione and thioacetamide				Removal of methylene blue and crystal violet with adsorption capacity
NiS microtubes	NiCl ₂ ·6H ₂ O thiourea and polyvinylpyrrolidone				Water disinfection and cold cathode emission
NiS NPs	Ni (NO ₃) ₂ ·6H ₂ O CH ₄ N ₂ S	Solvothermal 	Rhombohedral		

Table 4: (continued)

Materials	Precursors	Synthetic techniques	Crystal structures	Morphology	Applications
Mesopores thin film NiS ₂ 2020	Dimensional	Soft templating			Hydrogen evolution
NiS nanoflower	NiCl ₂ ·6H ₂ O Acetic acid and acetamide	Solvothermal 			Pseudocapacitive properties with capacitance 89.1 % at current density of 7.3 Ag ⁻¹
NiS NS					Oxygen evolution and supercapacitor with capacitances 1097 and 869 Fg ⁻¹ at current densities of 2 and 20 mA cm ²
NiS nanowire	Ni (NO ₃) ₂ ·6H ₂ O, sodium diethyldithiocarbamate hydrate and diethyldithiocarbamate	Vapor deposition 			Electrochemical water oxidation with current density 500 mA cm ⁻² of potential 340 mV

these materials have demonstrated efficacy in substance extraction, with a mass extraction efficiency of 1946.61 mg per g, and in the production of supercapacitors, achieving a capacitance of 1745.50 F per g.

3.5 Copper sulfide

The stoichiometric compositions of Cu_xS, a P-type semi-conducting material, may range from Cu₂S to CuS₂.^{137,138} Other possible stoichiometric compositions are Cu_{1.94}S,

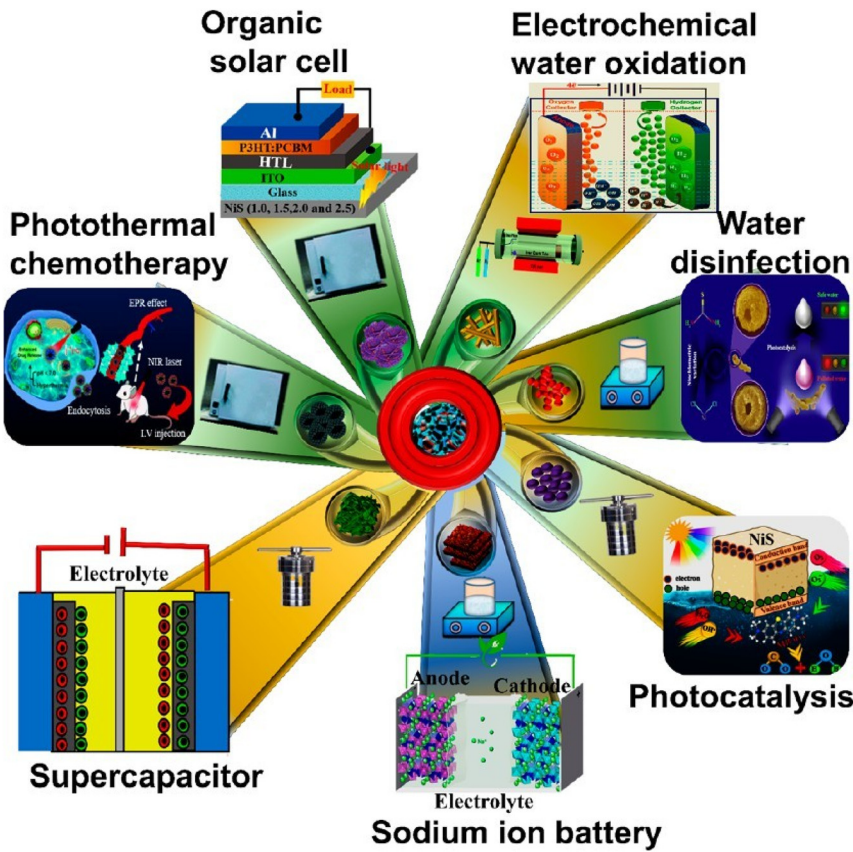


Figure 5: Diagram showing NiS manufacturing pathways, structures, and uses. Used with permission from.^{68,85,130,133,135,136}

$\text{Cu}_{1.8}\text{S}$, $\text{Cu}_{1.75}\text{S}$, CuS , and CuS_2 . Depending on the copper concentration, the E_g of Cu_xS might vary between 1.2 and 2.2 eV.¹³⁹ Because of its large band gap of 2.2 eV, CuS can soak up as much solar radiation as possible, regardless of its stoichiometric composition.^{140,141} Because of its larger band gap and ability to absorb visible light, CuS is a fortunate material.^{138,139,142} According to references,^{143–147} CuS may take on a variety of forms, such as nanoparticles (NPs), nanorods (NRs), nano structures resembling flowers and spheres, nanowires, plates, belts, and nanoribbons.¹⁴⁸ Methods for synthesizing CuS are currently extensively documented, including chemical vapor deposition, template-assisted growth, hydrothermal treatment, sol–gel synthesis, solvothermal processes, microwave use, and polyol methods.^{149,150} Among the many uses for CuS as a photocatalyst are in photovoltaics, optical filters, photoelectric devices, chemical sensors, thermoelectric cooling materials, photoelectric devices, photoelectric devices, liquid batteries,^{151–153} and photoelectric devices.¹⁵⁴ A possible stumbling block for solar light-prompted photocatalysis, CuS is nontoxic, has excellent photosensitivity, great physical and chemical stability, and is inexpensive.^{155,156} As a disinfectant for medical therapies, CuS is the main since it is harmless to human cells and has great antibacterial properties.¹⁵⁷ The large specific capacity (560 mAh g^{-1}) of CuS makes it an excellent cathode material for rechargeable Mg batteries, which leads to remarkable electrical properties.^{158,159} Typically, the reversible capacity of CuS is lower than its real value at ordinary temperature because Mg^{2+} is trapped in the host material.¹⁶⁰ As a result of a scalable technique based on two factors, CuS is also used in sodium ion batteries. The present collector regards Cu as an intimate substance first and foremost, which is a key component of batteries. Additionally, sulfur reacts strongly with several transition metals, copper specifically. At 80°C , CuS was consistently produced on a Cu current collector.¹⁶¹ Electrodes made of CuS are utilized in lithium-ion batteries due to the material's outstanding ability to conduct electricity.^{162,163} Thorough discussion was captivated by the CuS plasmonic property.¹⁶⁴ The vacancies are often caused by inadequate filling of sulfur's $3p$ orbitals, which happens when copper is scarce and belongs to the non-stoichiometric class. Because of the free holes created by the vacancies, pure, self-doped CuS may conduct electricity. There are more carriers of electricity as the compound's copper content drops, reaching higher concentrations of carriers at around $1020\text{--}1021 \text{ cm}^{-3}$. The particular structure determines whether the covellite CuS has an abnormally high number of holes, up to 1022 cm^{-3} . Covellite CuS has inherent high-extremity hole delocalization and a distinct anisotropic metallic conductivity.¹⁶⁵ Of all the semiconductor


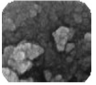

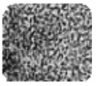

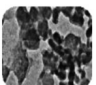
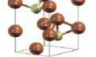


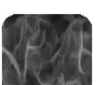











photothermal brokers, CuS has been the most extensively researched.^{166,167} Nanomagnets derived from copper show a strong photothermal sequel for the targeted removal of tumors when exposed to near-infrared laser light.^{168–170} The majority of these CuS -based NSs often include polymers (polyvinylpyrrolidone, or PVP), oleyl amine, sodium citrate, or PEGDMA-based gel¹⁷¹ attached to their surfaces as ligands. Although these CuS nano agents coated with organic molecules or polymers disperse readily in water, their presence in biological fluids does not endure. As a result, improving the biocompatibility and stability of CuS -based NSs using an eco-friendly, straightforward manufacturing method with superior ligands is crucial.¹⁷²

Several research organizations have dedicated substantial resources to obtaining specific shapes, crystal structures, and uses for CuS NSs produced using various synthesis methods, as seen in Table 5 and Figure 6. Table 5 displays literature that shows whether CuS NSs are used in $\text{Mg}/\text{Na}/\text{Li}$ -ion batteries, with 100 Ag^{-1} , 350 mAh g^{-1} , and 300 mAh g^{-1} functions, correspondingly. The decomposition of various colorants, such as the green color of malachite, the orange color of methyl, safranin O, and rhodamine B, has been accomplished using CuS nanomaterials. The corresponding clearance rates were 95.5 %, 99–100 %, 80.53 %, and 83.22–99 %. In addition, a remarkable 47 % productivity was achieved in the radiation treatment of tumors using CuS quantum dots (QDs) that were green synthesized.

3.6 Zinc sulfide

ZnS is a compound made up of transition metals and semiconductors from the II–VI group. Its band gap approximates 3.7 eV, a short Bohr radius, and a significant excitation binding energy of 40 meV.^{192–195} Multiple forms of ZnS , such as nanoparticles (NPs), nanowires, nanorods (NRs), nanoclusters, nanosheets, nanoflowers, hollow spheres, and nanotubes, have been created.^{196–202} The shape of NPs is influenced by many parameters, including the choice of a zinc and sulfur precursor, reaction duration, and temperature, due to its notable characteristics such as non-toxicity and temperature regulation. There are two different crystalline forms of ZnS : wurtzite and zinc blende, the latter of which has an energy bandgap of 3.77 eV. Zinc blende's rectangular shape appears more persistent than wurtzite's hexagonal structure, since the latter is created at temperatures above 1000°C . Various efforts have already been made^{203–212} to track the shape and dimensions of the crystals in ZnS nanostructures. Various methodologies were used to create these

Table 5: Current research on CuS synthesis, structure, crystalline system, particle dimensions, and its uses.^{140,154,161,165,172–187}

Materials	Precursors	Synthetic techniques	Crystal structures	Morphology	Applications
CuS NPs 2021	$C_{18}H_{35}NH_2$ /1-octadecene $C_{18}H_{36}$, copper nitrate		Hexagonal 		
CuS QDs 2019	Copper chloride dehydrates, sodium sulfide hydrates, chitosan, folic acid		Hexagonal 		Photothermal therapy of tumor efficiency 47 %
CuS Ns 2021	Cupric		Hexagonal 		
CuS NRs 2019	Cobalt chloride and thiourea		Hexagonal 		In optoelectronic devices with energy band gap in visible region
CuS nanosheets 2020	Thioacetamide		Hexagonal 		
CuS Nps 2019			Hexagonal 		
CuS Nps 2019	Sulfur powder, current collector		Hexagonal 	Sodium-ion batteries with ultra-high rate capability 100 Ag^{-1}	
CuS hollow micro flower 2018	Ionic liquids 1-butyl-3-methylimidazolium chloride, copper chloride dehydrates and thioacetamide.		Hexagonal 	Asymmetric supercapacitor exhibited energy density 15.97 Wh kg^{-1} power density 185.4 W kg^{-1}	
CuS NPL 2019	$\text{Cu}(\text{NO}_3)_2 \cdot 3\text{H}_2\text{O}$, thiourea and $\text{NiCl}_2 \cdot 6\text{H}_2\text{O}$		Hexagonal 		
CuS nano-spheres 2019			Hexagonal 		
CuS NPs 2017	Copper acetate and sodium sulfide		Hexagonal 		

structures, such as hydrothermal, template route, ultrasonic, template-free, solid–liquid reaction, solvothermal, coprecipitation, and electrospray pyrolysis.^{213–220} Compared to bulk, ZnS NPs have several desirable characteristics, such as (a) Intense light absorption, (b) an increased ratio of surface area to volume, (c) optical tunnelling's little impact, and (d) a lower melting point due to outstanding properties like nontoxicity and thermal stability. Among the many fields where ZnS finds

use are photocatalytic wastewater treatment, sensors for gases, photoelectric components, SSCs, photovoltaic window coverings, FET, light-emitting diodes, solar cells, and electroluminescent devices.^{199,221–226}

Table 6 and Figure 7 describe certain synthesis approaches for monitoring the shape and dimension of the crystals in ZnS NSs, along with their relevant applications. According to recent investigations (Table 6), ZnS NPs

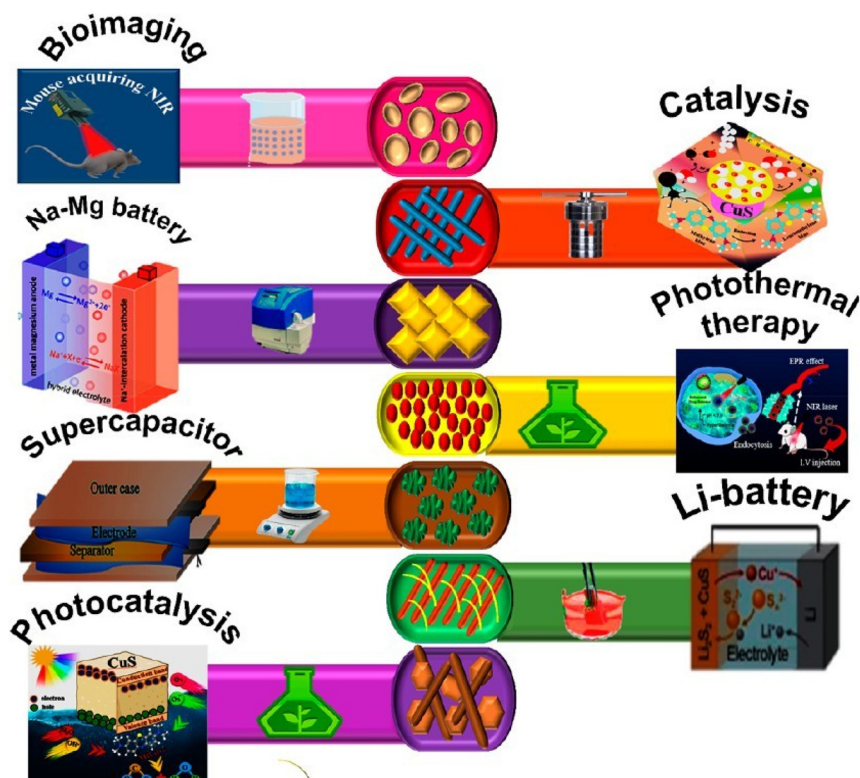


Figure 6: Diagram showing CuS synthesis methods, structures, and uses. Permission to reproduce provided. ^{133,188–191} 2020, 2018, 2008, 2019, and 2022 reproduction rights.


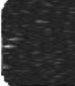
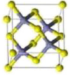

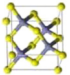
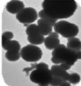
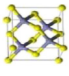


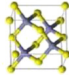
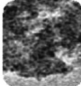
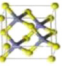
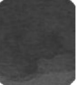
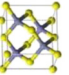
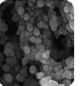
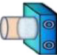
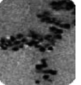

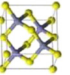
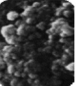
produced using the Sono chemical approach had an efficiency of 86.36 % for blue 14 degradation, whereas those synthesized using the hydrothermal method had an efficiency of 100 %. More than that, ZnS NPs have degraded MB, the elimination rates of mety orange at 75 %, blue 21 at 100 %, and cyano blue at 75 %.

3.7 Molybdenum disulfide

Many ground-breaking innovations have been made possible by the exceptional electrical and physical characteristics of 2D materials.²⁴⁵ 2D materials' exceptional properties might revolutionize several industries, examples of which are batteries for storing energy and electronic technology.^{246–248} Stretching these 2-D substances across their entire region gives compounds precisely thick layers, that in turn renders them sensitive to forces of gravity, gives molecules a lot of room to interact with one another, and affects quantum confinement. The impact was caused by unexpected features that set these materials apart from their 3D equivalents.^{249–251} More and more applications for MoS₂ have emerged in fields such as electrochemistry, solid lubricants, capacitors, catalysis, hydrogen storage, and electrochemical devices. The primary rationale for such applications is the sheet-like framework, which takes use of the enormous surface area of

intermediate double-layer storage, the high intrinsic and rapid ion conductivity, and the weak van der Waals interactions in the sandwich layers, which enable nanoparticles to split from the outermost layer of the layers. With a 0.62 nm interlayer spacing and mainly covalent MoS₂ bonds, the material is highly conductive. When molybdenum is in an oxidation state between +2 and +6, it shows a faradic capacitance, which means it can store more energy. When stacked with MoS₂ sections, the loss of capability, specific capacitance, and conductivity for electricity was less severe than with carbon materials. To overcome these limitations, researchers have created several nanocomposites that combine MoS₂ with conductive polymer to get better electrochemical characteristics.^{252,253} The electrode materials' capacitance and cycle life were enhanced because of the complementary actions of the MoS₂ nanosheet's contact with the CFC at the interface. Because the produced materials have a fast charge transfer rate and a low polarization resistance value, the electrode capacitance is quite high. Energy storage systems may use MoS₂ nanospheres as electrode materials.^{1–3} Rechargeable Li-ion batteries may employ MoS₂ as an electrode material because of its layered structure and its substantial theoretical capacity of 670 mAh g⁻¹ that comes through the 4 electrons transfer process upon discharging. This exceeds the most common graphite material by 1.8 times, with 372 mAh g⁻¹. According to the estimated redox potential, MoS₂ has an

Table 6: Latest research on ZnS production, structure, crystallization framework, dimension of particles, and uses.

Materials	Precursor	Synthesis techniques	Crystal structure	Morphology	Applications	MnS morphology	Precursor	Synthesis technique	Crystal structure	Morphology	Applications
Chemical bath											
ZnS NPs	Zinc acetate				Photocatalysis with 63–75 % efficiency	ZnS NPs		Chemical reaction	Wurtzite		Potential applications in nonlinear optics
ZnS NPs	Zinc acetate, Na ₂ S	Microwave assisted				ZnS NPs		Chemical reaction			Efficiency photocatalysis against methyl orange shows 75 %
ZnS NPs	Zn (CH ₃ COO) ₂ 2H ₂ O SC (NH ₂) ₂					ZnS NPs	Zn (CH ₃ COO) ₂ 2H ₂ O	Wet chemical 			Optical devices
ZnS NPs	Zn (CH ₃ COO) ₂ 2H ₂ O ethanol				Optoelectronics due to its large band gap	ZnS NPs	Zn(NO ₃) ₂ ·6H ₂ O C ₂ H ₅ NS				Photo catalytic activity against reactive efficiency 100 %
ZnS NPs		Sol-gel precipitation 			Anti-bacterial	ZnS NPs	Zinc acetate dihydrate and sodium sulfide	Sonochemical 			Photocatalytic degradation against direct blue 14 shows 86.36 %

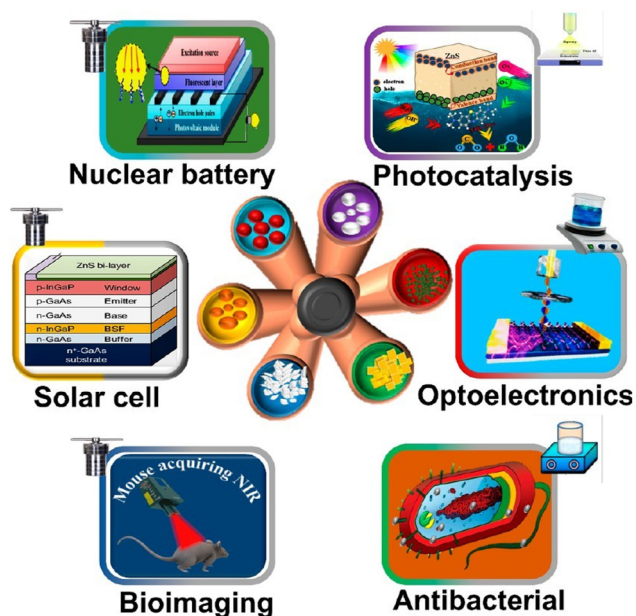


Figure 7: Diagram showing ZnS production methods, structures, and uses. Permission from.^{70,191,243,244} 2019–2022, 2020, and 2013.


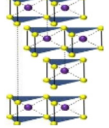

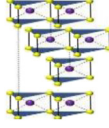


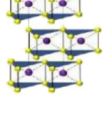
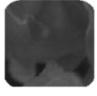


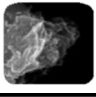
electrical conductivity of $10^{-4} \Omega^{-1} \text{cm}^{-1}$ versus Li^+/Li . When using nanosized MoS_2 to avoid problems, it is important to note that the reaction volume increases by 107 % for the MoS_2 electrode and by 21.7 % for the cell reaction.²⁵⁴

Both Table 7 and Figure 8 detail the most up to date MoS_2 morphologies and phases that have been synthesized utilizing various techniques, along with their respective applications. Table 2 shows the current state of the art in preparing MoS_2 nanosheets. Different synthesis routes, techniques that include exfoliation, liquid phase exfoliation, and microwaves have found usage in a range of contexts. Among them, one may find a 98 % reduction in dye rate in supercapacitors operating at 0.5 Ag^{-1} per unit of current, and a different one in Li-ion batteries with a capacity of 439 mAh g^{-1} .

3.8 Silver sulfide

Many other chemical processes, such as microwave, water-phase, hydrothermal treatment, thermal breakdown, conjugation, and opposite microemulsion manufacturing, have

Table 7: Current research on MoS_2 production, structure, crystallization system, dimensions of particles, and their uses.^{253–263}

Materials	Precursors	Synthesis techniques	Crystal structure	Morphology	Applications
	Sodium oxalic acid	Microwave-assisted. 	Rhombohedral 		Super-capacitors with high specific capacitance of 348 F/g at 0.5 A/g
MoS_2 -SDS	Molybdate disulfide powder, sodium dodecyl sulfate		Rhombohedral 		Photo-catalytic dye degradation (efficiency 91.84 %) and dye-sensitized solar cell
MoS_2 nanosheets	Molybdenum disulfide, boron nitride, hydrazine hydrate and sodium	Liquid phase-exfoliation 	Hexagonal 		Dye degradation (efficiency 98 %) and anti-bacterial behavior.
1T- MoS_2 2H- MoS_2 NF-2021		Solvothermal Combustion			Anti-bacterial activity
MoS_2 2020	Polystyrene microspheres, sodium molybdate, thiourea, polyvinyl pyrrolidone				NO_2 gas sensors
MoS_2 nanosheets	NaBr, KBr Bulk MoS_2				Super-capacitors with capacitance 76 Fg^{-1} at 5 mVs^{-1} with an aerial capacitance of 58.5 mF/cm^{-2}

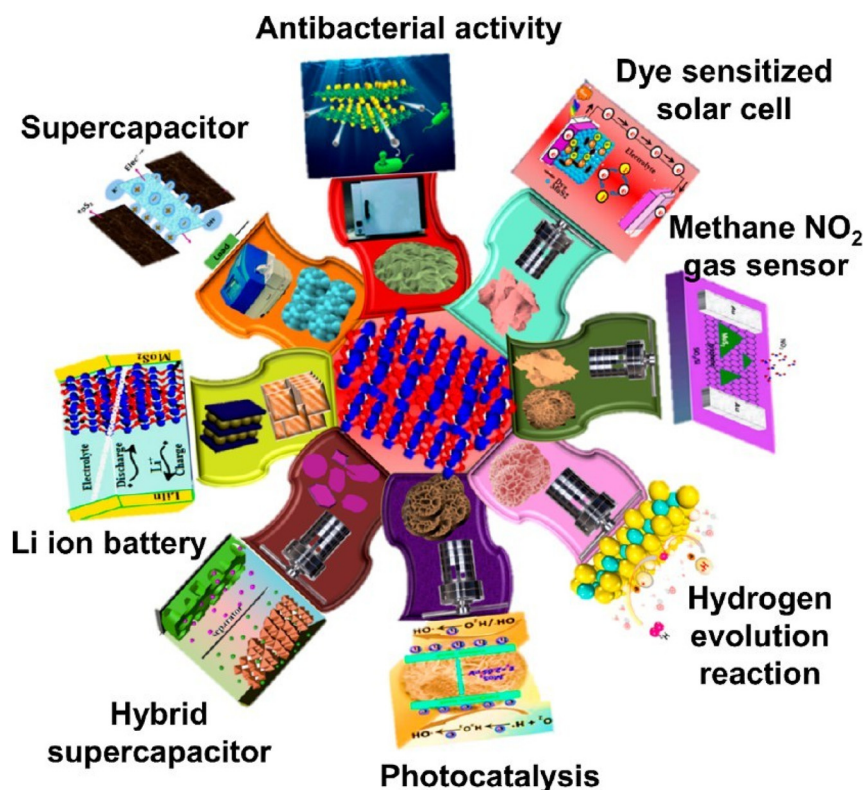


Figure 8: Diagram showing MoS₂ synthesis pathways, structures, and uses. Permission to reproduce.^{254,256,264–269} The copyrights are valid for the years 2019, 2021, 2020, 2016, 2018, and 2020.

been used to produce Ag₂S nanomaterials.^{270,271} In the presence of organic ligands, Ag₂S quantum dots (QDs) typically undergo physical and chemical transformations into their hydrophobic inorganic phase; the stage of transformation has practical uses in the biomedical field throughout the NIR and IR wavelength ranges.^{272,273} Additionally, colloidal Ag₂S NPs were created using synthesis of green method with the use of water-based extracts from various plant parts (for instance, rhizomes, vegetables, seeds, and stems) and macronutrient-containing albumins or royal jelly as stabilizing agents.²⁷⁴ The chemical element Ag₂S may undergo three different polymorphic changes: acanthine, a body-centered cubic (bcc) superionic phase of β -Ag₂S called argentite, and sulfide, a face-centered cubic (fcc) phase of γ -Ag₂S. These modifications occur at temperatures below 450 K, between 452 and 859 K, and approximately at 860 K, respectively. The Ag₂S compound exhibits a monoclinic crystal structure with a particle size less than 60 nm, as reported in reference.²⁷⁵ Bioimaging, cancer photothermal therapy, food packaging, solar cells, and photocatalysis are just a few of the many areas that benefit from this material's unique combination of near-infrared (NIR) emission, antimicrobial qualities, high quantum yield, efficient photothermal conversion, chemical stability, outstanding photostability, narrow bandgap energy (0.9–1.1 eV), high optical absorption coefficient, and lack of toxicity.^{270,271}

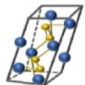
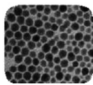
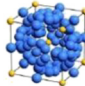
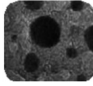

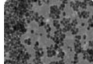
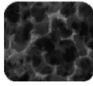
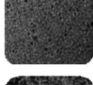
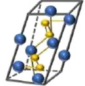

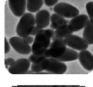

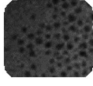
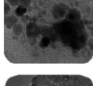
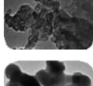
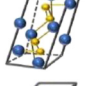


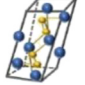

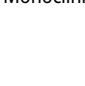

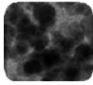
Recently, researchers have explored many important uses of distinct Ag₂S nanomaterials with varying structures, which

were synthesized using diverse methods. These findings are detailed in Table 8 and Figure 9. The study demonstrates that Ag₂S nanospheres (NSs) have been synthesized using different methods such as coprecipitation, precipitation, and green synthesis. These NSs have shown potential in various applications, containing properties that inhibit the growth of bacteria and fungi, with MIC values between 5 and 75 $\mu\text{g mL}^{-1}$ for bacteria and 80–310 $\mu\text{g mL}^{-1}$ for fungi. Additionally, they have exhibited a high efficiency of 58.6 % in cancer photothermal therapy. Furthermore, they have demonstrated bioimaging capabilities and efficiency in inhibiting the growth of both Gram-negative *Escherichia coli* and Gram-positive *Bacillus thuringiensis* (70 % and 90 %, respectively). Also, methyl green dye was removed, and a photodetector was used using Ag₂S nanoparticles made using a mix of sonochemical and microwave processes. When subjected to light with a wavelength of 550 nm and an intensity of 0.89 mW cm⁻², the photodetector had a response of 2723.2–4146.0 A W⁻¹. The nanoparticles also achieved a degradation efficiency of 99 % in the removal of methyl green dye.

3.9 Cadmium sulfide

Material having three dimensions less than a nanometer and a diameter of a few nanometers, like that of a molecule, is called a nanoparticle.²⁸⁶ The optical characteristics, size, and

Table 8: Recent research on Ag₂S synthesis, structure, crystallization framework, dimensions of particles, and uses.^{191,270–273,275–285}

Materials	Precursors	Synthesis techniques	Crystal structure	Morphology	Applications
Ag ₂ S QDs 2022	Silver nitrate, sodium	Thermal			
Ag ₂ S QDs 2022	AgNO ₃ , Na ₂ S·9H ₂ O		Monoclinic 		Antibacterial and antifungal activities
Ag ₂ S QDs 2022					
Ag ₂ S NPs 2022	Ag/AgCl Na ₂ SO ₄				Electrochemical monitoring nitrite in food potential with sensitivity of 0.05 uA umol L ⁻¹ cm ⁻²
Ag ₂ S QDs 2021					Bio-imaging of Hela cells with promising compatibility
Ag ₂ S QDs 2021	Diphenyl tetra zoilum bromide, glutathione	Aqueous precipitation	Mono clinic 		Photo-thermal therapy with photo thermal conversion efficiency 58.6 %
Ag ₂ S NPs 2021	AgNO ₃ and polyvinylpyrrolidone				
Ag ₂ S QDs 2018	Trioctyl phosphine		Monoclinic		Photovoltaic performance with power conversion efficiency 0.1 % at current density 0.62 mA/cm ²
Ag ₂ S NPs 2020	AgNO ₃ , Na ₂ S Pleurotus Ostreatus mycelium				Bioimaging/Antibacterial activity against –ve <i>E. coli</i> (90 %) and + ve <i>thuringiensis</i> (70 %)
Ag ₂ S NPs 2020	AgNO ₃ and bay leaf extract				Inflammatory activity against drug acetyl salicylic acid
Ag ₂ S NPs 2020	AgNO ₃ ·6H ₂ O Na ₂ S·6H ₂ O		Monoclinic 		
Ag ₂ S NPs 2020	AgNO ₃ Na ₂ S	Microwave 			Degradation of methyl green dye UV and visible light with efficiency (99 %) and (62–85 %)
Ag ₂ S QDs 2019	AgNO ₃ Na ₂ S		Monoclinic 		
Ag ₂ S NPs 2019	AgNO ₃ , Na ₂ S·9H ₂ O and rose-mary plant leaves				Antibacterial activity

structure of NSs sulfide and selenides, namely CdS, CdSe, ZnS, and ZnSe, have been the subject of a great deal of research.²⁸⁷ Typically, since they are easy to make in the

right size range, there is more focus on II–VI semiconductor NPs. The wide range of fields that have found uses for CdS – from photovoltaics and photodetectors to photocatalysts and

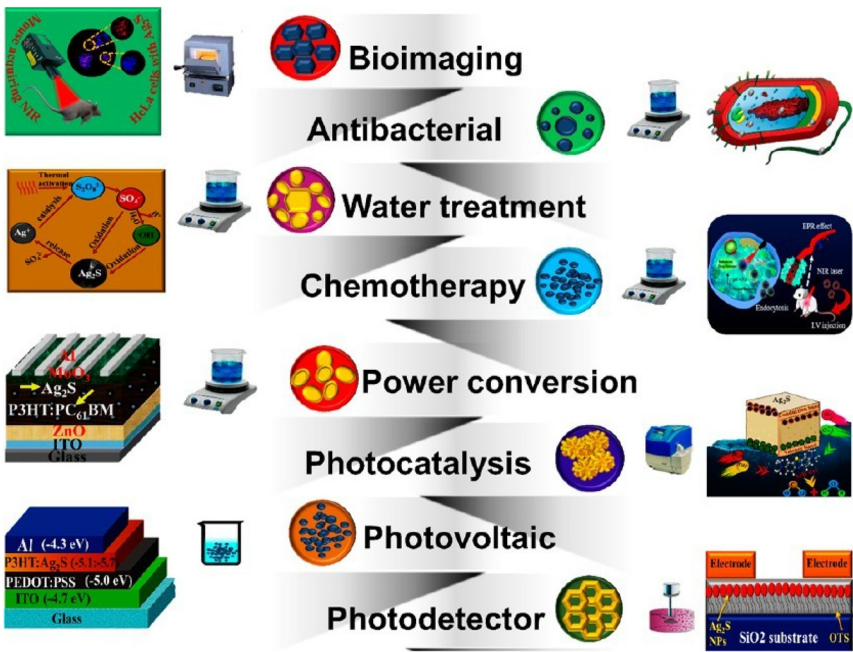


Figure 9: Diagrams showing Ag_2S production pathways, structures, and uses. By permission of. ^{191,271,277,279,280,284,285} Copyrights: 2022, 2021, 2020, 2020, 2018, and 2018.


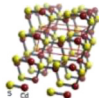
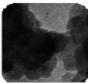

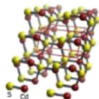
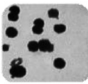

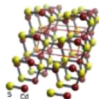
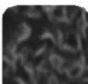
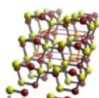
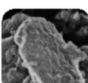

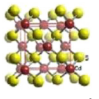
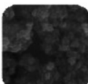
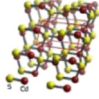
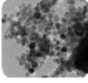


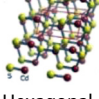


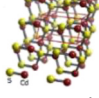
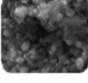
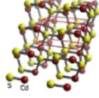
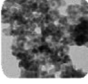
nonlinear optical materials – as well as its antibacterial potential – transformed it into a very interesting straight bandgap semiconductor.^{288–294} The crystal structure of CdS might be cubic, hexagonal, cubic, or deformed rock. With a value of 2.4 eV, CdS bulk semiconductors have a bandgap.²⁹⁵ In solar cells, it acts as a layer that lets light in.²⁹⁶ Its n-type semi conductivity makes it a perfect match for hetero-junction solar cells that use p-type materials.^{297,298} The photo-catalytic degradation of dyes may be facilitated by CdS NPs because of their wide surface area, strong oxygen

adsorption capabilities, rapidly recombining electron–hole pairs, and enhanced surface absorption of target molecules. Enhancement of CdS NPs photocatalytic activity via decreased hole–electron rearrangement and extremely effective light absorption is possible, depending on their crystal structure and band gap.²⁸⁷ Along with a more negative conduction band and apparent absorbance, CdS also has a lower reduction potential than H^+/H_2 .^{299,300} Table 9 and Figure 10 indicate that different phases and morphologies of CdS NSs, which were synthesized using different routes,

Table 9: Recent CdS NS synthesis, structure, crystalline system, dimension of particle, and uses. Studies.^{287,295,298,300–310}

Materials	Precursors	Synthesis techniques	Crystal structure	Morphology	Applications
	Cadmium nitrate, nitric acid and acetamide	Co-precipitation			In photodetectors
	Cadmium acetate dehydrates, sodium sulfide and 2 mercaptothion.	Chemical bath			Solar cell efficiency (1.15 %)
CdS NRs and cubes	Cadmium acetate, methanol, nickel chloride				Photocatalytic degradation efficiency 94 % for MO dye in 75 min
Spherical 2020		Solution	Hexagonal 		Super-capacitors exhibited energy density of 8.4 Wh kg^{-1} power density of 7.56 kW kg^{-1} at current density of 20 Ag^{-1}

Table 9: (continued)

Materials	Precursors	Synthesis techniques	Crystal structure	Morphology	Applications
CdS 2020		Chemical solution 	Hexagonal 		Solar cells and hydrogen production via photo-electrical water splitting
		Pulsed laser ablation 	Hexagonal 		Anti-microbial activity
Needle shaped	Cadmium chloride monohydrate, thiourea, ammonium and triethanolamine		Hexagonal 		
Spherical 2019	Cadmium chloride, thioglycolic acid		Hexagonal 		Dye degradation
Spherical 2019	Cadmium chloride, Na ₂ S, 2-mercaptoethano				Dye degradation
	Cadmium acetate and thiourea		Hexagonal 		
	Cadmium acetate, sodium sulfide nanohydrate				In solar cell power conversion efficiency at 0.5 M upon Mn incorporation efficiency was 0.42
			Hexagonal 		RhB dye degradation rate 78 %
Spherical 2018	Cadmium sulphide		Hexagonal 		In photovoltaic cells
Spherical 2017	Cadmium sulphide		Hexagonal 		

were widely used in various applications. New studies have shown that CdS nanoparticles excel in a variety of uses, using the use of photocatalytic dye degradation, solar cells, and supercapacitors among others. Crystals of CdS NSs with hexagonal structures have been produced using sol gel. The

hydrothermal method was shown to be appropriate for degrading methyl orange by 94 % and RhB dye by 78 %. They demonstrated an efficiency of 1.15 % in solar cells and a supercapacitor with an energy density of 8.4 Wh kg⁻¹ and a current density of 20 Ag⁻¹.

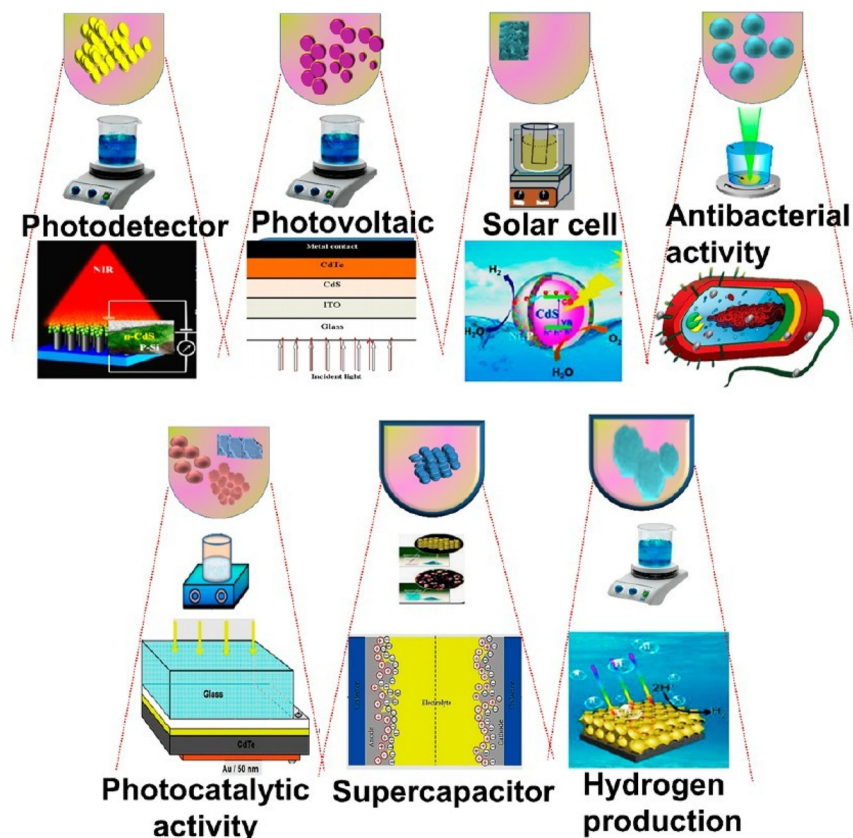


Figure 10: Diagram showing CdS production pathways, structures, and uses. Permission for a reproduction.^{311–316} Copyrights for 2021, 2013, 2018, 2016, 2020, and 2014.

3.10 Tungsten sulfide

Impressive electrical conductivity, exceptional catalytic activity, and great thermochemical stability are some of WS₂'s fascinating properties.^{317–319} Research on various WS₂ morphologies has been thorough.^{320–322} Chemical vapor deposition, sonication, and hydrothermal processes may all produce WS₂ in single or multiple layers. Catalytic activity toward H₂ generation is very high in both single and multi-layer WS₂.^{323–326} Research has been conducted on WS₂ NPs, nanoflakes, and nanoflowers.^{327–331} Several techniques for synthesis have been reported for NSs with desirable features, including biological compatibility, large surface area, effective photocatalyst, excellent electrochemical activity, benign technological properties, and high mobility.^{332–343} These methods include hydrothermal, sonochemical, solvothermal, ultrasonic spray pyrolysis, colloidal, chemical vapor deposition, and electrochemical approaches.

Figure 11 and Table 10 demonstrate the many synthesis pathways that have been devised in recent years to create CdS NSs with the necessary phases and morphologies for a range of applications. Photocatalytic activity was well-suited to WS₂ nanosheets produced by a hydrothermal synthesis technique, which degraded the MB dye with 90 % efficiency. Also, supercapacitors made of hydrothermally prepared

WS₂ NPs with hexagonal and tetragonal structures may be used capacitance is 102.909 mAh g⁻¹ at 226.67 mF cm⁻², and the current density is 1 Ag⁻¹. The synthesis of WS₂ QDs and NRs, on one hand, and electrochemical detection of psychotropic compounds on the other, are two areas where these materials excel, was accomplished using ultrasonic, electrochemical, and sonochemical technique methods.

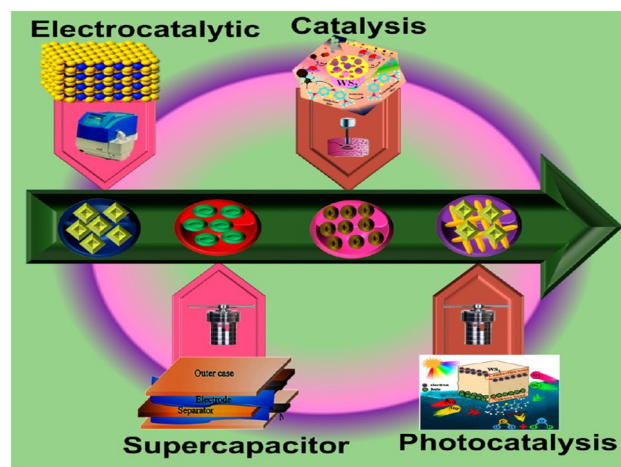
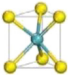

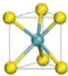
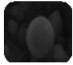
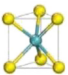
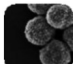
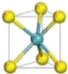


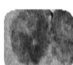
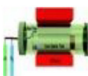
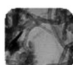
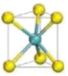
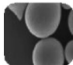

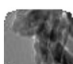
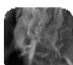
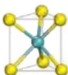



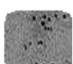



Figure 11: Diagram showing WS₂ manufacturing pathways, structures, and uses. Used with authorization by.^{344,345} 2016 and 2019 copyrights.

Table 10: Recent developments on WS₂ production, structure, crystallization system, dimensions of particles, and uses.^{332–338,346–352}

Materials	Precursors	Synthesis techniques	Crystal structure	Particles	Morphology	Applications
WS ₂ MSs		Hydrothermal		300 nm length		Photocatalytic degradation efficiency 90 % against MB dye
		Solvothermal		500–600 nm		Supercapacitor with capacity 102.909 mAh g ⁻¹ at current density 1 Ag
		Ultrasound assisted (liquid phase exfoliation)				Electrocatalytic activity exhibited low potential 172 mV at 10 mA cm ⁻²
		Horizontal reaction		20–150 nm diameter		Photocatalytic activity
				100 nm		
				200 nm		
WS ₂ hollow sphere 2020	Tungsten chloride, thioacetamide	Hydrothermal		300 nm ² um		Electrochemical activity
WS ₂ NRs 2019			Hexagonal	80–100 nm		Electrochemical detection of psychoactive drug
		Ultrasonic spray pyrolysis	Hexagonal	200–300 nm		
WS NSs 2018						Supercapacitor with specific capacitance 107.93 Fg ⁻¹
WS ₂ QDS 2017				5 nm		Catalytic activity
WS ₂ powder, ethanol U 2017				118 nm		
Bulk WS ₂ , propylene carbonate LiClO ₄ 2017			Hexagonal	3 nm		Photo electrochemical

3.11 Tin sulfide

Due to their strong light-harvesting capabilities and low band gap energy, there was extensive usage of Sn-based metal chalcogenides in optoelectronic devices.³⁵³ Tin sulfide (SnS) has strong anisotropic optoelectronic and mechanical properties, in addition to two band gaps, either direct or

indirect. According to publications,^{354–356} the band gap energy of SnS may be found between 1.07 and 1.25 eV when measured indirectly, and between 1.30 and 1.39 eV when measured directly. In the UV, visible, and near-infrared parts of the spectrum, its absorption constants are quite high, exceeding 104 cm⁻¹.^{357,358} In addition, the materials used to make it are plentiful, inexpensive, and safe.^{359,360} The

synthesis of WS_2 from amphoteric SnS is a very significant development since WS_2 may, depending on the circumstances of production, conduct p-type or n-type currents.^{361,362} Chalcogenide material SnS has garnered significant interest due to its possible uses in several industrial applications, the range of applications include photodetectors (such as photodiodes and photovoltaic cells), optoelectronic devices, solar cells, gas sensors, wastewater treatment, and biological applications.^{363–367} Although there have been claims of the presence of cubic-structured SnS , in most cases, the material exhibits a van der Waals force structure that is orthogonal to the c-axis, which holds the orthorhombic layers together.^{368,369} Because of its layered structure, which facilitates ion intercalation, SnS has good electrochemical characteristics (e.g., Na^+ and Li^+), and it is also an efficient layer for photovoltaic absorption.³⁵⁶ Therefore, SnS shows promise as an electrode material for electrochemical energy storage methods. Several researchers have used SnS as anode components for Li-ion batteries and as electrode components for supercapacitors.³⁷⁰ Thermal evaporation, chemical misting and immersion, radiofrequency (RF) sputtering and spin coating are some of the physical and chemical methods that may be used to create SnS thin films.^{368,371–375} Loferski calculated the bandgap efficiency to be 24 %, which was the theoretical limit for the SnS absorber's power conversion efficiencies (PCE). Thus, SnS has become the best alternative material for solar cells of the future. So far, 4.36 % PCE has been recorded for SnS solar cells.³⁷⁶ The chalcogenide NSs semiconductor SnS has a small electronic bandgap (E_g) of 1.3–1.6 eV, a high absorption coefficient, hole mobility, and is both inexpensive and non-toxic, making it one

of the most appealing choices for organic pollutant degradation.^{377,378} Because of its narrow E_g , which covers the whole visible spectrum, light shorter than one thousand nanometers (nm) may be absorbed by SnS . But, particularly for industrial applications, there is a pressing need to enhance SnS 's photocatalytic efficacy, which is currently limited because of photogenerated electron and hole recombination. An intriguing avenue to enhancing photocatalytic efficiency is the fabrication of SnS semiconductor-based nanocomposite with precious metals. This might lead to a boost in the reduction process and charge separation at the interface.³⁷⁹ Gas sensors based on 2D sulfide might potentially respond quickly because of the fast charge transfer that happens when gas molecules meet substrates.^{380,381}

Due to the S atom's decreased electronegativity and increased ability to absorb atmospheric oxygen, gas sensors based on sulfide nanosheets can function at far lower temperatures than their oxides semiconductor-based counterparts.³⁸¹ The SnS -based sensor does not show much selectivity when exposed to gaseous VOCs at room temperature.³⁸² The gas-sensing capabilities of 2D semiconductors have been improved using many realistic methods, including doping, nanocomposites, and modification with precious metals.^{383–385} To improve gas sensitivity, a simple and successful method is to dope with impurity atoms.^{384–386} Additionally, it has been shown that 2D nano sheets may be kept from aggregating or stacking when a hierarchical framework is built.³⁸⁷ High gas sensing responses are often achieved by loose hierarchical structures with huge active surface areas for gas adsorption/diffusion.³⁸² Table 11 and Figure 12 display several synthesis

Table 11: Present research on SnS synthesis, structure, crystallization system, dimensions of particles, and uses.^{353,362,365,370,376,379,381,382,388–392}

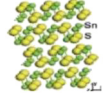

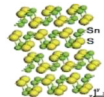

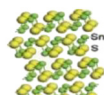
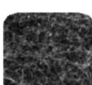

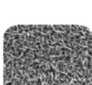

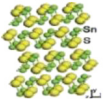


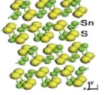
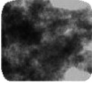
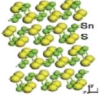


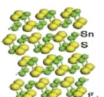
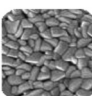
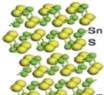


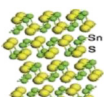


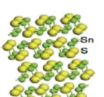


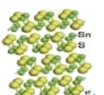

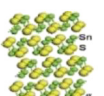
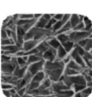
Materials	Precursors	Synthesis techniques	Crystal structure	Morphology	Applications
Nanosheets with spherical particle 2022	Tin chloride salt, thiourea	Conventional	Orthorhombic 		Anti-bacterial activity
Cubic NPs	Oleic acid, oleylamine, tri-octylphosphine, $SnCl_2$,		Orthorhombic 		Photo detector
	SnS powder, sulfur powder, argon and hydrogen		Orthorhombic 		Photodetectors with high sensitivity, fast response speed and wide spectrum detection
Nano films	Sn and S	Thermal	Orthorhombic 		Photo detectors with specific detectivity of 6.89×10^{30}

Table 11: (continued)

Materials	Precursors	Synthesis techniques	Crystal structure	Morphology	Applications
Nanoflakes	$\text{SnCl}_2 \cdot 2\text{H}_2\text{O}$ Ethylene glycol, thiourea,	Solvothermal 	Orthorhombic 		Gas sensing
Nanosheets	$\text{SnCl}_2 \cdot 2\text{H}_2\text{O}$ Thioacetamide, PVP	Microwave-assisted Thermal 	Orthorhombic 		Photo-detector with excellent opto-electronic stability reproducible photo-switching for 200 cycles
SnSe/SnS	$\text{SnCl}_2 \cdot 2\text{H}_2\text{O}$ Na_2S , NaOH, SnSe		Orthorhombic 		Anti-microbial activity
SnS thin film	SLG-substrate and Mo-coated soda-lime glass substrate	RF magnetron sputtering 	Orthorhombic 		In solar cell at pressure 2 Pa with highest power conversion efficiency 0.58 %
Ag-SnS spherical 2020	$\text{SnCl}_2 \cdot 2\text{H}_2\text{O}$ HAD, TOP, sulfur, Ag		Orthorhombic 		Photocatalytic efficiency enhanced with increasing the amount of Ag and 100 %
Nanosheets	$\text{SnCl}_2 \cdot 2\text{H}_2\text{O}$ Ethylene glycol	Solvothermal 	Orthorhombic 		Highly sensitive methanol
Thin film	Sodalime glass and Mo-coated SLG	Sputtering 	Orthorhombic 		In solar cells with power conversion efficiency of 0.38 % along J_{sc} of 3.56 mA/cm^2 and FF of 50 %
Nanosheets	$\text{SnCl}_4 \cdot 5\text{H}_2\text{O}$ and S powders	Chemical bath 	Orthorhombic 		Gas sensor exhibited an excellent response of 14.86–100 ppm ethanol vapor when operating at 160 °C
SnS honey comb like structures	Thiourea, stannous chloride, methanol, 2-methoxy ethanol	Solution-based	Orthorhombic 		Photovoltaic supercapacitors represented high specific capacitance of 42 Fg^{-1} At current density of 2 Ag^{-1}

methods that have been used lately, together with CdS NS architectures, structures, and applications. Using hydrothermal and solvothermal processes, SnS nanosheets and nanoflakes were produced, respectively, and shown antimicrobial properties in gas sensing and photodetector systems. With an efficiency of 0.38 and 0.58 % in converting electricity, respectively, SnS thin films used in solar cells have been synthesized using the sputtering technique.

3.12 Lead sulfide

Cubic lead sulfide (PbS) possesses distinctive optical properties due to its cubic structure.³⁹⁵ At room temperature, bulk PbS exhibits a narrow energy band gap of 0.41 eV in the near-infrared range, which can be increased to approximately 2 eV in the visible spectrum when formed into nanoclusters.³⁹⁶ Various morphologies of PbS, including

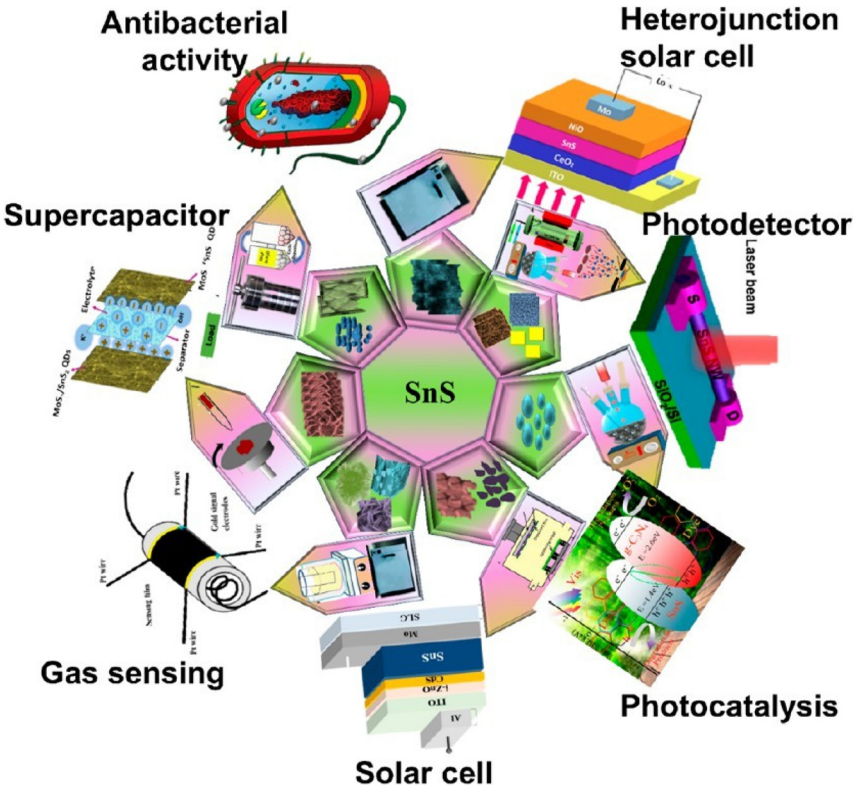


Figure 12: Diagrams showing SnS synthetic pathways, structures, and uses. Permission granted from.^{264,381,389,392–394} Copyrights: 2019, 2022, 2020, 2020, and 2021.

nanoparticles (NPs), microflowers, thin films, nanosheets (NSs), quantum dots (QDs), and nanorods (NRs), have been reported using different synthesis methods such as hydrothermal, microwave, spray pyrolysis, diffusion-controlled, green, aqueous-based, and plasma chemical methods.^{397–411}

PbS finds potential applications in optical switching devices, infrared detectors, Pb²⁺ ion-selective sensors, and solar absorption due to its versatile properties. Colloidal PbS is utilized in solar cells, photodetectors, LEDs, and optical switches.

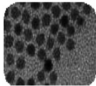





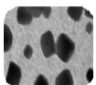





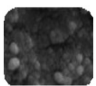
PbS nanoparticles exhibit intriguing optoelectrical characteristics such as tunable optical band gap, nonlinear optical behavior, enhanced electronic conductivity, and efficient multiple exciton generation (MEG) via single-photon absorption. The relatively small confinement radii of PbS nanoparticles, less than 20 nm,^{412–417} make them highly desirable as they offer greater control over optical and optoelectrical properties.⁴¹⁸

Table 12 and Figure 13 describe some recent research on the uses and structures of PbS nanomaterials synthesized

Table 12: Current investigation on lead sulfide synthesis, structure, crystalline system, particle dimension, and uses.^{397–402,404,405,419–422}

Materials	Precursors	Synthesis techniques	Crystal structure	Morphology	Applications
PbS NPs 2022	Lead acetate trihydrate, copper nitrate trihydrate and ammonium sulfide	Aqueous based	Cubic		Thermo electronics with charge carrier concentration $1.8 \times 10^{18} \text{ cm}^{-3}$
PbS Thin film 2021	Lead acetate, thiourea, lanthanum acetate and methanol	Spray pyrolysis	Cubic		Gas sensing with small concentration of 200 ppm target gas
ZnO–PbS Hetero junction 2020		Microwave	Cubic		Degradation of methyl orange dye (efficiency 96 %)

Table 12: (continued)

Materials	Precursors	Synthesis techniques	Crystal structure	Morphology	Applications
PbS (Quantum dots) QDs 2019	Sulfur, lead chloride, 3-mercaptopropionic acid, 1,2-ethanedithiol and tetrabutylammonium iodide	Diffusion-controlled	Cubic		Photocatalytic activity methyl orange dye shows 96 % efficiency
PbS NRS 2019	Lead acetate, trihydrate, carbon disulfide	Green synthesis 	Cubic		
PbS Nanosheets 2019	Pb(II) dithiocarbonate, ethylenediamine	Microwave-assisted 	Cubic		
PbS NPS 2019	Pb(NO ₃) ₂ ·Na ₂ S Cetyltrimethylammonium, silver nitrate	Microwave 	Cubic		Optoelectronic
		Co-precipitation 	Cubic		Optoelectronic devices
PbS NPS 2017	Lead nitrate, thiourea	Hydrothermal 	Cubic		In semiconductor devices attributed to higher enband gap
PbS Flower like 2017			Cubic		

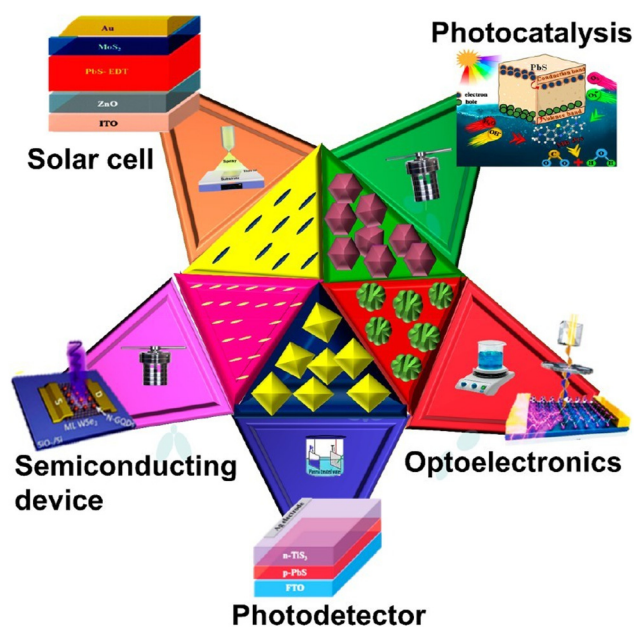


Figure 13: Diagram showing PbS production pathways, structures, and uses. Used with permission from. ^{70,409,423,424} Copies 2019, 2020, and 2022.

utilizing various methods. Cubic PbS NPs with structures appropriate for thermoelectric and optoelectronic applications were synthesized using microwave and water-based synthesis, respectively. A spray pyrolysis produced PbS thin film with a 40.32 nm diameter was used for gas sensing. An acceptable photocatalytic degradation of methyl orange was 96 % with QDs and hydrothermal, diffusion-controlled, and nanoflowers like PbS; acid brown was 95 %, acid violet was 75 %, and acid blue dye was 85 %.

4 Challenges and future prospects

MSs have great potential in fields such as biology, energy storage, environmental cleanup, sensing devices, and imaging and imaging. Further investigation, however, must overcome huge obstacles, such as the need to improve electrochemical performance and develop highly selective and sensitive MSs sensors. They are capable of cleaning industrial emissions of SiO₂ and other dangerous contaminants. Future research into Fenton-like reactions and the

advanced oxidation process (AOP) should make use of highly active MSs catalysts and native carriers. The structure of the catalyst also determines its electrocatalytic performance. Better kinetic performances are a direct result of a bigger catalyst surface area, raising the total number of sites that are actively used. Although MSs have enhanced the competence of electrochemical supercapacitors in energy storage, their wide range of energy and faradic reactions during charging and discharging reduce their operating voltage, energy density, and cycle durability. Hybrid battery super-capacitors allow us to circumvent the problem of low energy density. Consequently, MSs would exhibit superior performance at low temperatures, quick charging time, high energy density, maintained long life cycle, and fast ionic diffusivity. Supercapacitor hybrid systems powered by Li/Na/K and Mg ion batteries also display impressive power and energy values. Another possibility is that doping or composites with different nanomaterials might increase electrochemical activity. By comparison to 2D NSs, 3D NSs have more surface-active sites, allowing them to produce a higher capacitance. Despite their limited direct application in the OER, layered MSs (such as MoS_2 and WS_2) have outstanding inherent electrocatalytic HER activity owing to their highly electrically conductive and well-exposed active regions. Due to their abundance, affordability, chemical stability, and exceptional activity, nonlayered MSs (FeS_2 , Ni_3S_2 , NiS_2 , CoS_2 , and Co_3S_4) have been extensively studied as electrocatalysts for water splitting. Researchers have looked at ways to increase electrical conductivity, inherent activity, and active sites in electrocatalysts by strain, facet, edge, and defect engineering, heteroatom doping, and composite design.

The mass transfer capability of the catalyst may be enhanced by water splitting, a process that produces gas. One promising approach to addressing energy scarcity, climate change, and environmental pollution is photocatalyst water splitting for hydrogen generation; however, this technique is limited due to photo corrosion of MSs photocatalysts. Nevertheless, constructing an interconnected network of porous structures with a large specific surface area and rapid mass transfer remains a formidable challenge. To build better MSs as catalysts/photocatalysts, to make them more stable when water is being divided and to protect them from photo corrosion attack, anticorrosion coatings must be added to their structure. They are not stable under high working circumstances, hence stronger MSs are needed. Within this framework, there is still much to learn about the surface chemistry of MS and how it is affected by experimental conditions. Another challenge is determining how stable these materials are for certain uses over the long run.

5 Novelty and significance

This comprehensive review article presents a novel and significant contribution to the field of metal sulfide nanoparticles by offering a thorough analysis of recent advancements in their synthesis and applications. By encompassing a wide range of metal sulfides, including MnS , FeS , CoS , NiS , CuS , ZnS , AgS , CdS , WS , SnS , PbS , and MoS_2 , the article highlights their potential in addressing pressing challenges such as environmental contamination and sustainable energy storage demands. The article underscores the diverse applications of metal sulfide nanoparticles in various sectors, including health, biology, environmental remediation, and energy generation and storage, emphasizing their optical properties, specific capacitance, photocatalytic abilities, and light-absorbing capacities. Moreover, it discusses recent advancements in utilizing these nanoparticles as electrode materials for solar cells, supercapacitors, and ion batteries, as well as their roles in gas sensing, chemical sensing, electrocatalysis, and remediation of polluted areas. The article's unique focus on cost-effective synthesis methods and control over structures and compositions adds significant value, making it an essential resource for researchers and practitioners seeking to harness the full potential of metal sulfide nanoparticles across diverse applications.

6 Conclusions

There are several well-studied applications for MSs, which constitute a complex and diverse family of nanomaterials, and new concepts and examples of their use appear on a regular basis. MSs have great electrochemical activity, are environmentally friendly, and are inexpensive, making them ideal for application in energy conversion and storage systems. A synopsis of current knowledge on the efficient synthesis and regulated morphology, size, and crystal structure of MSs is given in this work. Using both top-down and bottom-up approaches, several monos- or bi-MSs have been produced. Hydrothermal, solvothermal, precipitation, and template methods are used to create MSs with nano- and microstructures. But combustion synthesis as a method for MS synthesis has seldom been investigated. Optimal control during production has allowed MSs nanocrystals to retain their chemical, physical, optical, and nano- and microstructural characteristics. The synthesis paths were dictated by factors such as the accessibility of raw materials, possible uses, and other monetary and ecological constraints. The existing literature was briefly linked to in terms of synthesis techniques, the dimension of particles, structure of crystals, and particular to the application geometries. Recent studies

have shown that MSs have many practical uses in various fields, in fields as diverse as biomedicine (including bio-imaging, photothermal tumor treatment, and antibacterial agents), solar cells (for energy production), batteries (for energy storage, including supercapacitors and Li/Mg/Na ion cells), and photocatalytic dye degradation. The destruction of a wide variety of dyes using photocatalysis, including methyl orange, crystal violet, malachite green, rhodamine B, and MB, and others, has been shown in earlier research using a variety of MSs, including MnS, CoS, NiS, CuS, ZnS, MoS₂, Ag₂S, CdS, WS₂, and PbS.

By using CoS, the maximum degradation of MB dye was 89.5 %, whereas WS₂ achieved 90 %; CdS achieved 94 %, 96 %, and 99 %; and MnS achieved 56 % and 95.5 % destruction of malachite green dye, separately. On top of that, CdS had an efficiency of around 1.15 % in solar cell applications, whereas SnS had efficiencies of 0.3 and 0.5 %, respectively. Additionally, the most efficient materials for supercapacitors were CoS, NiS, MoS₂, and WS₂, with capacitance values of 1072 Fg⁻¹, 1745.50 Fg⁻¹, 348 Fg⁻¹, and 107.93 Fg⁻¹, respectively. Future study into the possible energy and environmental advantages of MSs nanoparticles with different morphologies and their applications in many areas may be made possible by this review.

In conclusion, this review highlights the significant potential of metal sulfide nanoparticles in addressing contemporary challenges in environmental remediation and sustainable energy storage. By exploring diverse synthesis methods and applications across various fields, it underscores the versatility and promise of these materials. However, further research is needed to optimize production methods and fully exploit their capabilities in practical applications.

Research ethics: Not applicable.

Author contributions: The authors have accepted responsibility for the entire content of this manuscript and approved its submission.

Competing interests: The authors states no conflict of interest.

Research funding: Supported from the Princess Nourah bint Abdulrahman University (PNURSP2024R24) and Prince Sat-tam bin Abdulaziz University (PSAU/2023/R/1444) funds.

Data availability: The raw data can be obtained on request from the corresponding author.

References

1. Shahzad, U.; Saeed, M.; Marwani, H. M.; Al-Humaidi, J. Y.; ur Rehman, S.; Althomali, R. H.; Rahman, M. M. Transition Metal-Based Chalcogenides as Electrocatalysts for Overall Water Splitting in

- Hydrogen Energy Production. *Int. J. Hydrogen Energy* **2024**, *65*, 215–224.
2. Shi, E.; Gao, Y.; Finkenauer, B. P.; Coffey, A. H.; Dou, L. Two-Dimensional Halide Perovskite Nanomaterials and Heterostructures. *Chem. Soc. Rev.* **2018**, *47* (16), 6046–6072.
3. Alivisatos, A. P. Semiconductor Clusters, Nanocrystals, and Quantum Dots. *Science* **1996**, *271* (5251), 933–937.
4. Shahzad, U.; Saeed, M.; Marwani, H. M.; Al-Humaidi, J. Y.; Rehman, S. U.; Althomali, R. H.; Awual, M. R.; Rahman, M. M. Recent Progress on Potentiometric Sensor Applications Based on Nanoscale Metal Oxides: A Comprehensive Review. *Crit. Rev. Anal. Chem.* **2024**, 1–18; <https://doi.org/10.1080/10408347.2024.2337876>.
5. Wang, Z. L.; Song, J. Piezoelectric Nanogenerators Based on Zinc Oxide Nanowire Arrays. *Science* **2006**, *312* (5771), 242–246.
6. Fang, X.; Bando, Y.; Gautam, U. K.; Zhai, T.; Gradecak, S.; Golberg, D. Heterostructures and Superlattices in One-Dimensional Nanoscale Semiconductors. *J. Mater. Chem.* **2009**, *19* (32), 5683–5689.
7. Lai, C.-H.; Lu, M.-Y.; Chen, L.-J. Metal Sulfide Nanostructures: Synthesis, Properties and Applications in Energy Conversion and Storage. *J. Mater. Chem.* **2012**, *22* (1), 19–30.
8. Aziz, M. I.; Mughal, F.; Naeem, H. M.; Zeb, A.; Tahir, M. A.; Basit, M. A. Evolution of Photovoltaic and Photocatalytic Activity in Anatase-TiO₂ under Visible Light via Simplistic Deposition of CdS and PbS Quantum-Dots. *Mater. Chem. Phys.* **2019**, *229*, 508–513.
9. Mughal, F.; Muhyuddin, M.; Rashid, M.; Ahmed, T.; Akram, M. A.; Basit, M. A. Multiple Energy Applications of Quantum-Dot Sensitized TiO₂/PbS/CdS and TiO₂/CdS/PbS Hierarchical Nanocomposites Synthesized via P-SILAR Technique. *Chem. Phys. Lett.* **2019**, *717*, 69–76.
10. Naeem, H. M.; Muhyuddin, M.; Rasheed, R.; Noor, A.; Akram, M. A.; Aashiq, M. N.; Basit, M. A. Simplistic Wet-Chemical Coalescence of ZnO with Al₂O₃ and SnO₂ for Enhanced Photocatalytic and Electrochemical Performance. *J. Mater. Sci. Mater. Electron.* **2019**, *30* (15), 14508–14518.
11. Butt, S.; Farooq, M. U.; Mahmood, W.; Salam, S.; Sultan, M.; Basit, M. A.; Ma, J.; Lin, Y.; Nan, C. One-Step Rapid Synthesis of Cu₂Se with Enhanced Thermoelectric Properties. *J. Alloys Compd.* **2019**, *786*, 557–564.
12. Genovese, M. P.; Lightcap, I. V.; Kamat, P. V. Sun-Believable Solar Paint. A Transformative One-Step Approach for Designing Nanocrystalline Solar Cells. *ACS Nano* **2012**, *6* (1), 865–872.
13. Fajrina, N.; Tahir, M. A Critical Review in Strategies to Improve Photocatalytic Water Splitting towards Hydrogen Production. *Int. J. Hydrogen Energy* **2019**, *44* (2), 540–577.
14. Chandrasekaran, S.; Yao, L.; Deng, L.; Bowen, C.; Zhang, Y.; Chen, S.; Lin, Z.; Peng, F.; Zhang, P. Recent Advances in Metal Sulfides: From Controlled Fabrication to Electrocatalytic, Photocatalytic and Photoelectrochemical Water Splitting and Beyond. *Chem. Soc. Rev.* **2019**, *48* (15), 4178–4280.
15. Cox, P. A. *Transition Metal Oxides: An Introduction to Their Electronic Structure and Properties*; Oxford University Press: Oxford, 2010.
16. Burton, B. P.; Singh, A. K. Prediction of Entropy Stabilized Incommensurate Phases in the System MoS₂–MoTe₂. *J. Appl. Phys.* **2016**, *120* (15), 155101.
17. Shannon, R. D. Revised Effective Ionic Radii and Systematic Studies of Interatomic Distances in Halides and Chalcogenides. *Acta Crystallogr. Sect. A Cryst. Phys. Diffraction Theory Gen. Crystallogr.* **1976**, *32* (5), 751–767.
18. Miller, T. M.; Bederson, B. Atomic and Molecular Polarizabilities-A Review of Recent Advances. In *Advances in Atomic and Molecular Physics*; Bates, D. R.; Bederson, B., Eds. Academic Press: New York, 1978; pp. 1–55.
19. Lide, D. R. *CRC Handbook of Chemistry and Physics*; CRC Press: Boca Raton, FL, 2004.

20. Weber, T.; Prins, R.; van Santen, R. A. *Transition Metal Sulphides: Chemistry and Catalysis*; Springer Science & Business Media: Dordrecht, 1998.
21. Sarker, J. C.; Hogarth, G. Dithiocarbamate Complexes as Single Source Precursors to Nanoscale Binary, Ternary and Quaternary Metal Sulfides. *Chem. Rev.* **2021**, *121* (10), 6057–6123.
22. Rui, X.; Tan, H.; Yan, Q. Nanostructured Metal Sulfides for Energy Storage. *Nanoscale* **2014**, *6* (17), 9889–9924.
23. Huang, X.; Zeng, Z.; Zhang, H. Metal Dichalcogenide Nanosheets: Preparation, Properties and Applications. *Chem. Soc. Rev.* **2013**, *42* (5), 1934–1946.
24. Zhu, W.; Yue, X.; Zhang, W.; Yu, S.; Zhang, Y.; Wang, J.; Wang, J. Nickel Sulfide Microsphere Film on Ni Foam as an Efficient Bifunctional Electrocatalyst for Overall Water Splitting. *Chem. Commun.* **2016**, *52* (7), 1486–1489.
25. Argueta-Figueroa, L.; Martinez-Alvarez, O.; Santos-Cruz, J.; Garcia-Contreras, R.; Acosta-Torres, L.; De la Fuente-Hernandez, J.; Arenas-Arrocena, M. C. Nanomaterials Made of Non-toxic Metallic Sulfides: A Systematic Review of Their Potential Biomedical Applications. *Mater. Sci. Eng. C* **2017**, *76*, 1305–1315.
26. Xu, G.; Zeng, S.; Zhang, B.; Swihart, M. T.; Yong, K.-T.; Prasad, P. N. New Generation Cadmium-Free Quantum Dots for Biophotonics and Nanomedicine. *Chem. Rev.* **2016**, *116* (19), 12234–12327.
27. Vlasova, N.; Sorokin, M.; Oborina, E. Carbofunctional Sulfur-Containing Organosilicon Compounds: Synthesis and Application Fields. *Russ. J. Appl. Chem.* **2016**, *89* (7), 1031–1042.
28. Lee, S.-K.; Lee, Y. J.; Sun, Y.-K. Nanostructured Lithium Sulfide Materials for Lithium-Sulfur Batteries. *J. Power Sources* **2016**, *323*, 174–188.
29. Huffman, D. R.; Wild, R. L. Optical Properties of α - MnS. *Phys. Rev.* **1967**, *156* (3), 989–997.
30. Yang, X.; Wang, Y.; Wang, K.; Sui, Y.; Zhang, M.; Li, B.; Ma, Y.; Liu, B.; Zou, G.; Zou, B. Polymorphism and Formation Mechanism of Nanobipods in Manganese Sulfide Nanocrystals Induced by Temperature or Pressure. *J. Phys. Chem. C* **2012**, *116* (5), 3292–3297.
31. Lu, J.; Qi, P.; Peng, Y.; Meng, Z.; Yang, Z.; Yu, W.; Qian, Y. Metastable MnS Crystallites through Solvothermal Synthesis. *Chem. Mater.* **2001**, *13* (6), 2169–2172.
32. Yang, X.; Wang, Y.; Sui, Y.; Huang, X.; Cui, T.; Wang, C.; Liu, B.; Zou, G.; Zou, B. Size-Controlled Synthesis of Bifunctional Magnetic and Ultraviolet Optical Rock-Salt MnS Nanocube Superlattices. *Langmuir* **2012**, *28* (51), 17811–17816.
33. Hoekstra, D. C.; Nickmans, K.; Lub, J.; Debije, M. G.; Schenning, A. P. H. J. Air-Curable, High-Resolution Patternable Oxetane-Based Liquid Crystalline Photonic Films via Flexographic Printing. *ACS Appl. Mater. Interfaces* **2019**, *11* (7), 7423–7430.
34. Qi, K.; Wang, Y.-Q.; Rengaraj, S.; Al Wahaibi, B.; Jahangir, A. R. M. MnS Spheres: Shape-Controlled Synthesis and its Magnetic Properties. *Mater. Chem. Phys.* **2017**, *193*, 177–181.
35. Shahzad, U.; Saeed, M.; Rabbee, M. F.; Marwani, H. M.; Al-Humaidi, J. Y.; Altaf, M.; Althomali, R. H.; Rahman, M. M. Recent Progress in Two-Dimensional Metalloenes and Their Potential Application as Electrocatalyst. *J. Energy Chem.* **2024**, *94*, 577–598.
36. Vickers, N. J. Animal Communication: When I'm Calling You, Will You Answer Too? *Curr. Biol.* **2017**, *27* (14), R713–R715.
37. Li, M.; Liang, J.; Chai, Y.; Li, D.; Lu, J.; Li, L. One-Step Synthesis of Alpha-MnS Nanosheets for Supercapacitor Electrode Materials. *Micro & Nano Lett.* **2017**, *12* (10), 735–737.
38. Pujari, R. B.; Lokhande, A. C.; Yadav, A. A.; Kim, J. H.; Lokhande, C. D. Synthesis of MnS Microfibers for High Performance Flexible Supercapacitors. *Mater. Des.* **2016**, *108*, 510–517.
39. Wang, S.; Li, K.; Zhai, R.; Wang, H.; Hou, Y.; Yan, H. Synthesis of Metastable γ -Manganese Sulfide Crystallites by Microwave Irradiation. *Mater. Chem. Phys.* **2005**, *91* (2), 298–300.
40. Tiwari, P.; Malik, G.; Chandra, R. Phase-dependent Structural and Electrochemical Properties of Single Crystalline MnS Thin Films Deposited by DC Reactive Sputtering. *J. Appl. Phys.* **2018**, *124* (19), 195106.
41. Wei, C.; Chen, Q.; Cheng, C.; Liu, R.; Zhang, Q.; Zhang, L. Mesoporous Nickel Cobalt Manganese Sulfide Yolk–Shell Hollow Spheres for High-Performance Electrochemical Energy Storage. *Inorg. Chem. Front.* **2019**, *6* (7), 1851–1860.
42. Tang, Y.; Chen, T.; Yu, S. Morphology Controlled Synthesis of Monodispersed Manganese Sulfide Nanocrystals and Their Primary Application in Supercapacitors with High Performances. *Chem. Commun.* **2015**, *51* (43), 9018–9021.
43. Pathan, H. M.; Kale, S. S.; Lokhande, C. D.; Han, S.-H.; Joo, O.-S. Preparation and Characterization of Amorphous Manganese Sulfide Thin Films by SILAR Method. *Mater. Res. Bull.* **2007**, *42* (8), 1565–1569.
44. Michel, F. M.; Schoonen, M. A. A.; Zhang, X. V.; Martin, S. T.; Parise, J. B. Hydrothermal Synthesis of Pure α -Phase Manganese(II) Sulfide without the Use of Organic Reagents. *Chem. Mater.* **2006**, *18* (7), 1726–1736.
45. Zhang, L.; Zhou, L.; Wu, H. B.; Xu, R.; Lou, X. W. Unusual Formation of Single-Crystal Manganese Sulfide Microboxes Co-Mediated by the Cubic Crystal Structure and Shape. *Angew. Chem., Int. Ed.* **2012**, *51* (29), 7267–7270.
46. Peng, S.; Li, L.; Li, C.; Tan, H.; Cai, R.; Yu, H.; Mhaisalkar, S.; Srinivasan, M.; Ramakrishna, S.; Yan, Q. In Situ Growth of NiCo_2S_4 Nanosheets on Graphene for High-Performance Supercapacitors. *Chem. Commun.* **2013**, *49* (86), 10178–10180.
47. Quan, H.; Cheng, B.; Chen, D.; Su, X.; Xiao, Y.; Lei, S. One-Pot Synthesis of α -MnS/Nitrogen-Doped Reduced Graphene Oxide Hybrid for High-Performance Asymmetric Supercapacitors. *Electrochim. Acta* **2016**, *210*, 557–566.
48. Zhang, N.; Yi, R.; Wang, Z.; Shi, R.; Wang, H.; Qiu, G.; Liu, X. Hydrothermal Synthesis and Electrochemical Properties of Alpha-Manganese Sulfide Submicrocrystals as an Attractive Electrode Material for Lithium-Ion Batteries. *Mater. Chem. Phys.* **2008**, *111* (1), 13–16.
49. Chen, D.; Quan, H.; Wang, G.-S.; Guo, L. Hollow α -MnS Spheres and Their Hybrids with Reduced Graphene Oxide: Synthesis, Microwave Absorption, and Lithium Storage Properties. *ChemPlusChem* **2013**, *78* (8), 843–851.
50. Tang, Y.; Chen, T.; Yu, S.; Qiao, Y.; Mu, S.; Hu, J.; Gao, F. Synthesis of Graphene Oxide Anchored Porous Manganese Sulfide Nanocrystals via the Nanoscale Kirkendall Effect for Supercapacitors. *J. Mater. Chem. A* **2015**, *3* (24), 12913–12919.
51. Li, X.; Shen, J.; Li, N.; Ye, M. Fabrication of γ -MnS/rGO Composite by Facile One-Pot Solvothermal Approach for Supercapacitor Applications. *J. Power Sources* **2015**, *282*, 194–201.
52. Chen, T.; Tang, Y.; Qiao, Y.; Liu, Z.; Guo, W.; Song, J.; Mu, S.; Yu, S.; Zhao, Y.; Gao, F. All-solid-state High Performance Asymmetric Supercapacitors Based on Novel MnS Nanocrystal and Activated Carbon Materials. *Sci. Rep.* **2016**, *6* (1), 23289.
53. Zhang, G.; Kong, M.; Yao, Y.; Long, L.; Yan, M.; Liao, X.; Yin, G.; Huang, Z.; Asiri, A. M.; Sun, X. One-Pot Synthesis of γ -MnS/Reduced Graphene Oxide with Enhanced Performance for Aqueous Asymmetric Supercapacitors. *Nanotechnology* **2017**, *28* (6), 065402.
54. Ulutas, C.; Erken, O.; Gunes, M.; Ozkendir, O. M.; Gumus, C. Investigation on the Electronic and Physical Properties of Gamma-

- MnS Films as a Function of Thickness. *Mater. Sci. Semicond. Process.* **2022**, *140*, 106412.
55. Mariyappan, V.; Murugan, K.; Chen, S.-M. Solvothermal Synthesis of Carbon Incorporated MnS₂ Spheres; High Sensing Performance towards the Detection of Furazolidone in Bio-Fluids. *J. Alloys Compd.* **2021**, *882*, 160744.
 56. Heiba, Z. K.; Mohamed, M. B.; Badawi, A.; Farag, N. M. Effect of Sulfur Deficiency on the Structural, Optical and Electronic Properties of MnS Nanostructures. *Chem. Phys. Lett.* **2021**, *779*, 138877.
 57. Xaba, T.; Al-Shakban, M. Formation of the Green Stable α -MnS with Metastable γ -MnS Nanoparticles and Thin Films by Homogeneous Precipitation Route. *Chalcogenide Lett.* **2020**, *17* (8), 417–422.
 58. Biswas, B. D.; Purkayastha, M. D.; Majumder, T. P. Effect of DAS on the Optical and Photocatalytic Properties of Metastable γ -MnS Nanoparticles. *Surface. Interfac.* **2020**, *19*, 100469.
 59. Tiwari, P.; Jaiswal, J.; Chandra, R. Optical and Electrical Properties of Highly Ordered α - γ and α + γ -MnS Films Deposited by Reactive Sputtering Technique. *J. Appl. Phys.* **2019**, *126* (21), 213108.
 60. Paredes Camacho, R. A.; Wu, A.-M.; Jin, X.-Z.; Dong, X.-F.; Li, X.-N.; Huang, H. Effective Carbon Constraint of MnS Nanoparticles as High-Performance Anode of Lithium-Ion Batteries. *J. Power Sources* **2019**, *437*, 226931.
 61. Hosseini-Hajivar, M. M.; Jamali-Sheini, F.; Yousefi, R. Microwave-Assisted Solvothermal Synthesis and Physical Properties of Zn-Doped MnS Nanoparticles. *Solid State Sci.* **2019**, *93*, 31–36.
 62. Hussain, W.; Malik, H.; Hussain, R. A.; Hussain, H.; Green, I. R.; Marwat, S.; Bahadur, A.; Iqbal, S.; Farooq, M. U.; Li, H.; Badshah, A. Synthesis of MnS from Single- and Multi-Source Precursors for Photocatalytic and Battery Applications. *J. Electron. Mater.* **2019**, *48* (4), 2278–2288.
 63. Ghanbari, B.; Jamali-Sheini, F.; Yousefi, R. Microwave-Assisted Solvothermal Synthesis and Optoelectronic Properties of γ -MnS Nanoparticles. *J. Mater. Sci. Mater. Electron.* **2018**, *29* (13), 10976–10985.
 64. Dhandayuthapani, T.; Girish, M.; Sivakumar, R.; Sanjeeviraja, C.; Gopalakrishnan, C.; Nagarajan, R. S.; Mathew, S.; Jun, D.; Venkatesan, T.; Kalai Selvan, G.; Manikandan, K.; Arumugam, S. γ -MnS Films with 3D Microarchitectures: Comprehensive Study of the Synthesis, Microstructural, Optical and Magnetic Properties. *CrystEngComm* **2018**, *20* (5), 578–589.
 65. Mohamed, S. G.; Attia, S. Y.; Barakat, Y. F.; Hassan, H. H.; Zoubi, W. A. Hydrothermal Synthesis of α -MnS Nanoflakes@Nitrogen and Sulfur Co-Doped rGO for High-Performance Hybrid Supercapacitor. *ChemistrySelect* **2018**, *3* (22), 6061–6072.
 66. Fatolahi, L.; Feizbakhsh, A.; Kono, E.; Panahi, H. A. Synthesis and Characterization of ZnS Quantum Dots on MnS₂ Nanoparticles for Photo-Assisted Electrochemical Degradation of Drug Compound. *J. Inorg. Organomet. Polym. Mater.* **2019**, *29* (1), 80–86.
 67. Arul, N. S.; Cavalcante, L. S.; Han, J. Facile Synthesis of ZnS/MnS Nanocomposites for Supercapacitor Applications. *J. Solid State Electrochem.* **2018**, *22* (1), 303–313.
 68. Satpathy, S.; Das, S.; Bhattacharyya, B. K. How and Where to Use Super-capacitors Effectively, an Integration of Review of Past and New Characterization Works on Super-Capacitors. *J. Energy Storage* **2020**, *27*, 101044.
 69. Zhang, J.; Zhang, L.; Sun, F.; Wang, Z. An Overview on Thermal Safety Issues of Lithium-Ion Batteries for Electric Vehicle Application. *IEEE Access* **2018**, *6*, 23848–23863.
 70. Wang, X.; Cui, Y.; Li, T.; Lei, M.; Li, J.; Wei, Z. Recent Advances in the Functional 2D Photonic and Optoelectronic Devices. *Adv. Opt. Mater.* **2019**, *7* (3), 1801274.
 71. Malek, T. J.; Chaki, S. H.; Deshpande, M. P. Structural, Morphological, Optical, Thermal and Magnetic Study of Mackinawite FeS Nanoparticles Synthesized by Wet Chemical Reduction Technique. *Phys. B Condens. Matter* **2018**, *546*, 59–66.
 72. Thomas, M. P.; Ullah, A.; Pham, R. H.; Djieutedjeu, H.; Selegue, J. P.; Guiton, B. S. Morphology Control in the Hydrothermal Synthesis of FeS Nanoplatelets. *Cryst. Growth Des.* **2020**, *20* (9), 5728–5735.
 73. Bhattacharjee, S.; Habib, F.; Darwish, N.; Shanableh, A. Iron Sulfide Nanoparticles Prepared Using Date Seed Extract: Green Synthesis, Characterization and Potential Application for Removal of Ciprofloxacin and Chromium. *Powder Technol.* **2021**, *380*, 219–228.
 74. Wu, J.; Zeng, R. J. In Situ Preparation of Stabilized Iron Sulfide Nanoparticle-Impregnated Alginate Composite for Selenite Remediation. *Environ. Sci. Technol.* **2018**, *52* (11), 6487–6496.
 75. Liu, D.; Yang, L.; Wu, J.; Li, C. Gaseous Elemental Mercury Capture by Magnetic FeS₂ Nanorods Synthesized via a Molten Salt Method. *ACS Appl. Nano Mater.* **2022**, *5* (2), 2626–2635.
 76. Wu, Y.; Wang, Y.; Shao, S.; Ma, Y.; Zhang, J.; Kang, W.; Xu, J. Transformation of Two-Dimensional Iron Sulfide Nanosheets from FeS₂ to FeS as High-Rate Anodes for Pseudocapacitive Sodium Storage. *ACS Appl. Energy Mater.* **2020**, *3* (12), 12672–12681.
 77. Zhang, Z.-W.; Zhong, X.-B.; Zhang, Y.-H.; Tang, M.-Y.; Li, S.-X.; Zhang, H.-H.; Hu, P.; Liang, J. Scalable Synthesis of Mesoporous FeS₂ Nanorods as High-Performance Anode Materials for Sodium-Ion Batteries. *Rare Met.* **2022**, *41* (1), 21–28.
 78. Tripathi, J.; Chandawat, G. S.; Singh, J.; Tripathi, S.; Sharma, A. Correlation Among Local Structure, Magnetic, Structural and Electronic Properties in Polyol Synthesized Iron Sulfide (FeS₂) Nanoparticles. *J. Alloys Compd.* **2021**, *861*, 157977.
 79. Song, C.; Ding, W.; Zhao, W.; Liu, H.; Wang, J.; Yao, Y.; Yao, C. High Peroxidase-like Activity Realized by Facile Synthesis of FeS₂ Nanoparticles for Sensitive Colorimetric Detection of H₂O₂ and Glutathione. *Biosens. Bioelectron.* **2020**, *151*, 111983.
 80. Kaur, H.; Tian, R.; Roy, A.; McCrystall, M.; Horvath, D. V.; Lozano Onrubia, G.; Smith, R.; Ruether, M.; Griffin, A.; Backes, C.; Nicolosi, V.; Coleman, J. N. Production of Quasi-2D Platelets of Nonlayered Iron Pyrite (FeS₂) by Liquid-Phase Exfoliation for High Performance Battery Electrodes. *ACS Nano* **2020**, *14* (10), 13418–13432.
 81. Suroshe, J. S.; Mlowe, S.; Garje, S. S.; Revaprasadu, N. Preparation of Iron Sulfide Nanomaterials from Iron(II) Thiosemi-Carbazone Complexes and Their Application in Photodegradation of Methylene Blue. *J. Inorg. Organomet. Polym. Mater.* **2018**, *28* (3), 603–611.
 82. Gadisa, B. T.; Appiah-Ntiemoah, R.; Kim, H. Amorphous Iron Sulfide Nanowires as an Efficient Adsorbent for Toxic Dye Effluents Remediation. *Environ. Sci. Pollut. Control Ser.* **2019**, *26* (3), 2734–2746.
 83. Ahmad, M. W.; Farva, U.; Khan, M. A. Low Temperature Synthesis of Iron Pyrite (FeS₂) Nanospheres as a Strong Solar Absorber Material. *Mater. Lett.* **2018**, *228*, 129–132.
 84. Prabukanthan, P.; Thamaraiselvi, S.; Harichandran, G. Structural, Morphological, Electrocatalytic Activity and Photocurrent Properties of Electrochemically Deposited FeS₂ Thin Films. *J. Mater. Sci. Mater. Electron.* **2018**, *29* (14), 11951–11963.
 85. Zhu, X.; Wang, L. Advances in Materials for All-Climate Sodium-Ion Batteries. *EcoMat* **2020**, *2* (3), e12043.
 86. Khalid, S.; Ahmed, E.; Khan, Y.; Riaz, K. N.; Malik, M. A. Nanocrystalline Pyrite for Photovoltaic Applications. *ChemistrySelect* **2018**, *3* (23), 6488–6524.

87. Madian, M.; Eychmüller, A.; Giebler, L. Current Advances in TiO₂-Based Nanostructure Electrodes for High Performance Lithium Ion Batteries. *Batteries* **2018**, *4* (1), 7.
88. Ayodhya, D.; Veerabhadram, G. A Review on Recent Advances in Photodegradation of Dyes Using Doped and Heterojunction Based Semiconductor Metal Sulfide Nanostructures for Environmental Protection. *Mater. Today Energy* **2018**, *9*, 83–113.
89. Huang, G.; Chen, T.; Wang, Z.; Chang, K.; Chen, W. Synthesis and Electrochemical Performances of Cobalt Sulfides/graphene Nanocomposite as Anode Material of Li-Ion Battery. *J. Power Sources* **2013**, *235*, 122–128.
90. Hoodless, R. C.; Moyes, R. B.; Wells, P. B. D-Tracer Study of Butadiene Hydrogenation and Tetrahydrothiophen Hydrodesulphurisation Catalysed by Co₉S₈. *Catal. Today* **2006**, *114* (4), 377–382.
91. Wang, H.; Liang, Y.; Li, Y.; Dai, H. Co_{1-x}S-graphene Hybrid: A High-Performance Metal Chalcogenide Electrocatalyst for Oxygen Reduction. *Angew. Chem.* **2011**, *123* (46), 11161–11164.
92. Justin, P.; Ranga Rao, G. CoS Spheres for High-Rate Electro-Chemical Capacitive Energy Storage Application. *Int. J. Hydrogen Energy* **2010**, *35* (18), 9709–9715.
93. Wang, Q.; Jiao, L.; Du, H.; Yang, J.; Huan, Q.; Peng, W.; Si, Y.; Wang, Y.; Yuan, H. Facile Synthesis and Superior Supercapacitor Performances of Three-Dimensional Cobalt Sulfide Hierarchitectures. *CrystEngComm* **2011**, *13* (23), 6960–6963.
94. Dong, W.; Wang, X.; Li, B.; Wang, L.; Chen, B.; Li, C.; Li, X.; Zhang, T.; Shi, Z. Hydrothermal Synthesis and Structure Evolution of Hierarchical Cobalt Sulfide Nanostructures. *Dalton Trans.* **2011**, *40* (1), 243–248.
95. Apostolova, R.; Shembel, I.; Talyosef, I.; Grinblat, J.; Markovsky, A.; Aurbach, D. Study of Electrolytic Cobalt Sulfide Co₉S₈ as an Electrode Material in Lithium Accumulator Prototypes. *Russ. J. Electrochem.* **2009**, *45* (3), 311–319.
96. Kim, Y.; Goodenough, J. B. Lithium Insertion into Transition-Metal Monosulfides: Tuning the Position of the Metal 4s Band. *J. Phys. Chem. C* **2008**, *112* (38), 15060–15064.
97. Shin, J.; Kang, H.; Lee, Y.; Ha, S. H.; Cho, E. Core-Shell Structured Li-Fe Electrode for High Energy and Stable Thermal Battery. *RSC Adv.* **2022**, *12* (8), 4795–4804.
98. Chen, X.; Zhang, Z.; Qiu, Z.; Shi, C.; Li, X. Hydrothermal Fabrication and Characterization of Polycrystalline Linneite (Co₃S₄) Nanotubes Based on the Kirkendall Effect. *J. Colloid Interface Sci.* **2007**, *308* (1), 271–275.
99. Wang, Z.; Pan, L.; Hu, H.; Zhao, S. Co₉S₈ Nanotubes Synthesized on the Basis of Nanoscale Kirkendall Effect and Their Magnetic and Electrochemical Properties. *CrystEngComm* **2010**, *12* (6), 1899–1904.
100. Bao, S.-J.; Li, C. M.; Guo, C.-X.; Qiao, Y. Biomolecule-Assisted Synthesis of Cobalt Sulfide Nanowires for Application in Supercapacitors. *J. Power Sources* **2008**, *180* (1), 676–681.
101. Wang, Q.; Jiao, L.; Han, Y.; Du, H.; Peng, W.; Huan, Q.; Song, D.; Si, Y.; Wang, Y.; Yuan, H. CoS₂ Hollow Spheres: Fabrication and Their Application in Lithium-Ion Batteries. *J. Phys. Chem. C* **2011**, *115* (16), 8300–8304.
102. Zhou, Y. X.; Yao, H. B.; Wang, Y.; Liu, H. L.; Gao, M. R.; Shen, P. K.; Yu, S. Hierarchical Hollow Co₉S₈ Microspheres: Solvothermal Synthesis, Magnetic, Electrochemical, and Electrocatalytic Properties. *Chem. Eur. J.* **2010**, *16* (39), 12000–12007.
103. Lewis, A. E. Review of Metal Sulphide Precipitation. *Hydrometallurgy* **2010**, *104* (2), 222–234.
104. Rickard, D.; Luther, G. W. III. Metal Sulfide Complexes and Clusters. *Rev. Mineral. Geochem.* **2006**, *61* (1), 421–504.
105. Swanner, E. D.; Planavsky, N. J.; Lalonde, S. V.; Robbins, L. J.; Bekker, A.; Rouxel, O. J.; Saito, M. A.; Kappler, A.; Mojzsis, S. J.; Konhauser, K. O. Cobalt and Marine Redox Evolution. *Earth Planet. Sci. Lett.* **2014**, *390*, 253–263.
106. Moore, E. K.; Hao, J.; Prabhu, A.; Zhong, H.; Jelen, B. I.; Meyer, M.; Hazen, R. M.; Falkowski, P. G. Geological and Chemical Factors that Impacted the Biological Utilization of Cobalt in the Archean Eon. *J. Geophys. Res.: Biogeosciences* **2018**, *123* (3), 743–759.
107. Shi, W.; Zhu, J.; Rui, X.; Cao, X.; Chen, C.; Zhang, H.; Hng, H. H.; Yan, Q. Controlled Synthesis of Carbon-Coated Cobalt Sulfide Nanostructures in Oil Phase with Enhanced Li Storage Performances. *ACS Appl. Mater. Interfaces* **2012**, *4* (6), 2999–3006.
108. Bavar, S.; Alamolhoda, S.; Bafghi, M. S.; Masoudpanah, S. Photocatalytic Performances of Cobalt Sulfides Prepared by Solution Combustion Synthesis Using Mixed Fuels. *J. Phys. Chem. Solid.* **2021**, *149*, 109805.
109. Wu, Y.; Gaddam, R. R.; Zhang, C.; Lu, H.; Wang, C.; Golberg, D.; Zhao, X. S. Stabilising Cobalt Sulphide Nanocapsules with Nitrogen-Doped Carbon for High-Performance Sodium-Ion Storage. *Nano-Micro Lett.* **2020**, *12* (1), 1–12.
110. Wang, B.; Cheng, Y.; Su, H.; Cheng, M.; Li, Y.; Geng, H.; Dai, Z. Boosting Transport Kinetics of Cobalt Sulfides Yolk-Shell Spheres by Anion Doping for Advanced Lithium and Sodium Storage. *ChemSusChem* **2020**, *13* (16), 4078–4085.
111. Samal, R.; Mondal, S.; Gangan, A. S.; Chakraborty, B.; Rout, C. S. Comparative Electrochemical Energy Storage Performance of Cobalt Sulfide and Cobalt Oxide Nanosheets: Experimental and Theoretical Insights from Density Functional Theory Simulations. *Phys. Chem. Chem. Phys.* **2020**, *22* (15), 7903–7911.
112. El-Gendy, D. M.; Afifi, I. M.; Allam, N. K. Eco-Friendly, One-Step Synthesis of Cobalt Sulfide-Decorated Functionalized Graphene for High-Performance Supercapacitors. *J. Energy Storage* **2019**, *24*, 100760.
113. Li, M.; Feng, W.; Su, W.; Wang, X. Complex Hollow Structures of Cobalt (II) Sulfide as a Cathode for Lithium-Sulfur Batteries. *Int. J. Electrochem. Sci.* **2020**, *15*, 526–534.
114. Muradov, M. B.; Balayeva, O. O.; Azizov, A. A.; Maharramov, A. M.; Qahramanli, L. R.; Eyvazova, G. M.; Aghamaliyev, Z. A. Synthesis and Characterization of Cobalt Sulfide Nanoparticles by Sonochemical Method. *Infrared Phys. Technol.* **2018**, *89*, 255–262.
115. Zhang, C.; Shi, Y.; Yu, Y.; Du, Y.; Zhang, B. Engineering Sulfur Defects, Atomic Thickness, and Porous Structures into Cobalt Sulfide Nanosheets for Efficient Electrocatalytic Alkaline Hydrogen Evolution. *ACS Catal.* **2018**, *8* (9), 8077–8083.
116. Masikhwa, T. M.; Madito, M. J.; Bello, A.; Lekitima, J.; Manyala, N. Microwave-Assisted Synthesis of Cobalt Sulphide Nanoparticle Clusters on Activated Graphene Foam for Electrochemical Supercapacitors. *RSC Adv.* **2017**, *7* (33), 20231–20240.
117. Zhou, Y.; Zhu, Y.; Xu, B.; Zhang, X.; Al-Ghanim, K. A.; Mahboob, S. Cobalt Sulfide Confined in N-Doped Porous Branched Carbon Nanotubes for Lithium-Ion Batteries. *Nano-Micro Lett.* **2019**, *11* (1), 1–9.
118. Irshad, A.; Munichandraiah, N. Electrodeposited Nickel-Cobalt-Sulfide Catalyst for the Hydrogen Evolution Reaction. *ACS Appl. Mater. Interfaces* **2017**, *9* (23), 19746–19755.
119. Muniyappa, M.; Kalegowda, S. N.; Shetty, M.; Sriramoju, J. B.; Shastri, M.; Navakoteswara Rao, S. V.; De, D.; Shankar, M. V.; Rangappa, D. Cocatalyst Free Nickel Sulphide Nanostructure for Enhanced Photocatalytic Hydrogen Evolution. *Int. J. Hydrogen Energy* **2022**, *47* (8), 5307–5318.
120. Karthikeyan, R.; Thangaraju, D.; Prakash, N.; Hayakawa, Y. Single-Step Synthesis and Catalytic Activity of Structure-Controlled Nickel Sulfide Nanoparticles. *CrystEngComm* **2015**, *17* (29), 5431–5439.

121. Bhardwaj, R.; Jha, R.; Bhushan, M.; Sharma, R. Enhanced Electrochemical Activity of the Solvothermally Synthesized Mesoporous Rhombohedral Nickel Sulphide. *Mater. Sci. Semicond. Process.* **2020**, *118*, 105194.
122. Luo, P.; Zhang, H.; Liu, L.; Zhang, Y.; Deng, J.; Xu, C.; Hu, N.; Wang, Y. Targeted Synthesis of Unique Nickel Sulfide (NiS, NiS₂) Microarchitectures and the Applications for the Enhanced Water Splitting System. *ACS Appl. Mater. Interfaces* **2017**, *9* (3), 2500–2508.
123. Karakaya, C.; Solati, N.; Savacı, U.; Keles, E.; Turan, S.; Çelebi, S.; Kaya, S. Mesoporous Thin-Film NiS₂ as an Idealized Pre-Electrocatalyst for a Hydrogen Evolution Reaction. *ACS Catal.* **2020**, *10* (24), 15114–15122.
124. Mehmood, A.; Rahman, G.; Ul Haq Ali Shah, A.; Joo, O.-S.; Mian, S. A. Template-Free Hydrothermal Growth of Nickel Sulfide Nanorods as High-Performance Electroactive Materials for Oxygen Evolution Reaction and Supercapacitors. *Energy Fuel.* **2021**, *35* (8), 6868–6879.
125. Nareesh, B.; Punnoose, D.; Rao, S. S.; Subramanian, A.; Raja Ramesh, B.; Kim, H.-J. Hydrothermal Synthesis and Pseudocapacitive Properties of Morphology-Tuned Nickel Sulfide (NiS) Nanostructures. *New J. Chem.* **2018**, *42* (4), 2733–2742.
126. Zhao, J.; Guan, B.; Hu, B.; Xu, Z.; Wang, D.; Zhang, H. Vulcanizing Time Controlled Synthesis of NiS Microflowers and its Application in Asymmetric Supercapacitors. *Electrochim. Acta* **2017**, *230*, 428–437.
127. Sadan, M. K.; Jeon, M.; Yun, J.; Song, E.; Cho, K.-K.; Ahn, J.-H.; Ahn, H.-J. Excellent Electrochemical Performance of a Mesoporous Nickel Sulfide Anode for Na/K-Ion Batteries. *ACS Appl. Energy Mater.* **2021**, *4* (12), 14537–14545.
128. Khosravi, M.; Saeednia, S.; Iranmanesh, P.; Hatefi Ardakani, M. Cauliflower-Like Nickel Sulfide Nanostructures: Preparation, Optical Properties, Catalytic and Photocatalytic Activities. *J. Cluster Sci.* **2023**, *34*, 311–322.
129. Iqbal, M. F.; Yousef, A. K. M.; Hassan, A.; Hussain, S.; Ashiq, M. N.; Ul-Hassan, M.; Razaq, A. Significantly Improved Electrochemical Characteristics of Nickel Sulfide Nanoplates Using Graphene Oxide Thin Film for Supercapacitor Applications. *J. Energy Storage* **2021**, *33*, 102091.
130. Khan, R.; Das, N. S.; Das, B.; Das, B.; Chattopadhyay, K. K. Hierarchical Nickel Sulphide Microstructures for Controlled Water Disinfection and Cold Cathode Emission. *J. Photochem. Photobiol., A* **2021**, *412*, 113212.
131. Nandhini, S.; Muralidharan, G. Facile Microwave-Hydrothermal Synthesis of NiS Nanostructures for Supercapacitor Applications. *Appl. Surf. Sci.* **2018**, *449*, 485–491.
132. Ehsan, M. A.; Khan, A.; Zafar, M. N.; Akber, U. A.; Hakeem, A. S.; Nazar, M. F. Aerosol-Assisted Chemical Vapor Deposition of Nickel Sulfide Nanowires for Electrochemical Water Oxidation. *Int. J. Hydrogen Energy* **2022**, *47*, 42001.
133. Yang, R.; Li, R.; Zhang, L.; Xu, Z.; Kang, Y.; Xue, P. Facile Synthesis of Hollow Mesoporous Nickel Sulfide Nanoparticles for Highly Efficient Combinatorial Photothermal–Chemotherapy of Cancer. *J. Mater. Chem. B* **2020**, *8* (34), 7766–7776.
134. Kumari, S.; Khan, A. A.; Chowdhury, A.; Bhakta, A. K.; Mekhalif, Z.; Hussain, S. Efficient and Highly Selective Adsorption of Cationic Dyes and Removal of Ciprofloxacin Antibiotic by Surface Modified Nickel Sulfide Nanomaterials: Kinetics, Isotherm and Adsorption Mechanism. *Colloids Surf., A* **2020**, *586*, 124264.
135. Hilal, M.; Han, J. I. Preparation of Hierarchical Flower-like Nickel Sulfide as Hole Transporting Material for Organic Solar Cells via a One-Step Solvothermal Method. *Sol. Energy* **2019**, *188*, 403–413.
136. Shah, S. S.; Aziz, M.; Mohamedkhair, A. K.; Qasem, M. A. A.; Hakeem, A. S.; Nazal, M. K.; Yamani, Z. H. Preparation and Characterization of Manganese Oxide Nanoparticles-Coated Albizia Procera Derived Carbon for Electrochemical Water Oxidation. *J. Mater. Sci. Mater. Electron.* **2019**, *30* (17), 16087–16098.
137. Jiang, X.; Xie, Y.; Lu, J.; He, W.; Zhu, L.; Qian, Y. Preparation and Phase Transformation of Nanocrystalline Copper Sulfides (Cu₉S₈, Cu₇S₄ and CuS) at Low Temperature. *J. Mater. Chem.* **2000**, *10* (9), 2193–2196.
138. Gorai, S.; Ganguli, D.; Chaudhuri, S. Synthesis of Copper Sulfides of Varying Morphologies and Stoichiometries Controlled by Chelating and Nonchelating Solvents in a Solvothermal Process. *Cryst. Growth Des.* **2005**, *5* (3), 875–877.
139. Kundu, J.; Pradhan, D. Controlled Synthesis and Catalytic Activity of Copper Sulfide Nanostructured Assemblies with Different Morphologies. *ACS Appl. Mater. Interfaces* **2014**, *6* (3), 1823–1834.
140. Mezgebe, M. M.; Ju, A.; Wei, G.; Macharia, D. K.; Guang, S.; Xu, H. Structure Based Optical Properties and Catalytic Activities of Hydrothermally Prepared CuS Nanostructures. *Nanotechnology* **2019**, *30* (10), 105704.
141. Basu, M.; Sinha, A. K.; Pradhan, M.; Sarkar, S.; Negishi, Y.; Pal, T. Evolution of Hierarchical Hexagonal Stacked Plates of CuS from Liquid–Liquid Interface and its Photocatalytic Application for Oxidative Degradation of Different Dyes Under Indoor Lighting. *Environ. Sci. Technol.* **2010**, *44* (16), 6313–6318.
142. Islam, D. A.; Chakraborty, A.; Bhattacharya, B.; Sarkar, U.; Acharya, H. Tailored Synthesis of CuS Nanodisks from a New Macrocyclic Precursor and Their Efficient Catalytic Properties on Methylene Blue Dye Degradation. *J. Nanoparticle Res.* **2016**, *18* (5), 114.
143. Ayodhya, D.; Venkatesham, M.; Santoshi kumari, A.; Reddy, G. B.; Ramakrishna, D.; Veerabhadram, G. Photocatalytic Degradation of Dye Pollutants Under Solar, Visible and UV Lights Using Green Synthesised CuS Nanoparticles. *J. Exp. Nanosci.* **2016**, *11* (6), 418–432.
144. Solanki, J. N.; Sengupta, R.; Murthy, Z. V. P. Synthesis of Copper Sulphide and Copper Nanoparticles with Microemulsion Method. *Solid State Sci.* **2010**, *12* (9), 1560–1566.
145. Thongtem, T.; Phuruangrat, A.; Thongtem, S. Formation of CuS with Flower-Like, Hollow Spherical, and Tubular Structures Using the Solvothermal-Microwave Process. *Curr. Appl. Phys.* **2009**, *9* (1), 195–200.
146. Aziz, S. B.; Abdulwahid, R. T.; Rsaul, H. A.; Ahmed, H. M. In Situ Synthesis of CuS Nanoparticle with a Distinguishable SPR Peak in NIR Region. *J. Mater. Sci. Mater. Electron.* **2016**, *27* (5), 4163–4171.
147. Palve, B. M.; Jadkar, S. R.; Pathan, H. M. A Simple Chemical Route to Synthesis the CuS Nanocrystal Powder at Room Temperature and Phase Transition. *J. Mater. Sci. Mater. Electron.* **2016**, *27* (11), 11783–11789.
148. Maeda, K.; Tanaka, K.; Fukui, Y.; Uchiki, H. Influence of H₂S Concentration on the Properties of Cu₂ZnSnS₄ Thin Films and Solar Cells Prepared by Sol–gel Sulfurization. *Sol. Energy Mater. Sol. Cells* **2011**, *95* (10), 2855–2860.
149. Rajagopal, S.; Nataraj, D.; Khyzhun, O. Y.; Djauoued, Y.; Robichaud, J.; Kim, C.-K. Controlled Synthesis of MoO₃ Microcrystals by Subsequent Calcination of Hydrothermally Grown pyrazine–MoO₃ Nanorod Hybrids and Their Photodecomposition Properties. *Mater. Chem. Phys.* **2013**, *141* (1), 383–392.
150. Saranya, M.; Santhosh, C.; Ramachandran, R.; Kollu, P.; Saravanan, P.; Vinoba, M.; Jeong, S. K.; Grace, A. N. Hydrothermal Growth of CuS Nanostructures and its Photocatalytic Properties. *Powder Technol.* **2014**, *252*, 25–32.
151. Li, M.; Wu, Q.; Shi, J. A Simple Route to Synthesize CuS Framework with Porosity. *J. Alloys Compd.* **2010**, *489* (2), 343–347.
152. Xu, H.; Wang, W.; Zhu, W. Sonochemical Synthesis of Crystalline CuS Nanoplates via an In Situ Template Route. *Mater. Lett.* **2006**, *60* (17), 2203–2206.

153. Shen, G.; Chen, D.; Tang, K.; Liu, X.; Huang, L.; Qian, Y. General Synthesis of Metal Sulfides Nanocrystallines via a Simple Polyol Route. *J. Solid State Chem.* **2003**, 173 (1), 232–235.
154. Subramanyam, K.; Sreelekha, N.; Amaranatha Reddy, D.; Murali, G.; Rahul Varma, K.; Vijayalakshmi, R. P. Chemical Synthesis, Structural, Optical, Magnetic Characteristics and Enhanced Visible Light Active Photocatalysis of Ni Doped CuS Nanoparticles. *Solid State Sci.* **2017**, 65, 68–78.
155. Hou, G.; Cheng, Z.; Kang, L.; Xu, X.; Zhang, F.; Yang, H. Controllable Synthesis of CuS Decorated TiO₂ Nanofibers for Enhanced Photocatalysis. *CrystEngComm* **2015**, 17 (29), 5496–5501.
156. Manzar, R.; Saeed, M.; Shahzad, U.; Al-Humaidi, J. Y.; ur Rehman, S.; Althomali, R. H.; Rahman, M. M. Recent Advancements in Boron Carbon Nitride (BNC) Nanoscale Materials for Efficient Supercapacitor Performances. *Prog. Mater. Sci.* **2024**, 144, 101286.
157. Huang, J.; Zhou, J.; Zhuang, J.; Gao, H.; Huang, D.; Wang, L.; Wu, W.; Li, Q.; Yang, D.-P.; Han, M.-Y. Strong Near-Infrared Absorbing and Biocompatible CuS Nanoparticles for Rapid and Efficient Photothermal Ablation of Gram-Positive and -Negative Bacteria. *ACS Appl. Mater. Interfaces* **2017**, 9 (42), 36606–36614.
158. Duffort, V.; Sun, X.; Nazar, L. F. Screening for Positive Electrodes for Magnesium Batteries: A Protocol for Studies at Elevated Temperatures. *Chem. Commun.* **2016**, 52 (84), 12458–12461.
159. Xiong, F.; Fan, Y.; Tan, S.; Zhou, L.; Xu, Y.; Pei, C.; An, Q.; Mai, L. Magnesium Storage Performance and Mechanism of CuS Cathode. *Nano Energy* **2018**, 47, 210–216.
160. Yoo, H. D.; Shterenberg, I.; Gofer, Y.; Gershinshy, G.; Pour, N.; Aurbach, D. Mg Rechargeable Batteries: An On-Going Challenge. *Energy Environ. Sci.* **2013**, 6 (8), 2265–2279.
161. Kim, H.; Sadan, M. K.; Kim, C.; Choe, S.-H.; Cho, K.-K.; Kim, K.-W.; Ahn, J.-H.; Ahn, H.-J. Simple and Scalable Synthesis of CuS as an Ultrafast and Long-Cycling Anode for Sodium Ion Batteries. *J. Mater. Chem. A* **2019**, 7 (27), 16239–16248.
162. Wang, Y.; Zhang, Y.; Li, H.; Peng, Y.; Li, J.; Wang, J.; Hwang, B. J.; Zhao, J. Realizing High Reversible Capacity: 3D Intertwined CNTs Inherently Conductive Network for CuS as an Anode for Lithium Ion Batteries. *Chem. Eng. J.* **2018**, 332, 49–56.
163. Li, H.; Wang, Y.; Huang, J.; Zhang, Y.; Zhao, J. Microwave-Assisted Synthesis of CuS/Graphene Composite for Enhanced Lithium Storage Properties. *Electrochim. Acta* **2017**, 225, 443–451.
164. Faucheaux, J. A.; Stanton, A. L.; Jain, P. K. Plasmon Resonances of Semiconductor Nanocrystals: Physical Principles and New Opportunities. *J. Phys. Chem. Lett.* **2014**, 5 (6), 976–985.
165. Al-Jawad, S. M.; Taha, A. A.; Muhsen, M. M. Preparation and Characterization of CuS Nanoparticles Prepared by Two-phase Colloidal Method. *J. Phys. Conf.* **2021**, 1795, 012053.
166. Li, Y.; Lu, W.; Huang, Q.; Li, C.; Chen, W. Copper Sulfide Nanoparticles for Photothermal Ablation of Tumor Cells. *Nanomedicine* **2010**, 5 (8), 1161–1171.
167. Huang, X.; Zhang, W.; Guan, G.; Song, G.; Zou, R.; Hu, J. Design and Functionalization of the NIR-Responsive Photothermal Semiconductor Nanomaterials for Cancer Theranostics. *Accounts Chem. Res.* **2017**, 50 (10), 2529–2538.
168. Tian, Q.; Jiang, F.; Zou, R.; Liu, Q.; Chen, Z.; Zhu, M.; Yang, S.; Wang, J.; Wang, J.; Hu, J. Hydrophilic Cu₉S₅ Nanocrystals: A Photothermal Agent with a 25.7% Heat Conversion Efficiency for Photothermal Ablation of Cancer Cells In Vivo. *ACS Nano* **2011**, 5 (12), 9761–9771.
169. Yang, K.; Zhu, L.; Nie, L.; Sun, X.; Cheng, L.; Wu, C.; Niu, G.; Chen, Z.; Liu, Z. Visualization of Protease Activity In Vivo Using an Activatable Photo-Acoustic Imaging Probe Based on CuS Nanoparticles. *Theranostics* **2014**, 4 (2), 134.
170. Tian, Q.; Tang, M.; Sun, Y.; Zou, R.; Chen, Z.; Zhu, M.; Yang, S.; Wang, J.; Wang, J.; Hu, J. Hydrophilic Flower-Like CuS Superstructures as an Efficient 980 Nm Laser-Driven Photothermal Agent for Ablation of Cancer Cells. *Adv. Mater.* **2011**, 23 (31), 3542–3547.
171. Meng, Z.; Wei, F.; Wang, R.; Xia, M.; Chen, Z.; Wang, H.; Zhu, M. NIR-Laser-Switched In Vivo Smart Nanocapsules for Synergic Photothermal and Chemotherapy of Tumors. *Adv. Mater.* **2016**, 28 (2), 245–253.
172. Yu, W.; Yu, N.; Wang, Z.; Li, X.; Song, C.; Jiang, R.; Geng, P.; Li, M.; Yin, S.; Chen, Z. Chitosan-Mediated Green Synthesis and Folic-Acid Modification of CuS Quantum Dots for Photoacoustic Imaging Guided Photothermal Therapy of Tumor. *J. Colloid Interface Sci.* **2019**, 555, 480–488.
173. Deb, S.; Kalita, P. Green Synthesis of Copper Sulfide (CuS) Nanostructures for Heterojunction Diode Applications. *J. Mater. Sci. Mater. Electron.* **2021**, 32 (19), 24125–24137.
174. Rouchdi, M.; Mamori, H.; Salmani, E.; Ait Syad, B.; Mounkachi, O.; Essajai, R.; Ez-zahraoui, H.; Chakchak, H.; Hassanain, N.; Benyoussef, A.; El Kenz, A.; Mzerd, A. Physicochemical Characterization and Catalytic Performance of Fe Doped CuS Thin Films Deposited by the Chemical Spray Pyrolysis Technique. *Appl. Phys. A: Mater. Sci. Process.* **2021**, 127 (6), 1–14.
175. Wang, Z.; Rafai, S.; Qiao, C.; Jia, J.; Zhu, Y.; Ma, X.; Cao, C. Microwave-Assisted Synthesis of CuS Hierarchical Nanosheets as the Cathode Material for High-Capacity Rechargeable Magnesium Batteries. *ACS Appl. Mater. Interfaces* **2019**, 11 (7), 7046–7054.
176. Shawky, A.; El-Sheikh, S.; Gaber, A.; El-Hout, S. I.; El-Sherbiny, I. M.; Ahmed, A. I. Urchin-Like CuS Nanostructures: Simple Synthesis and Structural Optimization with Enhanced Photocatalytic Activity under Direct Sunlight. *Appl. Nanosci.* **2020**, 10 (7), 2153–2164.
177. Iqbal, S.; Bahadur, A.; Anwer, S.; Shoaib, M.; Liu, G.; Li, H.; Raheel, M.; Javed, M.; Khalid, B. Designing Novel Morphologies of L-Cysteine Surface Capped 2D Covellite (CuS) Nanoplates to Study the Effect of CuS Morphologies on Dye Degradation Rate Under Visible Light. *CrystEngComm* **2020**, 22 (24), 4162–4173.
178. Pejjai, B.; Reddivari, M.; Kotte, T. R. R. Phase Controllable Synthesis of CuS Nanoparticles by Chemical Co-Precipitation Method: Effect of Copper Precursors on the Properties of CuS. *Mater. Chem. Phys.* **2020**, 239, 122030.
179. Al-Jawad, S. M.; Taha, A. A.; Redha, A. M. Studying the Structural, Morphological, and Optical Properties of CuS: Ni Nanostructure Prepared by a Hydrothermal Method for Biological Activity. *J. Sol. Gel Sci. Technol.* **2019**, 91 (2), 310–323.
180. Jeyabanu, K.; Devendran, P.; Manikandan, A.; Packiaraj, R.; Ramesh, K.; Nallamuthu, N. Preparation and Characterization Studies of La Doped CuS Nanospheres by Microwave Irradiation for High Performance Supercapacitors. *Phys. B Condens. Matter* **2019**, 573, 92–101.
181. Pal, D.; Singh, G.; Goswami, Y. C.; Kumar, V. Synthesis of Randomly Oriented Self Assembled CuS Nanorods by Co-Precipitation Route. *J. Mater. Sci. Mater. Electron.* **2019**, 30 (16), 15700–15704.
182. Zeinodin, R.; Jamali-Sheini, F. In-Doped CuS Nanostructures: Ultrasonic Synthesis, Physical Properties, and Enhanced Photocatalytic Behavior. *Phys. B Condens. Matter* **2019**, 570, 148–156.
183. Li, Y.-H.; Wang, Z. Green Synthesis of Multifunctional Copper Sulfide for Efficient Adsorption and Photocatalysis. *Chem. Pap.* **2019**, 73 (9), 2297–2308.
184. Liu, Y.; Zhou, Z.; Zhang, S.; Luo, W.; Zhang, G. Controllable Synthesis of CuS Hollow Microflowers Hierarchical Structures for Asymmetric Supercapacitors. *Appl. Surf. Sci.* **2018**, 442, 711–719.

185. Wang, Z.; Zhang, X.; Zhang, Y.; Li, M.; Qin, C.; Bakenov, Z. Chemical Dealloying Synthesis of CuS Nanowire-on-Nanoplate Network as Anode Materials for Li-Ion Batteries. *Metals* **2018**, *8* (4), 252.
186. Diwate, K.; Rondia, S.; Mayabadi, A.; Rokade, A.; Waykar, R.; Borate, H.; Funde, A.; Shinde, M.; Rajendra Prasad, M. B.; Pathan, H.; Jadkar, S. Chemical Spray Pyrolysis Synthesis of Covellite Copper Sulphide (CuS) Thin Films for Economical Counter Electrode for DSSCs. *J. Mater. Sci. Mater. Electron.* **2018**, *29* (6), 4940–4947.
187. Ayodhya, D.; Veerabhadram, G. Preparation, Characterization, Photocatalytic, Sensing and Antimicrobial Studies of Calotropis Gigantea Leaf Extract Capped CuS NPs by a Green Approach. *J. Inorg. Organomet. Polym. Mater.* **2017**, *27* (1), 215–230.
188. Zhang, R.; Tutusaus, O.; Mohtadi, R.; Ling, C. Magnesium-Sodium Hybrid Battery with High Voltage, Capacity and Cyclability. *Front. Chem.* **2018**, *6*, 611.
189. Jana, S.; Thapa, R.; Maity, R.; Chattopadhyay, K. Optical and Dielectric Properties of PVA Capped Nanocrystalline PbS Thin Films Synthesized by Chemical Bath Deposition. *Phys. E Low-dimens. Syst. Nanostruct.* **2008**, *40* (10), 3121–3126.
190. Palchoudhury, S.; Ramasamy, K.; Gupta, R. K.; Gupta, A. Flexible Supercapacitors: A Materials Perspective. *Front. Mater.* **2019**, *5*, 83.
191. Gutierrez, I. Z.; Gerke, C.; Shen, Y.; Ximendes, E.; Silvan, M. M.; Marin, R.; Jaque, D.; Calderón, O. G.; Melle, S.; Rubio-Retama, J. Boosting the Near-Infrared Emission of Ag₂S Nanoparticles by a Controllable Surface Treatment for Bioimaging Applications. *ACS Appl. Mater. Interfaces* **2022**, *14*, 4871.
192. Iranmanesh, P.; Saeednia, S.; Nourzpoor, M. Characterization of ZnS Nanoparticles Synthesized by Co-Precipitation Method. *Chin. Phys. B* **2015**, *24* (4), 046104.
193. Murugadoss, G.; Rajamannan, B.; Ramasamy, V. Photoluminescence Properties of Monodispersed Mn²⁺ Doped ZnS Nanoparticles Prepared in High Temperature. *J. Mol. Struct.* **2011**, *991* (1–3), 202–206.
194. Zhang, Y. C.; Wang, G. Y.; Hu, X. Y.; Chen, W. W. Solvothermal Synthesis of Uniform Hexagonal-Phase ZnS Nanorods Using a Single-Source Molecular Precursor. *Mater. Res. Bull.* **2006**, *41* (10), 1817–1824.
195. Biswas, S.; Kar, S. Fabrication of ZnS Nanoparticles and Nanorods with Cubic and Hexagonal Crystal Structures: A Simple Solvothermal Approach. *Nanotechnology* **2008**, *19* (4), 045710.
196. Wang, J.; You, T.; Feng, H.; Chen, K.; Xu, B. Selective Synthesis of ZnS Nanowire-Bundles and Nanowires via Different Growth Mechanisms. *J. Cryst. Growth* **2013**, *374*, 60–64.
197. Lan, C.; Hong, K.; Wang, W.; Wang, G. Synthesis of ZnS Nanorods by Annealing Precursor ZnS Nanoparticles in NaCl Flux. *Solid State Commun.* **2003**, *125* (9), 455–458.
198. Ashwini, K.; Pandurangappa, C. Solvothermal Synthesis, Characterization and Photoluminescence Studies of ZnS: Eu Nanocrystals. *Opt. Mater.* **2014**, *37*, 537–542.
199. Liu, H.; Ni, Y.; Han, M.; Liu, Q.; Xu, Z.; Hong, J.; Ma, Z. A Facile Template-Free Route for Synthesis of Hollow Hexagonal ZnS Nano- and Submicro-Spheres. *Nanotechnology* **2005**, *16* (12), 2908.
200. Li, J.-R.; Huang, J.-F.; Cao, L.-Y.; Wu, J.-P.; He, H.-Y. Synthesis and Kinetics Research of ZnS Nanoparticles Prepared by Sonochemical Process. *Mater. Sci. Technol.* **2010**, *26* (10), 1269–1272.
201. Akhtar, M. S.; Riaz, S.; Mehmood, R. F.; Ahmad, K. S.; Alghamdi, Y.; Malik, M. A.; Naseem, S. Surfactant and Template Free Synthesis of Porous ZnS Nanoparticles. *Mater. Chem. Phys.* **2017**, *189*, 28–34.
202. She, Y.-Y.; Yang, J.; Qiu, K.-Q. Synthesis of ZnS Nanoparticles by Solid-Liquid Chemical Reaction with ZnO and Na₂S under Ultrasonic. *Trans. Nonferrous Metals Soc. China* **2010**, *20*, s211.
203. Sandana Mala, J. G.; Rose, C. Facile Production of ZnS Quantum Dot Nanoparticles by *Saccharomyces cerevisiae* MTCC 2918. *J. Biotechnol.* **2014**, *170*, 73–78.
204. Singh, A.; Viswanath, V.; Janu, V. Synthesis, Effect of Capping Agents, Structural, Optical and Photoluminescence Properties of ZnO Nanoparticles. *J. Lumin.* **2009**, *129* (8), 874–878.
205. Moore, D.; Wang, Z. L. Growth of Anisotropic One-Dimensional ZnS Nanostructures. *J. Mater. Chem.* **2006**, *16* (40), 3898–3905.
206. Yang, Z.; Li, Z.; Xu, M.; Ma, Y.; Zhang, J.; Su, Y.; Gao, F.; Wei, H.; Zhang, L.; Zhang, L. Controllable Synthesis of Fluorescent Carbon Dots and Their Detection Application as Nanoprobes. *Nano-Micro Lett.* **2013**, *5* (4), 247–259.
207. Lin, K. B.; Su, Y. H. Photoluminescence of Cu: ZnS, Ag: ZnS, and Au: ZnS Nanoparticles Applied in Bio-LED. *Appl. Phys. B Laser Opt.* **2013**, *113* (3), 351–359.
208. Al-Rasoul, K. T.; Abbas, N. K.; Shanan, Z. J. Structural and Optical Characterization of Cu and Ni Doped ZnS Nanoparticles. *Int. J. Electrochem. Sci.* **2013**, *8* (4), 5594–5604.
209. Chauhan, R.; Kumar, A.; Chaudhary, R. P. Photocatalytic Degradation of Methylene Blue with Fe Doped ZnS Nanoparticles. *Spectrochim. Acta Mol. Biomol. Spectrosc.* **2013**, *113*, 250–256.
210. Yang, Z.; Gao, D.; Zhu, Z.; Zhang, J.; Shi, Z.; Zhang, Z.; Xue, D. Ferromagnetism in Sphalerite and Wurtzite CdS Nanostructures. *Nanoscale Res. Lett.* **2013**, *8* (1), 1–9.
211. Kumar, S.; Verma, N. Room Temperature Magnetism in Cobalt-Doped ZnS Nanoparticles. *J. Supercond. Nov. Magnetism* **2015**, *28* (1), 137–142.
212. Murugadoss, G.; Ramasamy, V.; Rajesh Kumar, M. Photoluminescence Enhancement of Hexagonal-Phase ZnS: Mn Nanostructures Using 1-Thioglycolic Acid. *Appl. Nanosci.* **2014**, *4* (4), 449–454.
213. Rahdar, A. Effect of 2-mercaptoethanol as Capping Agent on ZnS Nanoparticles: Structural and Optical Characterization. *J. Nanostruct. Chem.* **2013**, *3* (1), 1–5.
214. Lenggoro, I. W.; Okuyama, K.; de la Mora, J. F.; Tohge, N. Preparation of ZnS Nanoparticles by Electrospray Pyrolysis. *J. Aerosol Sci.* **2000**, *31* (1), 121–136.
215. Salavati-Niasari, M.; Davar, F.; Mazaheri, M. Synthesis and Characterization of ZnS Nanoclusters via Hydrothermal Processing from [Bis (Salicylidene) Zinc (II)]. *J. Alloys Compd.* **2009**, *470* (1–2), 502–506.
216. Fang, X.-S.; Ye, C.-H.; Peng, X.-S.; Wang, Y.-H.; Wu, Y.-C.; Zhang, L.-D. Large-Scale Synthesis of ZnS Nanosheets by the Evaporation of ZnS Nanopowders. *J. Cryst. Growth* **2004**, *263* (1–4), 263–268.
217. Xiao, N.; Dai, Q.; Wang, Y.; Ning, J.; Liu, B.; Zou, G.; Zou, B. ZnS Nanocrystals and Nanoflowers Synthesized by a Green Chemistry Approach: Rare Excitonic Photoluminescence Achieved by the Tunable Molar Ratio of Precursors. *J. Hazard Mater.* **2012**, *211*, 62–67.
218. Shao, H.-F.; Qian, X.-F.; Zhu, Z.-K. The Synthesis of ZnS Hollow Nanospheres with Nanoporous Shell. *J. Solid State Chem.* **2005**, *178* (11), 3522–3528.
219. Malarkodi, C.; Annadurai, G. A Novel Biological Approach on Extracellular Synthesis and Characterization of Semiconductor Zinc Sulfide Nanoparticles. *Appl. Nanosci.* **2013**, *3* (5), 389–395.
220. Azizi, S.; Ahmad, M. B.; Namvar, F.; Mohamad, R. Green Biosynthesis and Characterization of Zinc Oxide Nanoparticles Using Brown Marine Macroalga *Sargassum muticum* Aqueous Extract. *Mater. Lett.* **2014**, *116*, 275–277.
221. Fu, L.; Fu, Z. *Plectranthus Amboinicus* Leaf Extract–Assisted Biosynthesis of ZnO Nanoparticles and Their Photocatalytic Activity. *Ceram. Int.* **2015**, *41* (2), 2492–2496.

222. Karthikeyan, B.; Arun, A.; Harini, L.; Sundar, K.; Kathiresan, T. Role of ZnS Nanoparticles on Endoplasmic Reticulum Stress-Mediated Apoptosis in Retinal Pigment Epithelial Cells. *Biol. Trace Elem. Res.* **2016**, 170 (2), 390–400.
223. Usman, M.; Fareed, A. G.; Amin, M. A Bibliometric Analysis of CO₂ Methanation: Research Trends and Comprehension of Effective Catalysts. *J. Iran. Chem. Soc.* **2024**, 1–17; <https://doi.org/10.1007/s13738-024-02998-9>.
224. Dash, C. S.; Prabakaran, S. Nano Resistive Memory (Re-RAM) Devices and Their Applications. *Rev. Adv. Mater. Sci.* **2019**, 58 (1), 248–270.
225. Zhang, H.; Zhang, S.; Pan, S.; Li, G.; Hou, J. A Simple Solution Route to ZnS Nanotubes and Hollow Nanospheres and Their Optical Properties. *Nanotechnology* **2004**, 15 (8), 945.
226. Zhang, H.; Banfield, J. F. Aggregation, Coarsening, and Phase Transformation in ZnS Nanoparticles Studied by Molecular Dynamics Simulations. *Nano Lett.* **2004**, 4 (4), 713–718.
227. Kozhevnikova, N.; Melkozerova, M.; Enyashin, A.; Tyutyunnik, A.; Pasechnik, L.; Baklanova, I. V.; Suntsov, A. Y.; Yushkov, A. A.; Buldakova, L. Y.; Yanchenko, M. Y. Janus ZnS Nanoparticles: Synthesis and Photocatalytic Properties. *J. Phys. Chem. Solid.* **2022**, 161, 110459.
228. Dhupar, A.; Sharma, V.; Kumar, S.; Gaur, A.; Sharma, J. K. Role of Aluminium Concentration on the Structural, Morphological, and Optical Properties of ZnS Nanoparticles. *J. Electron. Mater.* **2021**, 50 (12), 7174–7187.
229. Jubeer, E.; Manthrammel, M. A.; Shkir, M.; Subha, P.; Yahia, I.; Alfaify, S. Microwave Assisted Synthesis of Quantum Dots like ZnS Nanoparticles for Optoelectronic Applications: An Effect of CTAB Concentrations. *Optik* **2021**, 240, 166812.
230. Messalti, A. S.; El-Ghozzi, M.; Zambon, D.; Mahiou, R.; Setifi, Z. Investigating Photoluminescence Properties of Ca-Doped ZnS Nanoparticles Prepared via Hydrothermal Method. *J. Lumin.* **2021**, 238, 118227.
231. Mote, V. D.; Dole, B. Structural, Optical, and Magnetic Properties of Mn-Doped ZnS Nanoparticles. *J. Mater. Sci. Mater. Electron.* **2021**, 32 (1), 420–429.
232. Vijayan, S.; Dash, C. S.; Umadevi, G.; Sundararajan, M.; Mariappan, R. Investigation of Structural, Optical and Antibacterial Activity of ZnS Nanoparticles. *J. Cluster Sci.* **2021**, 32 (6), 1601–1608.
233. Ramki, K.; RajaPriya, A.; Sakthivel, P.; Murugadoss, G.; Thangamuthu, R.; Rajesh Kumar, M. Rapid Degradation of Organic Dyes under Sunlight Using Tin-Doped ZnS Nanoparticles. *J. Mater. Sci. Mater. Electron.* **2020**, 31 (11), 8750–8760.
234. Liu, J.; Ma, J.; Liu, Y.; Song, Z.; Sun, Y.; Fang, J.; Liu, Z. Preparation of ZnS Nanoparticles by Hydrothermal Method. *J. Phys. Conf.* **2009**, 486, L40–L43.
235. Fakher Alfahed, R.; Al-Asadi, A. S.; Badran, H. A.; Ajeel, K. I. Structural, Morphological, and Z-Scan Technique for a Temperature-Controllable Chemical Reaction Synthesis of Zinc Sulfide Nanoparticles. *Appl. Phys. B Laser Opt.* **2019**, 125 (3), 1–11.
236. Boulkroune, R.; Sebais, M.; Messai, Y.; Bourzami, R.; Schmutz, M.; Blanck, C.; Halimi, O.; Boudine, B. Hydrothermal Synthesis of Strontium-Doped ZnS Nanoparticles: Structural, Electronic and Photocatalytic Investigations. *Bull. Mater. Sci.* **2019**, 42 (5), 1–8.
237. Suganthi, N.; Pushpanathan, K. Photocatalytic Degradation and Antimicrobial Activity of Transition Metal Doped Mesoporous ZnS Nanoparticles. *Int. J. Environ. Sci. Technol.* **2019**, 16 (7), 3375–3388.
238. Naz, H.; Ali, R. N.; Zhu, X.; Xiang, B. Effect of Mo and Ti Doping Concentration on the Structural and Optical Properties of ZnS Nanoparticles. *Phys. E Low-dimens. Syst. Nanostruct.* **2018**, 100, 1–6.
239. Sabaghi, V.; Davar, F.; Fereshteh, Z. ZnS Nanoparticles Prepared via Simple Reflux and Hydrothermal Method: Optical and Photocatalytic Properties. *Ceram. Int.* **2018**, 44 (7), 7545–7556.
240. Bakhtkhosh, P.; Mehrizad, A. Sonochemical Synthesis of Sm-Doped ZnS Nanoparticles for Photocatalytic Degradation of Direct Blue 14: Experimental Design by Response Surface Methodology and Development of a Kinetics Model. *J. Mol. Liq.* **2017**, 240, 65–73.
241. Motejaddad Emrooz, H. B.; Rahmani, A. Synthesis, Characterization and Photocatalytic Behavior of Mesoporous ZnS Nanoparticles Prepared by Hybrid Salt Extraction and Structure Directing Agent Method. *Mater. Sci. Semicond. Process.* **2017**, 72, 15–21.
242. Jothibas, M.; Manoharan, C.; Johnson Jeyakumar, S.; Praveen, P.; Kartharinal Punithavathy, I.; Prince Richard, J. Synthesis and Enhanced Photocatalytic Property of Ni Doped ZnS Nanoparticles. *Sol. Energy* **2018**, 159, 434–443.
243. Xu, Z.; Liu, Y.; Tang, X. Radioluminescent Nuclear Battery Technology Development for Space Exploration. *Adv. Astronaut. Sci. Technol.* **2020**, 3 (2), 125–131.
244. Leem, J. W.; Jun, D.-H.; Heo, J.; Park, W.-K.; Park, J.-H.; Cho, W. J.; Kim, D. E.; Yu, J. S. Single-material Zinc Sulfide Bi-layer Antireflection Coatings for GaAs Solar Cells. *Opt Express* **2013**, 21 (105), A821–A8.
245. Mannix, A. J.; Kiraly, B.; Hersam, M. C.; Guisinger, N. P. Synthesis and Chemistry of Elemental 2D Materials. *Nat. Rev. Chem* **2017**, 1 (2), 1–14.
246. Si, K. J.; Dong, D.; Shi, Q.; Zhu, W.; Premaratne, M.; Cheng, W. Ultrathin Fresnel Lens Based on Plasmonic Nanosheets. *Mater. Today* **2019**, 23, 9–15.
247. Fan, F. R.; Wang, R.; Zhang, H.; Wu, W. Emerging Beyond-Graphene Elemental 2D Materials for Energy and Catalysis Applications. *Chem. Soc. Rev.* **2021**, 50, 10983.
248. Geng, X.; Yi, J. The Development of High-Temperature Superconductors and 2D Iron-Based Superconductors. In *Nano-Sized Multifunctional Materials*; Elsevier: Chatswood, 2019; pp. 117–144.
249. Late, D. J.; Bhat, A.; Rout, C. S. Fundamentals and Properties of 2D Materials in General and Sensing Applications. In *Fundamentals and Sensing Applications of 2D Materials*; Elsevier: Bangalore, 2019; pp. 5–24.
250. Venkateshalu, S.; Grace, A. N. MXenes A New Class of 2D Layered Materials: Synthesis, Properties, Applications as Supercapacitor Electrode and Beyond. *Appl. Mater. Today* **2020**, 18, 100509.
251. Raza, A.; Hassan, J.; Ikram, M.; Naz, S.; Haider, A.; Ul-Hamid, A.; Shahzadi, I.; Haider, J.; Goumri-Said, S.; Kanoun, M. B.; Ali, S. Molecular Docking and DFT Analyses of Magnetic Cobalt Doped MoS₂ and BN Nanocomposites for Catalytic and Antimicrobial Explorations. *Surface. Interfac.* **2021**, 27, 101571.
252. Dutta, S.; De, S. MoS₂ Nanosheet/rGO Hybrid: An Electrode Material for High Performance Thin Film Supercapacitor. *Mater. Today: Proc.* **2018**, 5 (3), 9771–9775.
253. Krithika, S.; Balavijayalakshmi, J. Synthesis and Fabrication of Nanostructured MoS₂/PANI Nanocomposites by Microwave Assisted Method for Electrochemical Applications. *Mater. Today: Proc.* **2022**, 50, 17–25.
254. Santhosha, A.; Nayak, P. K.; Pollok, K.; Langenhorst, F.; Adelhelm, P. Exfoliated MoS₂ as Electrode for All-Solid-State Rechargeable Lithium-Ion Batteries. *J. Phys. Chem. C* **2019**, 123 (19), 12126–12134.
255. Dharamalingam, K.; Arjun Kumar, B.; Ramalingam, G.; Sasi Florence, S.; Raju, K.; Senthil Kumar, P.; Govindaraju, S.; Thangavel, E. The Role of Sodium Dodecyl Sulfate Mediated Hydrothermal Synthesis of MoS₂ Nanosheets for Photocatalytic Dye Degradation and Dye-Sensitized Solar Cell Application. *Chemosphere* **2022**, 294, 133725.

256. Mutalik, C.; Krisnawati, D. I.; Patil, S. B.; Khafid, M.; Atmojo, D. S.; Santoso, P.; Lu, S.-C.; Wang, D.-Y.; Kuo, T.-R. Phase-Dependent MoS₂ Nanoflowers for Light-Driven Antibacterial Application. *ACS Sustainable Chem. Eng.* **2021**, 9 (23), 7904–7912.
257. Li, Y.; Song, Z.; Li, Y.; Chen, S.; Li, S.; Li, Y.; Wang, H.; Wang, Z. Hierarchical Hollow MoS₂ Microspheres as Materials for Conductometric NO₂ Gas Sensors. *Sens. Actuators, B* **2019**, 282, 259–267.
258. Wang, H.; Tran, D.; Moussa, M.; Stanley, N.; Tung, T. T.; Yu, L.; Yap, P. L.; Ding, F.; Qian, J.; Losic, D. Improved Preparation of MoS₂/Graphene Composites and Their Inks for Supercapacitors Applications. *Mater. Sci. Eng., B* **2020**, 262, 114700.
259. Sabeeh, H.; Zulfiqar, S.; Aadil, M.; Shahid, M.; Shakir, I.; Khan, M. A.; Warsi, M. F. Flake-Like MoS₂ Nano-Architecture and its Nanocomposite with Reduced Graphene Oxide for Hybrid Supercapacitors Applications. *Ceram. Int.* **2020**, 46 (13), 21064–21072.
260. Solomon, G.; Mazzaro, R.; Morandi, V.; Concina, I.; Vomiero, A. Microwave-Assisted vs. Conventional Hydrothermal Synthesis of MoS₂ Nanosheets: Application Towards Hydrogen Evolution Reaction. *Crystals* **2020**, 10 (11), 1040.
261. Saha, S.; Chaudhary, N.; Mittal, H.; Gupta, G.; Khanuja, M. Inorganic–Organic Nanohybrid of MoS₂–PANI for Advanced Photocatalytic Application. *Int. Nano Lett.* **2019**, 9 (2), 127–139.
262. Wang, F.; Liu, H.; Hu, K.; Li, Y.; Zeng, W.; Zeng, L. Hierarchical Composites of MoS₂ Nanoflower Anchored on SnO₂ Nanofiber for Methane Sensing. *Ceram. Int.* **2019**, 45 (17), 22981–22986.
263. Ali, B. A.; Metwalli, O. I.; Khalil, A. S.; Allam, N. K. Unveiling the Effect of the Structure of Carbon Material on the Charge Storage Mechanism in MoS₂-Based Supercapacitors. *ACS Omega* **2018**, 3 (11), 16301–16308.
264. Enaganti, P. K.; Selamneni, V.; Sahatiya, P.; Goel, S. MoS₂/Cellulose Paper Coupled with SnS₂ Quantum Dots as 2D/0D Electrode for High-Performance Flexible Supercapacitor. *New J. Chem.* **2021**, 45 (19), 8516–8526.
265. Krishnamoorthy, D.; Prakasam, A. Preparation of MoS₂/Graphene Nanocomposite-Based Photoanode for Dye-Sensitized Solar Cells (DSSCs). *Inorg. Chem. Commun.* **2020**, 118, 108016.
266. Hong, H. S.; Phuong, N. H.; Huong, N. T.; Nam, N. H.; Hue, N. T. Highly Sensitive and Low Detection Limit of Resistive NO₂ Gas Sensor Based on a MoS₂/Graphene Two-Dimensional Heterostructures. *Appl. Surf. Sci.* **2019**, 492, 449–454.
267. Tang, Q.; Jiang, D.-e. Mechanism of Hydrogen Evolution Reaction on 1T-MoS₂ from First Principles. *ACS Catal.* **2016**, 6 (8), 4953–4961.
268. Zhang, X.; Suo, H.; Zhang, R.; Niu, S.; Zhao, X. q.; Zheng, J.; Guo, C. Photocatalytic Activity of 3D Flower-like MoS₂ Hemispheres. *Mater. Res. Bull.* **2018**, 100, 249–253.
269. Liu, H.; Liu, X.; Wang, S.; Liu, H.-K.; Li, L. Transition Metal Based Battery-Type Electrodes in Hybrid Supercapacitors: A Review. *Energy Storage Mater.* **2020**, 28, 122–145.
270. Shahri, N. N. M.; Taha, H.; Hamid, M. H. S. A.; Kusri, E.; Lim, J.-W.; Hobley, J.; Usman, A. Antimicrobial Activity of Silver Sulfide Quantum Dots Functionalized with Highly Conjugated Schiff Bases in a One-Step Synthesis. *RSC Adv.* **2022**, 12 (5), 3136–3146.
271. Ren, Q.; Ma, Y.; Zhang, S.; Ga, L.; Ai, J. One-Step Synthesis of Water-Soluble Silver Sulfide Quantum Dots and Their Application to Bioimaging. *ACS Omega* **2021**, 6 (9), 6361–6367.
272. Bao, W.; Ga, L.; Zhao, R.; Ai, J. Microwave Synthesis of Silver Sulfide Near-Infrared Fluorescent Quantum Dots and Their Detection of Dopamine. *Biosens. Bioelectron. X* **2022**, 10, 100112.
273. Borovaya, M.; Naumenko, A.; Horionova, I.; Plokhovska, S.; Blume, Y.; Yemets, A. “Green” Synthesis of Ag₂S Nanoparticles, Study of Their Properties and Bioimaging Applications. *Appl. Nanosci.* **2020**, 10 (12), 4931–4940.
274. Sadovnikov, S.; Gusev, A. Atomic Displacements in the α–β Phase Transition in Ag₂S and in Ag₂S/Ag Heterostructure. *J. Exp. Theor. Phys.* **2019**, 129 (6), 1005–1016.
275. Gao, M.; Zhao, H.; Wang, Z.; Zhao, Y.; Zou, X.; Sun, L. Controllable Preparation of Ag₂S Quantum Dots with Size-Dependent Fluorescence and Cancer Photothermal Therapy. *Adv. Powder Technol.* **2021**, 32 (6), 1972–1982.
276. Wong, A.; Santos, A. M.; Cardenas-Riojas, A. A.; Baena-Moncada, A. M.; Sotomayor, M. D. Voltammetric Sensor Based on Glassy Carbon Electrode Modified with Hierarchical Porous Carbon, Silver Sulfide Nanoparticles and Fullerene for Electrochemical Monitoring of Nitrite in Food Samples. *Food Chem.* **2022**, 383, 132384.
277. Huang, D.; Chen, N.; Zhu, C.; Fang, G.; Zhou, D. The Overlooked Oxidative Dissolution of Silver Sulfide Nanoparticles by Thermal Activation of Persulfate: Processes, Mechanisms, and Influencing Factors. *Sci. Total Environ.* **2021**, 760, 144504.
278. Kothari, R.; Sharma, D. Biofabrication of Silver Sulphide Nanoparticles from Cinnamomum Tamala Leaves: A Next Generation Anti-Inflammatory Agent. *World J. Pharmaceut. Res.* **2020**, 1.
279. Hamed, M. S.; Adediji, M. A.; Zhang, Y.; Mola, G. T. Silver Sulphide Nano-Particles Enhanced Photo-Current in Polymer Solar Cells. *Appl. Phys. A: Mater. Sci. Process.* **2020**, 126 (3), 1–9.
280. Al-Shehri, B. M.; Shkir, M.; Bawazeer, T. M.; AlFaify, S.; Hamdy, M. S. A Rapid Microwave Synthesis of Ag₂S Nanoparticles and Their Photocatalytic Performance under UV and Visible Light Illumination for Water Treatment Applications. *Phys. E Low-dimens. Syst. Nanostruct.* **2020**, 121, 114060.
281. Kondratenko, T. S.; Zvyagin, A. I.; Smirnov, M. S.; Grevtseva, I. G.; Perepelitsa, A. S.; Ovchinnikov, O. V. Luminescence and Nonlinear Optical Properties of Colloidal Ag₂S Quantum Dots. *J. Lumin.* **2019**, 208, 193–200.
282. Awwad, A. M.; Salem, N. M.; Aqarbeh, M. M.; Abdulaziz, F. M. Green Synthesis, Characterization of Silver Sulfide Nanoparticles and Antibacterial Activity Evaluation. *Chem. Int.* **2020**, 6 (1), 42–48.
283. Elsaedy, H. A Low Temperature Synthesis of Ag₂S Nanostructures and Their Structural, Morphological, Optical, Dielectric and Electrical Studies: An Effect of SDS Surfactant Concentration. *Mater. Sci. Semicond. Process.* **2019**, 93, 360–365.
284. Ahmad, R.; Srivastava, R.; Bhardwaj, H.; Yadav, S.; Nand Singh, V.; Chand, S.; Singh, N.; Sapra, S. Size-Tunable Synthesis of Colloidal Silver Sulfide Nanocrystals for Solution-Processed Photovoltaic Applications. *ChemistrySelect* **2018**, 3 (20), 5620–5629.
285. Kang, M. H.; Kim, S. H.; Jang, S.; Lim, J. E.; Chang, H.; Kong, K.-j.; Myung, S.; Park, J. K. Synthesis of Silver Sulfide Nanoparticles and Their Photodetector Applications. *RSC Adv.* **2018**, 8 (50), 28447–28452.
286. Rao, C.; Thomas, P.; Kulkarni, G. *Nanocrystals: Synthesis, Properties and Applications*; Springer: Berlin, 2007.
287. Sankar, M.; Jothibas, M.; Muthuvel, A.; Rajeshwari, A.; Jeyakumar, S. J. Structural, Optical and Photocatalytic Degradation of Organic Dyes by Sol Gel Prepared Ni Doped CdS Nanoparticles. *Surface. Interfac.* **2020**, 21, 100775.
288. Ismail, R. A.; Khashan, K. S.; Alwan, A. M. Study of the Effect of Incorporation of CdS Nanoparticles on the Porous Silicon Photodetector. *Silicon* **2017**, 9 (3), 321–326.
289. Abd El-Sadek, M.; Wasly, H.; Batoo, K. M. X-Ray Peak Profile Analysis and Optical Properties of CdS Nanoparticles Synthesized via the Hydrothermal Method. *Appl. Phys. Mater. Sci. Process* **2019**, 125 (4), 283.
290. Martínez-Alonso, C.; Rodríguez-Castañeda, C. A.; Moreno-Romero, P.; Coria-Monroy, C.; Hu, H. Cadmium Sulfide Nanoparticles Synthesized

- by Microwave Heating for Hybrid Solar Cell Applications. *Int. J. Photoenergy* **2014**, 2014, 2014.
291. Samadi-Maybodi, A.; Sadeghi-Maleki, M.-R. In-situ Synthesis of High Stable CdS Quantum Dots and Their Application for Photocatalytic Degradation of Dyes. *Spectrochim. Acta Mol. Biomol. Spectrosc.* **2016**, 152, 156–164.
 292. Talwatkar, S.; Tamgadge, Y.; Sunatkari, A.; Gambhire, A.; Muley, G. Amino Acids (L-Arginine and L-Alanine) Passivated CdS Nanoparticles: Synthesis of Spherical Hierarchical Structure and Nonlinear Optical Properties. *Solid State Sci.* **2014**, 38, 42–48.
 293. Shariati, M. R.; Samadi-Maybodi, A.; Colagar, A. H. Exploration of Charge Carrier Delocalization in the Iron Oxide/CdS Type-II Heterojunction Band Alignment for Enhanced Solar-Driven Photocatalytic and Antibacterial Applications. *J. Hazard Mater.* **2019**, 366, 475–481.
 294. Tandon, S.; Vats, S. Microbial Biosynthesis of Cadmium Sulfide (CdS) Nanoparticles and Their Characterization. *Eur. J. Pharm. Med. Res.* **2016**, 3 (9), 545–550.
 295. Rahul, Singh, S.; Singh, P. K.; Paul Sharma, J.; Kakroo, S.; Sonker, R.; Khan, Z. H. Encompassing Environment Synthesis, Characterization and Photovoltaic Utilization of Cadmium Sulphide Quantum Dots. *Mater. Today: Proc.* **2021**, 34, 767–770.
 296. Ramanathan, K.; Contreras, M. A.; Perkins, C. L.; Asher, S.; Hasoon, F. S.; Keane, J.; Young, D.; Romero, M.; Metzger, W.; Noufi, R.; Ward, J.; Duda, A. Properties of 19.2% Efficiency ZnO/CdS/CuInGaSe₂ Thin-Film Solar Cells. *Prog. Photovoltaics Res. Appl.* **2003**, 11 (4), 225–230.
 297. Krishnakumar, V.; Han, J.; Klein, A.; Jaegermann, W. CdTe Thin Film Solar Cells with Reduced CdS Film Thickness. *Thin Solid Films* **2011**, 519 (21), 7138–7141.
 298. Shaikh, S.; Shkir, M.; Masumdar, E. Facile Fabrication and Characterization of Modified Spray Deposited Cadmium Sulphide Thin Films. *Phys. B Condens. Matter* **2019**, 571, 64–70.
 299. Ertis, I. F.; Boz, I. Synthesis and Optical Properties of Sb-Doped CdS Photocatalysts and Their Use in Methylene Blue (MB) Degradation. *Int. J. Chem. React. Eng.* **2017**, 15 (2), 1.
 300. Junaid, M.; Imran, M.; Ikram, M.; Naz, M.; Aqeel, M.; Afzal, H.; Majeed, H.; Ali, S. The Study of Fe-Doped CdS Nanoparticle-Assisted Photocatalytic Degradation of Organic Dye in Wastewater. *Appl. Nanosci.* **2019**, 9 (8), 1593–1602.
 301. Hadi, I. H.; Khashan, K. S.; Sulaiman, D. Cadmium Sulphide (CdS) Nanoparticles: Preparation and Characterization. *Mater. Today: Proc.* **2021**, 42, 3054–3056.
 302. Rathinamala, I.; Babu, I. M.; William, J. J.; Muralidharan, G.; Prithivikumaran, N. CdS Microspheres as Promising Electrode Materials for High Performance Supercapacitors. *Mater. Sci. Semicond. Process.* **2020**, 105, 104677.
 303. Alhammadi, S.; Minnam Reddy, V. R.; Gedi, S.; Park, H.; Sayed, M. S.; Shim, J.-J.; Kim, W. K. Performance of Graphene–CdS Hybrid Nanocomposite Thin Film for Applications in Cu(In,Ga)Se₂ Solar Cell and H₂ Production. *Nanomaterials* **2020**, 10 (2), 245.
 304. Mostafa, A. M.; Mwafy, E. A.; Hasanin, M. S. One-Pot Synthesis of Nanostructured CdS, CuS, and SnS by Pulsed Laser Ablation in Liquid Environment and Their Antimicrobial Activity. *Opt Laser. Technol.* **2020**, 121, 105824.
 305. Rafiq, A.; Imran, M.; Aqeel, M.; Naz, M.; Ikram, M.; Ali, S. Study of Transition Metal Ion Doped CdS Nanoparticles for Removal of Dye from Textile Wastewater. *J. Inorg. Organomet. Polym. Mater.* **2020**, 30 (6), 1915–1923.
 306. Abd El-Sadek, M. S.; Wasly, H. S.; Batoo, K. M. X-Ray Peak Profile Analysis and Optical Properties of CdS Nanoparticles Synthesized via the Hydrothermal Method. *Appl. Phys. A: Mater. Sci. Process.* **2019**, 125 (4), 283.
 307. Jabeen, U.; Adhikari, T.; Pathak, D.; Shah, S. M.; Nunzi, J.-M. Structural, Optical and Photovoltaic Properties of P3HT and Mn-Doped CdS Quantum Dots Based Bulk Heterojunction Hybrid Layers. *Opt. Mater.* **2018**, 78, 132–141.
 308. Iqbal, M.; Ali, A.; Nahyoon, N. A.; Majeed, A.; Pothu, R.; Phulpoto, S.; Thebo, K. H. Photocatalytic Degradation of Organic Pollutant with Nanosized Cadmium Sulfide. *Mater. Sci. Energy Technol.* **2019**, 2 (1), 41–45.
 309. Muniyappan, S.; Murugakoothan, P. Oleic Acid Capped Cadmium Sulphide (CdS) Quantum Dots: Discussions on Synthesis, Structural, Optical and Morphological Behavior. *Mater. Lett.* **2018**, 220, 277–280.
 310. Muniyappan, S.; Solaiyammal, T.; Sudhakar, K.; Nandhini, S.; Murugakoothan, P. Effective Chemical Route for the Synthesis of Thiophenol Stabilized Cadmium Sulphide (CdS) Quantum Dots: Compact Discussions on the Structural, Morphological, Optical and Dielectric Properties. *J. Mater. Sci. Mater. Electron.* **2018**, 29 (4), 2899–2906.
 311. Chandra, A.; Giri, S.; Das, B.; Ghosh, S.; Sarkar, S.; Chattopadhyay, K. K. NIR Photodetector Based on p-Silicon Nanowires/n-Cadmium Sulfide Nanoscale Junctions. *Appl. Surf. Sci.* **2021**, 548, 149256.
 312. Mohamed, H. Dependence of Efficiency of Thin-Film CdS/CdTe Solar Cell on Optical and Recombination Losses. *J. Appl. Phys.* **2013**, 113, 093105.
 313. Zhen, W.; Ning, X.; Yang, B.; Wu, Y.; Li, Z.; Lu, G. The Enhancement of CdS Photocatalytic Activity for Water Splitting via Anti-Photocorrosion by Coating Ni₂P Shell and Removing Nascent Formed Oxygen with Artificial Gill. *Appl. Catal. B Environ.* **2018**, 221, 243–257.
 314. Saleem, A. M.; Desmaris, V.; Enoksson, P. Performance Enhancement of Carbon Nanomaterials for Supercapacitors. *J. Nanomater.* **2016**, 2016, 1.
 315. Zhang, R.; Wang, C.; Chen, H.; Zhao, H.; Liu, J.; Li, Y.; Su, B. Cadmium Sulfide Inverse Opal for Photocatalytic Hydrogen Production. *Acta Phys. Chim. Sin.* **2020**, 36, 1803014.
 316. Ordenes-Aenishanslins, N. A.; Saona, L. A.; Durán-Toro, V. M.; Monrás, J. P.; Bravo, D. M.; Pérez-Donoso, J. M. Use of Titanium Dioxide Nanoparticles Biosynthesized by *Bacillus Mycoides* in Quantum Dot Sensitized Solar Cells. *Microb. Cell Factories* **2014**, 13 (1), 90.
 317. Mayorga-Martinez, C. C.; Ambrosi, A.; Eng, A. Y. S.; Sofer, Z.; Pumera, M. Transition Metal Dichalcogenides (MoS₂, MoSe₂, WS₂ and WSe₂) Exfoliation Technique Has Strong Influence Upon Their Capacitance. *Electrochem. Commun.* **2015**, 56, 24–28.
 318. Lin, Y. C.; Li, S.; Komsa, H. P.; Chang, L. J.; Krashenninnikov, A. V.; Eda, G.; Suenaga, K. Revealing the Atomic Defects of WS₂ Governing its Distinct Optical Emissions. *Adv. Funct. Mater.* **2018**, 28 (4), 1704210.
 319. Kozawa, D.; Carvalho, A.; Verzhbitskiy, I.; Giustiniano, F.; Miyauchi, Y.; Mouri, S.; Castro Neto, A. H.; Matsuda, K.; Eda, G. Evidence for Fast Interlayer Energy Transfer in MoSe₂/WS₂ Heterostructures. *Nano Lett.* **2016**, 16 (7), 4087–4093.
 320. Zhang, D.; Liu, T.; Jia, Y.; Chai, J.; Yang, X.; Cheng, J.; Cao, M. Morphology and Structure of WS₂ Nanosheets Prepared by Solvothermal Method with Surfactants. *Integrated Ferroelectr.* **2018**, 188 (1), 24–30.
 321. Rothschild, A.; Popovitz-Biro, R.; Lourie, O.; Tenne, R. Morphology of Multiwall WS₂ Nanotubes. *J. Phys. Chem. B* **2000**, 104 (38), 8976–8981.
 322. Eftekhari, A. Tungsten Dichalcogenides (WS₂, WSe₂, and WTe₂): Materials Chemistry and Applications. *J. Mater. Chem. A* **2017**, 5 (35), 18299–18325.
 323. Yang, J.; Voiry, D.; Ahn, S. J.; Kang, D.; Kim, A. Y.; Chhowalla, M.; Shin, H. S. Two-Dimensional Hybrid Nanosheets of Tungsten Disulfide and

- Reduced Graphene Oxide as Catalysts for Enhanced Hydrogen Evolution. *Angew. Chem.* **2013**, 125 (51), 13996–13999.
324. Yan, Y.; Xia, B.; Li, N.; Xu, Z.; Fisher, A.; Wang, X. Vertically Oriented MoS₂ and WS₂ Nanosheets Directly Grown on Carbon Cloth as Efficient and Stable 3-dimensional Hydrogen-Evolving Cathodes. *J. Mater. Chem. A* **2015**, 3 (1), 131–135.
 325. Nguyen, T. P.; Choi, S.; Jeon, J.-M.; Kwon, K. C.; Jang, H. W.; Kim, S. Y. Transition Metal Disulfide Nanosheets Synthesized by Facile Sonication Method for the Hydrogen Evolution Reaction. *J. Phys. Chem. C* **2016**, 120 (7), 3929–3935.
 326. Akple, M. S.; Apeviyeku, H. K. Synthesis and Density-Functional-Theory Calculations of Electronic Band Structure of Hollow Sphere WS₂. *Mater. Sci.* **2018**, 36 (3), 409–418.
 327. Hasani, A.; Nguyen, T. P.; Tekalgne, M.; Van Le, Q.; Choi, K. S.; Lee, T. H.; Jung Park, T.; Jang, H. W.; Kim, S. Y. The Role of Metal Dopants in WS₂ Nanoflowers in Enhancing the Hydrogen Evolution Reaction. *Appl. Catal. Gen.* **2018**, 367, 73–79.
 328. Cao, S.; Zhao, C.; Peng, L.; Han, T. Synthesis of Uniform WS₂ Nanoflowers via a Sodium Silicate-Assisted Hydrothermal Process. *J. Mater. Sci. Mater. Electron.* **2016**, 27 (4), 3821–3825.
 329. Cheng, L.; Huang, W.; Gong, Q.; Liu, C.; Liu, Z.; Li, Y.; Dai, H. I. Innenrücktitelbild: Ultrathin WS₂ Nanoflakes as a High-Performance Electrocatalyst for the Hydrogen Evolution Reaction. *Angew. Chem.* **2014**, 126 (30), 8091.
 330. Kim, M.-J.; Jeon, S.-J.; Kang, T. W.; Ju, J.-M.; Yim, D.; Kim, H.-I.; Park, J. H.; Kim, J. H. 2H-WS₂ Quantum Dots Produced by Modulating the Dimension and Phase of 1T-Nanosheets for Antibody-Free Optical Sensing of Neurotransmitters. *ACS Appl. Mater. Interfaces* **2017**, 9 (14), 12316–12323.
 331. Li, W.; Chen, D.; Xia, F.; Tan, J. Z. Y.; Song, J.; Song, W.-G.; Caruso, R. A. Flowerlike WSe₂ and WS₂ Microspheres: One-Pot Synthesis, Formation Mechanism and Application in Heavy Metal Ion Sequestration. *Chem. Commun.* **2016**, 52 (24), 4481–4484.
 332. Fatima, T.; Husain, S.; Narang, J.; Khanuja, M.; Shetti, N. P.; Reddy, K. R. Novel Tungsten Disulfide (WS₂) Nanosheets for Photocatalytic Degradation and Electrochemical Detection of Pharmaceutical Pollutants. *J. Water Proc. Eng.* **2022**, 47, 102717.
 333. Chen, T.-W.; Rajaji, U.; Chen, S.-M.; Jothi Ramalingam, R. A Relative Study on Sonochemically Synthesized Mesoporous WS₂ Nanorods & Hydrothermally Synthesized WS₂ Nanoballs Towards Electrochemical Sensing of Psychoactive Drug (Clonazepam). *Ultrason. Sonochem.* **2019**, 54, 79–89.
 334. Sun, L.; Geng, J.; Gao, M.; Zheng, D.; Jing, Z.; Zhao, Q.; Lin, J. Novel WS₂/Fe_{0.95}S_{1.05} Hierarchical Nanosphere as a Highly Efficient Electrocatalyst for Hydrogen Evolution Reaction. *Chem. Eur J.* **2021**, 27 (42), 10998–11004.
 335. Fatima, T.; Husain, S.; Narang, J.; Khanuja, M.; Shetti, N. P.; Reddy, K. R. Synthesis of Tribological WS₂ Powder from WO₃ Prepared by Ultrasonic Spray Pyrolysis (USP). *Metals* **2019**, 9 (3), 277.
 336. Meza, E.; Diaz, R. E.; Li, C. W. Solution-Phase Activation and Functionalization of Colloidal WS₂ Nanosheets with Ni Single Atoms. *ACS Nano* **2020**, 14 (2), 2238–2247.
 337. Vaziri, H. S.; Shokuhfar, A.; Afghahi, S. S. Synthesis of WS₂/CNT Hybrid Nanoparticles for Fabrication of Hybrid Aluminum Matrix Nanocomposite. *Mater. Res. Express* **2020**, 7 (2), 025034.
 338. Valappil, M. O.; Anil, A.; Shaijumon, M.; Pillai, V. K.; Alwarappan, S. A Single-step Electrochemical Synthesis of Luminescent WS₂ Quantum Dots. *Chem. Eur J.* **2017**, 23 (38), 9144–9148.
 339. Goldman, E. B.; Zak, A.; Tenne, R.; Kartvelishvili, E.; Levin-Zaidman, S.; Neumann, Y.; Stiubea-Cohen, R.; Palmon, A.; Hovav, A.-H.; Aframian, D. J. Biocompatibility of Tungsten Disulfide Inorganic Nanotubes and Fullerene-Like Nanoparticles with Salivary Gland Cells. *Tissue Eng.* **2015**, 21 (5–6), 1013–1023.
 340. Ashraf, W.; Fatima, T.; Srivastava, K.; Khanuja, M. Superior Photocatalytic Activity of Tungsten Disulfide Nanostructures: Role of Morphology and Defects. *Appl. Nanosci.* **2019**, 9 (7), 1515–1529.
 341. Song, Y.; Yan, X.; Ostermeyer, G.; Li, S.; Qu, L.; Du, D.; Li, Z.; Lin, Y. Direct Cytosolic microRNA Detection Using Single-Layer Perfluorinated Tungsten Diselenide Nanoplateform. *Anal. Chem.* **2018**, 90 (17), 10369–10376.
 342. Rohaizad, N.; Mayorga-Martinez, C. C.; Sofer, Z.; Pumera, M. 1T-phase Transition Metal Dichalcogenides (MoS₂, MoSe₂, WS₂, and WSe₂) with Fast Heterogeneous Electron Transfer: Application on Second-Generation Enzyme-Based Biosensor. *ACS Appl. Mater. Interfaces* **2017**, 9 (46), 40697–40706.
 343. Kim, H.-C.; Kim, H.; Lee, J.-U.; Lee, H.-B.; Choi, D.-H.; Lee, J.-H.; Lee, W. H.; Jhang, S. H.; Park, B. H.; Cheong, H.; Lee, S.-W.; Chung, H.-J. Engineering Optical and Electronic Properties of WS₂ by Varying the Number of Layers. *ACS Nano* **2015**, 9 (7), 6854–6860.
 344. Mohamad Latiff, N.; Wang, L.; Mayorga-Martinez, C. C.; Sofer, Z.; Fisher, A. C.; Pumera, M. Valence and Oxide Impurities in MoS₂ and WS₂ Dramatically Change Their Electrocatalytic Activity Towards Proton Reduction. *Nanoscale* **2016**, 8 (37), 16752–16760.
 345. Palchoudhury, S.; Ramasamy, K.; Gupta, R. K.; Gupta, A. Flexible Supercapacitors: A Materials Perspective. *Front. Mater.* **2019**, 5, 1.
 346. Raghavendra, K. V. G.; Prasanna, A. L.; Sreekanth, T.; Kim, J.; Yoo, K. Novel Hydrothermal Synthesis of Time-Variant Tungsten Disulfide Electrode Material for High-Performance Supercapacitors. *J. Energy Storage* **2021**, 34, 102197.
 347. Jha, R. K.; Nanda, A.; Bhat, N. Ultrasonication Assisted Fabrication of a Tungsten Sulfide/tungstite Heterostructure for Ppb-Level Ammonia Detection at Room Temperature. *RSC Adv.* **2020**, 10 (37), 21993–22001.
 348. Sinha, S. S.; Yadgarov, L.; Aliev, S. B.; Feldman, Y.; Pinkas, I.; Chithaiah, P.; Ghosh, S.; Idelevich, A.; Zak, A.; Tenne, R. MoS₂ and WS₂ Nanotubes: Synthesis, Structural Elucidation, and Optical Characterization. *J. Phys. Chem. C* **2021**, 125 (11), 6324–6340.
 349. Nguyen, T. P.; Nguyen, D. L. T.; Nguyen, V.-H.; Le, T.-H.; Ly, Q. V.; Vo, D.-V. N.; Nguyen, Q. V.; Le, H. S.; Jang, H. W.; Kim, S. Y.; Le, Q. V. Facile Synthesis of WS₂ Hollow Spheres and Their Hydrogen Evolution Reaction Performance. *Appl. Surf. Sci.* **2020**, 505, 144574.
 350. Pazhamalai, P.; Krishnamoorthy, K.; Sahoo, S.; Mariappan, V. K.; Kim, S.-J. Copper Tungsten Sulfide Anchored on Ni-Foam as a High-Performance Binder Free Negative Electrode for Asymmetric Supercapacitor. *Chem. Eng. J.* **2019**, 359, 409–418.
 351. Bayat, A.; Saievar-Iranizad, E. Synthesis of Blue Photo-Luminescent WS₂ Quantum Dots via Ultrasonic Cavitation. *J. Lumin.* **2017**, 185, 236–240.
 352. Zhou, L.; Yan, S.; Wu, H.; Song, H.; Shi, Y. Facile Sonication Synthesis of WS₂ Quantum Dots for Photoelectrochemical Performance. *Catalysts* **2017**, 7 (1), 18.
 353. Qazi, A.; Nazir, M.; Shahid, M.; Butt, S.; Basit, M. A. Facile Development of Hybrid Bulk-Nanostructured SnSe/SnS for Anti-bacterial Activity with Negligible Cytotoxicity. *J. Cluster Sci.* **2021**, 32 (3), 665–672.
 354. Herron, S. M.; Tanskanen, J. T.; Roelofs, K. E.; Bent, S. F. Highly Textured Tin(II) Sulfide Thin Films Formed from Sheetlike Nanocrystal Inks. *Chem. Mater.* **2014**, 26 (24), 7106–7113.
 355. Banai, R. E.; Burton, L. A.; Choi, S. G.; Hofherr, F.; Sorgenfrei, T.; Walsh, A.; To, B.; Croll, A.; Brownson, J. R. S. Ellipsometric Characterization and Density-Functional Theory Analysis of Anisotropic Optical Properties of Single-Crystal α -SnS. *J. Appl. Phys.* **2014**, 116 (1), 013511.

356. Reddy, N. K.; Devika, M.; Gunasekhar, K.; Gopal, E. Fabrication of Photovoltaic Devices Using ZnO Nanostructures and SnS Thin Films. *Nano* **2016**, *11* (07), 1650077.
357. Xin, C.; Zheng, J.; Su, Y.; Li, S.; Zhang, B.; Feng, Y.; Pan, F. Few-Layer Tin Sulfide: A New Black-Phosphorus-Analogue 2D Material with a Sizeable Band Gap, Odd–Even Quantum Confinement Effect, and High Carrier Mobility. *J. Phys. Chem. C* **2016**, *120* (39), 22663–22669.
358. Brent, J. R.; Lewis, D. J.; Lorenz, T.; Lewis, E. A.; Savjani, N.; Haigh, S. J.; Seifert, G.; Derby, B.; O'Brien, P. Tin(II) Sulfide (SnS) Nanosheets by Liquid-Phase Exfoliation of Herzenbergite: IV–VI Main Group Two-Dimensional Atomic Crystals. *J. Am. Chem. Soc.* **2015**, *137* (39), 12689–12696.
359. Ettema, A. R. H. F.; de Groot, R. A.; Haas, C.; Turner, T. S. Electronic Structure of SnS Deduced from Photoelectron Spectra and Band-Structure Calculations. *Phys. Rev. B* **1992**, *46* (12), 7363–7373.
360. Lambros, A. P.; Geraleas, D.; Economou, N. A. Optical Absorption Edge in SnS. *J. Phys. Chem. Solid.* **1974**, *35* (4), 537–541.
361. Manukumar, K. N.; Nagaraju, G.; Kishore, B.; Madhu, C.; Munichandraiah, N. Ionic Liquid-Assisted Hydrothermal Synthesis of SnS Nanoparticles: Electrode Materials for Lithium Batteries, Photoluminescence and Photocatalytic Activities. *J. Energy Chem.* **2018**, *27* (3), 806–812.
362. Modi, K. H.; Pataniya, P. M.; Patel, V.; Sumesh, C. K. Microwave Assisted Synthesis of SnS Nanosheets for Fabrication of Large Area SnS/Si Heterojunction. *Sol. Energy* **2021**, *221*, 412–417.
363. Tian, H.; Fan, C.; Liu, G.; Yuan, S.; Zhang, Y.; Wang, M.; Li, E. Ultrafast Broadband Photodetector Based on SnS Synthesized by Hydrothermal Method. *Appl. Surf. Sci.* **2019**, *487*, 1043–1048.
364. Hegde, S. S.; Surendra, B. S.; Talapatadur, V.; Murahari, P.; Ramesh, K. Visible Light Photocatalytic Properties of Cubic and Orthorhombic SnS Nanoparticles. *Chem. Phys. Lett.* **2020**, *754*, 137665.
365. Gajendiran, J.; Gnanam, S.; Senthil, V. P.; Ramana Ramya, J.; Ramachandran, K.; Vijayakumar, V.; Gokul Raj, S.; Ramesh Kumar, G.; Sivakumar, N. Hydrothermal Synthesis of Undoped and Inner Transition Metals (Neodymium (Nd), Gadolinium (Gd)) Doped Tin Monosulfide (SnS) Nanostructures: Comparative Study of the Morphological, Opto-Magnetic Properties and Antibacterial Performance. *Chem. Phys. Lett.* **2022**, *796*, 139569.
366. Ma, Y. T.; Ma, S.; Tang, J.; Wu, Z. G.; Shi, J.; Zhao, Y.; Pei, S. T.; Cao, P. F. Hydrothermal-Synthesis Flower-like SnS Microspheres Gas Sensors Bonded Physically by PVDF for Detecting Ethanol. *Vacuum* **2020**, *181*, 109657.
367. Ali, S.; Wang, F.; Zubair Iqbal, M.; Ullah Shah, H.; Zafar, S. Hydrothermal Synthesis, Characterization and Optical Properties of SnS Prismatic Nanorods. *Mater. Lett.* **2017**, *206*, 22–25.
368. Chalapathi, U.; Poornaprakash, B.; Park, S.-H. Growth and Properties of Cubic SnS Films Prepared by Chemical Bath Deposition Using EDTA as the Complexing Agent. *J. Alloys Compd.* **2016**, *689*, 938–944.
369. Polivtseva, S.; Katerski, A.; Kärber, E.; Oja Acik, I.; Mere, A.; Mikli, V.; Krunk, M. Post-Deposition Thermal Treatment of Sprayed SnS Films. *Thin Solid Films* **2017**, *633*, 179–184.
370. Reddy, B. P.; Sekhar, M. C.; Vattikuti, S. V. P.; Suh, Y.; Park, S.-H. Solution-Based Spin-Coated Tin Sulfide Thin Films for Photovoltaic and Supercapacitor Applications. *Mater. Res. Bull.* **2018**, *103*, 13–18.
371. Banu, S.; Ahn, S. J.; Eo, Y. J.; Gwak, J.; Cho, A. Tin Monosulfide (SnS) Thin Films Grown by Liquid-Phase Deposition. *Sol. Energy* **2017**, *145*, 33–41.
372. Ceylan, A. Synthesis of SnS Thin Films via High Vacuum Sulfidation of Sputtered Sn Thin Films. *Mater. Lett.* **2017**, *201*, 194–197.
373. Al-Shakban, M.; Xie, Z.; Savjani, N.; Malik, M. A.; O'Brien, P. A Facile Method for the Production of SnS Thin Films from Melt Reactions. *J. Mater. Sci.* **2016**, *51* (13), 6166–6172.
374. Ray, S. C.; Karanjai, M. K.; DasGupta, D. Structure and Photoconductive Properties of Dip-Deposited SnS and SnS₂ Thin Films and Their Conversion to Tin Dioxide by Annealing in Air. *Thin Solid Films* **1999**, *350* (1), 72–78.
375. Shao, Z.; Shi, C.; Chen, J.; Zhang, Y. Preparation of SnS Thin Films with Gear-like Sheet Appearance by Close-Spaced Vacuum Thermal Evaporation. *Int. J. Mod. Phys. B* **2017**, *31* (16–19), 1744054.
376. Arepalli, V. K.; Shin, Y.; Kim, J. Photovoltaic Behavior of the Room Temperature Grown RF-Sputtered SnS Thin Films. *Opt. Mater.* **2019**, *88*, 594–600.
377. Zhang, G.; Fu, Z.; Wang, Y.; Wang, H. Facile Synthesis of Hierarchical SnS Nanostructures and Their Visible Light Photocatalytic Properties. *Adv. Powder Technol.* **2015**, *26* (4), 1183–1190.
378. de Kergommeaux, A.; Lopez-Haro, M.; Pouget, S.; Zuo, J.-M.; Lebrun, C.; Chandezon, F.; Aldakov, D.; Reiss, P. Synthesis Internal Structure, and Formation Mechanism of Monodisperse Tin Sulfide Nanoplatelets. *J. Am. Chem. Soc.* **2015**, *137* (31), 9943–9952.
379. Behera, C.; Ghosh, S. P.; Kar, J. P.; Samal, S. L. Facile Synthesis and Enhanced Photocatalytic Activity of Ag–SnS Nanocomposites. *New J. Chem.* **2020**, *44* (27), 11684–11693.
380. Zhu, H.; Yang, D.; Ji, Y.; Zhang, H.; Shen, X. Two-Dimensional SnS Nanosheets Fabricated by a Novel Hydrothermal Method. *J. Mater. Sci.* **2005**, *40* (3), 591–595.
381. Shan, W.; Fu, Z.; Ma, M.; Liu, Z.; Xue, Z.; Xu, J.; Zhang, F.; Li, Y. Facile Chemical Bath Synthesis of SnS Nanosheets and Their Ethanol Sensing Properties. *Sensors* **2019**, *19* (11), 2581.
382. Qin, Y.; Qiu, P.; Bai, Y. First-Principles Calculations Combined with Experiments to Study the Gas-Sensing Performance of Zn-Substituted SnS. *Phys. Chem. Chem. Phys.* **2020**, *22* (31), 17513–17522.
383. Zhong, F.; Wu, Z.; Guo, J.; Jia, D. Ni-Doped ZnS Nanospheres Decorated with Au Nanoparticles for Highly Improved Gas Sensor Performance. *Sensors* **2018**, *18* (9), 2882.
384. Wu, J.; Zhang, D.; Cao, Y. Fabrication of Iron-Doped Titanium Dioxide Quantum Dots/Molybdenum Disulfide Nanoflower for Ethanol Gas Sensing. *J. Colloid Interface Sci.* **2018**, *529*, 556–567.
385. Huang, Z.; Wei, D.; Wang, T.; Jiang, W.; Liu, F.; Chuai, X.; Liang, X.; Gao, Y.; Sun, P.; Yan, X.; Zheng, J.; Song, H.; Lu, G. Excellent Gas Sensing of Hierarchical Urchin-Shaped Zn Doped Cadmium Sulfide. *J. Alloys Compd.* **2019**, *773*, 299–304.
386. Kim, H.-J.; Choi, K.-I.; Kim, K.-M.; Na, C. W.; Lee, J.-H. Highly Sensitive C₂H₅OH Sensors Using Fe-Doped NiO Hollow Spheres. *Sens. Actuators, B* **2012**, *171–172*, 1029–1037.
387. Hao, J.; Zhang, D.; Sun, Q.; Zheng, S.; Sun, J.; Wang, Y. Hierarchical SnS₂/SnO₂ Nanoheterojunctions with Increased Active-Sites and Charge Transfer for Ultrasensitive NO₂ Detection. *Nanoscale* **2018**, *10* (15), 7210–7217.
388. Miranti, R.; Septianto, R. D.; Kikitsu, T.; Hashizume, D.; Matsushita, N.; Iwasa, Y.; Bisri, S. Z. π-SnS Colloidal Nanocrystals with Size-Dependent Band Gaps. *J. Phys. Chem. C* **2022**, *126* (11), 5323–5332.
389. Chen, R.; Li, L.; Jiang, L.; Yu, X.; Zhu, D.; Xiong, Y.; Zheng, D.; Yang, W. Small-Diameter P-type SnS Nanowire Photodetectors and Phototransistors with Low-Noise and High-Performance. *Nanotechnology* **2022**, *33* (13), 135707.
390. Alagarasan, D.; Hegde, S. S.; Varadarajaperumal, S.; Arun Kumar, K. D.; Naik, R.; Panjalingam, S. P.; Massoud, E. E. S.; Ganesan, R. Effect of Annealing Temperature on SnS Thin Films for Photodetector Applications. *J. Mater. Sci. Mater. Electron.* **2022**, *33* (8), 4794–4805.
391. Bai, Y.; Qin, Y.; Qiu, P. Boosting the Acetone Sensing of SnS Nanoflakes by Spin Mn Substitution: A Novel Adsorption–Desorption Perspective. *Environ. Sci.: Nano* **2021**, *8* (4), 1096–1108.

392. Son, S.-I.; Shin, D.; Son, Y. G.; Son, C. S.; Kim, D. R.; Park, J. H.; Kim, S.; Hwang, D.; Song, P. K. Effect of Working Pressure on the Properties of RF Sputtered SnS Thin Films and Photovoltaic Performance of SnS-Based Solar Cells. *J. Alloys Compd.* **2020**, *831*, 154626.
393. Ahmed, S.; Aktar, A.; Hossain, J.; Ismail, A. B. M. Enhancing the Open Circuit Voltage of the SnS Based Heterojunction Solar Cell Using NiO HTL. *Sol. Energy* **2020**, *207*, 693–702.
394. Jia, T.; Fu, F.; Li, J.; Deng, Z.; Long, F.; Yu, D.; Cui, Q.; Wang, W. Rational Construction of Direct Z-Scheme SnS/g-C₃N₄ Hybrid Photocatalyst for Significant Enhancement of Visible-Light Photocatalytic Activity. *Appl. Surf. Sci.* **2020**, *499*, 143941.
395. Baláž, P.; Pourghahramani, P.; Dutková, E.; Fabián, M.; Kováč, J.; Satka, A. PbS Nanostructures Synthesized via Surfactant Assisted Mechanochemical Route. *Cent. Eur. J. Chem.* **2009**, *7* (2), 215–221.
396. Salavati-Niasari, M.; Sobhani, A.; Khoshrooz, S.; Mirzanasiri, N. Preparation and Characterization of PbS Nanoparticles via Cyclic Microwave Radiation Using Precursor of Lead (II) Oxalate. *J. Cluster Sci.* **2014**, *25* (4), 937–947.
397. Ebnalwaleed, A.; Essai, M. H.; Hasaneen, B.; Mansour, H. E. Facile and Surfactant-Free Hydrothermal Synthesis of PbS Nanoparticles: The Role of Hydrothermal Reaction Time. *J. Mater. Sci. Mater. Electron.* **2017**, *28* (2), 1958–1965.
398. Shkir, M.; AlFaify, S. A Facile Low-Temperature Synthesis of Nanosheets Assembled PbS Microflowers and Their Structural, Morphological, Optical, Photoluminescence, Dielectric and Electrical Studies. *Mater. Res. Express* **2019**, *6* (10), 105013.
399. Hamdedein, A.; Aboud, A. A.; El Roubi, W. M. A.; Khan, M. D.; Farghali, A. A.; Khedr, M. H.; Revaprasadu, N. Effect of La Doping on the Structural and Gas Sensing Properties of PbS Thin Films Deposited by Spray Pyrolysis. *IOP Conf. Ser. Mater. Sci. Eng.* **2021**, *1046*, 012026.
400. Onwudiwe, D. C. Microwave-Assisted Synthesis of PbS Nanostructures. *Heliyon* **2019**, *5* (3), e01413.
401. Abargues, R.; Navarro, J.; Rodríguez-Cantó, P. J.; Maulu, A.; Sánchez-Royo, J. F.; Martínez-Pastor, J. P. Enhancing the Photocatalytic Properties of PbS QD Solids: The Ligand Exchange Approach. *Nanoscale* **2019**, *11* (4), 1978–1987.
402. Saah, S. A.; Khan, M. D.; Awudza, J. A.; Revaprasadu, N.; O'Brien, P. A Facile Green Synthesis of Ultranarrow PbS Nanorods. *J. Inorg. Organomet. Polym. Mater.* **2019**, *29* (6), 2274–2281.
403. Hamdedein, A.; Aboud, A. A.; El Roubi, W. M. A.; Khan, M. D.; Farghali, A. A.; Khedr, M. H.; Revaprasadu, N. Effect of La Doping on the Structural and Gas Sensing Properties of PbS Thin Films Deposited by Spray Pyrolysis. *IOP Conf. Ser. Mater. Sci. Eng.* **2021**, *1046* (1), 012026.
404. Li, M.; Liu, Y.; Zhang, Y.; Chang, C.; Zhang, T.; Yang, D.; Xiao, K.; Arbiol, J.; Ibanez, M.; Cabot, A. Room Temperature Aqueous-Based Synthesis of Copper-Doped Lead Sulfide Nanoparticles for Thermoelectric Application. *Chem. Eng. J.* **2022**, *433*, 133837.
405. Mochalov, L.; Logunov, A.; Prokhorov, I.; Sazanova, T.; Kudrin, A.; Yunin, P.; Zelentsov, S.; Letnianshchik, A.; Starostin, N.; Boreman, G.; Vorotyntsev, V. Plasma-Chemical Synthesis of Lead Sulphide Thin Films for Near-IR Photodetectors. *Plasma Chem. Plasma Process.* **2021**, *41* (1), 493–506.
406. Asunskis, D. J.; Bolotin, I. L.; Hanley, L. Nonlinear Optical Properties of PbS Nanocrystals Grown in Polymer Solutions. *J. Phys. Chem. C* **2008**, *112* (26), 9555–9558.
407. Colvin, V. L.; Schlamp, M. C.; Alivisatos, A. P. Light-emitting Diodes Made from Cadmium Selenide Nanocrystals and a Semiconducting Polymer. *Nature* **1994**, *370* (6488), 354–357.
408. Kane, R. S.; Cohen, R. E.; Silbey, R. Theoretical Study of the Electronic Structure of PbS Nanoclusters. *J. Phys. Chem.* **1996**, *100* (19), 7928–7932.
409. Tulsani, S. R.; Rath, A. K.; Late, D. J. 2D-MoS₂ Nanosheets as Effective Hole Transport Materials for Colloidal PbS Quantum Dot Solar Cells. *Nanoscale Adv.* **2019**, *1* (4), 1387–1394.
410. Hirata, H.; Higashiyama, K. Analytical Study of the Lead Ion-Selective Ceramic Membrane Electrode. *Bull. Chem. Soc. Jpn.* **1971**, *44* (9), 2420–2423.
411. Nam, M.; Park, J.; Kim, S.-W.; Lee, K. Broadband-Absorbing Hybrid Solar Cells with Efficiency Greater Than 3% Based on a Bulk Heterojunction of PbS Quantum Dots and a Low-Bandgap Polymer. *J. Mater. Chem. A* **2014**, *2* (11), 3978–3985.
412. Wise, F. W. Lead Salt Quantum Dots: The Limit of Strong Quantum Confinement. *Acc. Chem. Res.* **2000**, *33* (11), 773–780.
413. Shahzad, U.; Marwani, H. M.; Saeed, M.; Asiri, A. M.; Repon, M. R.; Althomali, R. H.; Rahman, M. M. Progress and Perspectives on Promising Covalent-Organic Frameworks (COFs) Materials for Energy Storage Capacity. *Chem. Rec.* **2023**, *24*, e202300285.
414. Shahzad, U.; Marwani, H. M.; Saeed, M.; Asiri, A. M.; Rahman, M. M. Two-Dimensional MXenes as Emerging Materials: A Comprehensive Review. *ChemistrySelect* **2023**, *8* (25), e202300737.
415. Shahzad, U.; Marwani, H. M.; Saeed, M.; Asiri, A. M.; Althomali, R. H.; Rahman, M. M. Exploration of Porous Metal-Organic Frameworks (MOFs) for an Efficient Energy Storage Applications. *J. Energy Storage* **2023**, *74*, 109518.
416. Saeed, M.; Marwani, H. M.; Shahzad, U.; Asiri, A. M.; Hussain, I.; Rahman, M. M. Utilizing Nanostructured Materials for Hydrogen Generation, Storage, and Diverse Applications. *Chem. Asian J.* **2023**, e202300593; <https://doi.org/10.1002/asia.202300593>.
417. Saeed, M.; Marwani, H. M.; Shahzad, U.; Asiri, A. M.; Rahman, M. M. Recent Advances, Challenges, and Future Perspectives of ZnO Nanostructure Materials Towards Energy Applications. *Chem. Rec.* **2023**, *24*, e202300106.
418. Freitas, J. N.; Gonçalves, A. S.; Nogueira, A. F. A Comprehensive Review of the Application of Chalcogenide Nanoparticles in Polymer Solar Cells. *Nanoscale* **2014**, *6* (12), 6371–6397.
419. Shkir, M.; Khan, M. T.; Ashraf, I.; AlFaify, S.; El-Toni, A. M.; Aldalbahi, A.; Ghaithan, H.; Khan, A. Rapid Microwave-Assisted Synthesis of Ag-Doped PbS Nanoparticles for Optoelectronic Applications. *Ceram. Int.* **2019**, *45* (17), 21975–21985.
420. Kord, M.; Hedayati, K.; Farhadi, M. Green Synthesis and Characterization of Flower-Like PbS and Metal-Doped Nanostructures via Hydrothermal Method. *Main Group Met. Chem.* **2017**, *40* (1–2), 35–40.
421. Saeed, M.; Shahzad, U.; Marwani, H. M.; Asiri, A. M.; Rehman, S. U.; Althomali, R. H.; Rahman, M. M. Recent Advancements on Sustainable Electrochemical Water Splitting Hydrogen Energy Applications Based on Nanoscale Transition Metal Oxides (TMO) Substrates. *Chem. Asian J.* **2024**, e202301107; <https://doi.org/10.1002/asia.202301107>.
422. Saeed, M.; Marwani, H. M.; Shahzad, U.; Asiri, A. M.; Rahman, M. M. Nanoscale Silicon Porous Materials for Efficient Hydrogen Storage Application. *J. Energy Storage* **2024**, *81*, 110418.
423. Fang, J.; Zhou, Z.; Xiao, M.; Lou, Z.; Wei, Z.; Shen, G. Recent Advances in Low-Dimensional Semiconductor Nanomaterials and Their Applications in High-Performance Photodetectors. *InfoMater* **2020**, *2* (2), 291–317.
424. Yao, H.; Liu, L. Design and Optimize the Performance of Self-Powered Photodetector Based on PbS/TiS₃ Heterostructure by SCAPS-1D. *Nanomaterials* **2022**, *12* (3), 325.